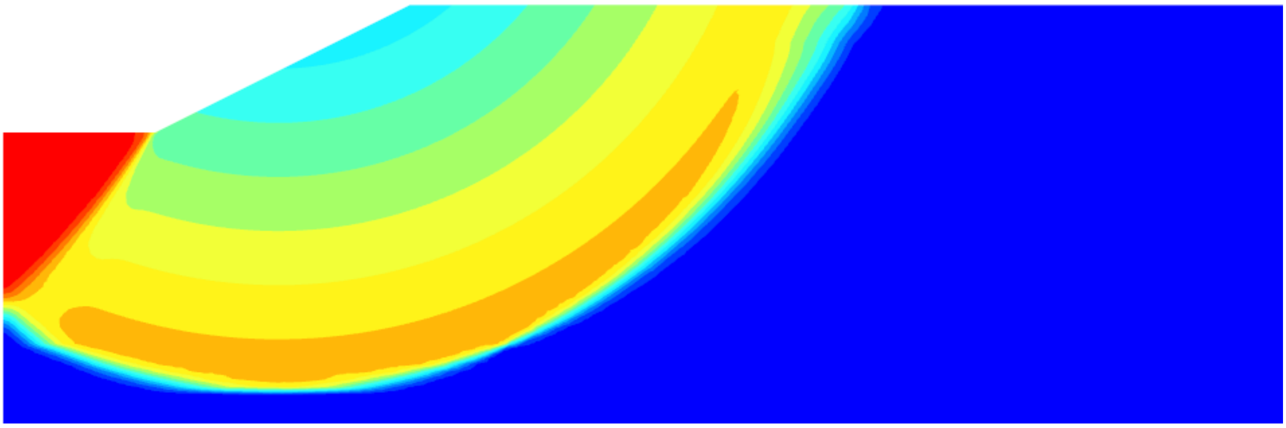

A comparison of analytical and numerical determination of hydraulic bottom-heave

A case study of lime-cement column implementation in underpass road 2970 in Hasslerör, Sweden

Master's thesis in Master's Programmes Structural Engineering and Building Technology & Infrastructure and Environmental Engineering

JOHAN EMMOTH
DANIEL WALLIN

DEPARTMENT OF ARCHITECTURE AND CIVIL ENGINEERING
DIVISION OF GEOLOGY & GEOTECHNICS

CHALMERS UNIVERSITY OF TECHNOLOGY
Gothenburg, Sweden 2021
www.chalmers.se

MASTER'S THESIS ACEX30

A comparison of analytical and numerical determination of hydraulic bottom-heave

A case study of lime-cement column implementation in underpass road 2970 in Hasslerör, Sweden

Master's Thesis in Master's Programmes Structural Engineering and Building Technology & Infrastructure and Environmental Engineering

JOHAN EMMOTH
DANIEL WALLIN

Department of Architecture and Civil Engineering
Division of Geology & Geotechnics
CHALMERS UNIVERSITY OF TECHNOLOGY

Gothenburg, Sweden 2021

A comparison of analytical and numerical determination of hydraulic bottom-heave

A case study of lime-cement column implementation in underpass road 2970 in Hasslerör, Sweden

Master's thesis in the Master's Programmes Structural Engineering and Building Technology & Infrastructure and Environmental Engineering

JOHAN EMMOTH

DANIEL WALLIN

Examensarbete ACEX30
Institutionen för arkitektur och samhällsbyggnadsteknik
Chalmers tekniska högskola, 2021

Department of Architecture and Civil Engineering
Division of Geology & Geotechnics
Chalmers University of Technology
SE-412 96 Gothenburg
Sweden
Telephone: + 46 (0)31-772 1000

Cover: Global slip surface due to hydraulic bottom-heave in Plaxis 2D.

Department of Architecture and Civil Engineering
Gothenburg, Sweden, 2021

A comparison of analytical and numerical determination of hydraulic bottom-heave

A case study of lime-cement column implementation in underpass road 2970 in Hasslerör, Sweden

Master's thesis in the Master's Programmes Structural Engineering and Building Technology & Infrastructure and Environmental Engineering

JOHAN EMMOTH

DANIEL WALLIN

Department of Architecture and Civil Engineering
Division of Geology & Geotechnics
Chalmers University of Technology

ABSTRACT

The determination of hydraulic bottom-heave is commonly derived by simplified analytical methodologies, which yields an overview but is unable to capture the complex behaviour as possible in numerical analyses. The use of numerical analyses is ever-increasing, but the accuracy of the methodology is highly sensitive. The thesis aims to establish the differences between the analytical and numerical modelling methodologies in determination of hydraulic bottom-heave. Furthermore, lime-cement columns are studied as a possible mitigation measure against slope stability and hydraulic bottom-heave failure. The analytical analyses are based on the Swedish design guidelines, total safety method and the direct method. The numerical analyses are divided into four scenarios which encompass the Mohr-Coulomb, Soft Soil, Hardening Soil and NGI-ADP constitutive model. The analyses are based on a case study of an underpass road in Hasslerör, Sweden. Additionally, key input parameters are established in a sensitivity analysis.

The analytical and numerical analyses predict that mitigation measures are required to ensure sufficient stability of the excavation. The predicted deformations and factor of safety depend on the selection of constitutive models. The sensitivity analysis implies that the selection of groundwater conditions, strength parameters and calculation type are of most importance to the results.

Conclusively, the thesis implies that the analytical analyses should serve as a first order estimate to establish whether numerical modelling is necessary. Furthermore, the sensitive nature of the numerical modelling clarifies the importance of representative input data and expertise of the geotechnical engineer. The numerical analyses conclude that lime-cement columns have a stabilizing impact with regards to both slope stability and hydraulic bottom-heave failure. However, the influence of the lime-cement columns with regards to hydraulic bottom-heave cannot be considered in the current Swedish design guidelines. The thesis recommends further research and development to verify the stabilizing effects of lime-cement columns with regards to hydraulic bottom-heave.

Key words: Hydraulic bottom-heave, analytical analysis, numerical analysis, lime-cement columns, excavation, constitutive models, Plaxis 2D

En jämförelse mellan analytiska och numeriska analyser för utvärdering av hydraulisk bottenupptryckning

En fallstudie av implementering av kalk-cementpelare i underfarten vid väg 2970 i Hasslerör, Sverige

Examensarbete inom masterprogrammen Konstruktionsteknik och Byggnadsteknologi & Infrastruktur och Miljöteknik

JOHAN EMMOTH

DANIEL WALLIN

Institutionen för arkitektur och samhällsbyggnadsteknik
Avdelningen för geologi & geoteknik
Chalmers tekniska högskola

SAMMANFATTNING

Utvärdering av hydraulisk bottenupptryckning genomförs vanligtvis med förenklande analytiska metoder. Analytiska metoder ger en översiktsbild men saknar egenskapen att fånga det komplexa beteendet såsom i numeriska analyser. Användandet av numeriska analyser ökar ständigt, men metodens träffsäkerhet är högst känslig för diverse faktorer. Tesens mål innefattar en etablering av skillnaderna mellan analytiska och numeriska beräkningsmetoder gällande hydraulisk bottenupptryckning. Vidare studeras kalk-cementpelare som en möjlig förstärkningsmetod för att förhindra brott som innefattar skred eller hydraulisk bottenupptryckning. De analytiska beräkningarna baseras på svensk standard, totalfilosofi och direktmetoden. De numeriska analyserna är uppdelade i fyra fall som innefattar Mohr-Coulomb, Soft Soil, Hardening Soil och NGI-ADP som konstitutiva modeller. Samtliga analyser baseras på en fallstudie av en underfart vid väg 2970 i Hasslerör, Sverige. Dessutom fastställs de mest påverkande parametrarna i en känslighetsanalys.

De analytiska och numeriska analyserna indikerar att förstärkningsmetoder krävs för att erhålla tillräcklig stabilitet i schaktet. De resulterande deformationerna och respektive säkerhetsfaktor fastställs vara beroende på valet av konstitutiv modell. Känslighetsanalysen indikerar att valet av grundvattentillstånd, hållfasthetsparametrar samt beräkningstyp har störst inverkan på resultaten.

Sammanfattningsvis antyder tesen att de analytiska beräkningsmetoderna bör användas som ett överslag för att utvärdera om en detaljerad numerisk analys är nödvändig. Vidare konstateras att känsligheten vid användning av numeriska analyser klargör vikten av representativ indata och erfarenhet hos utförande geotekniker. De numeriska analyserna fastställer att kalk-cementpelare har en stabiliserande effekt gällande både skred och hydraulisk bottenupptryckning. Däremot saknas möjligheten att tillgodoräkna de gynnsamma effekterna av kalk-cementpelare gällande hydraulisk bottenupptryckning inom ramen för svensk standard. Tesen rekommenderar vidare forskning och utveckling för att verifiera och fastställa den stabiliserande effekten av kalk-cementpelare med hänsyn till hydraulisk bottenupptryckning.

Nyckelord: Hydraulisk bottenupptryckning, analytisk analys, numerisk analys, kalk-cementpelare, schakt, konstitutiva modeller, Plaxis 2D

Contents

Preface

We would like to thank our supervisor Mats Karlsson at Chalmers University of Technology for continuous feedback and supervision throughout the project. Further, we would like to thank our supervisor at AFRY, Mikael Isaksson, for his support and for providing an inspiring and unique case study. We would also like to express our gratitude towards the geotechnical team at AFRY for welcoming us with open arms into their organisation.

Finally, we would like to show appreciation towards our families and our friends at Chalmers for their invaluable support and many years of laughter, hardship and development in life.

Gothenburg, June 2021

Johan Emmoth & Daniel Wallin

List of Figures

List of Tables

Notations

Abbreviations

1D	One-dimensional
2D	Two-dimensional
3D	Three-dimensional
CAUC	Consolidated anisotropic undrained compression triaxial test
CAUE	Consolidated anisotropic undrained extension triaxial test
CRS	Constant rate of strain
CPT	Cone penetration test
ESP	Effective stress path
FOS	Factor of safety
LCC	Lime-cement columns
NC	Normally consolidated
OC	Overconsolidated
OCR	Overconsolidation ratio
TSP	Total stress path
POP	Pre-overburden pressure

Greek lowercase letters

β	Inclination of slope
γ	Saturated unit weight
γ_w	Unit weight of water
γ'	Effective unit weight
γ_f^C	Shear strain at failure in triaxial compression
γ_f^E	Shear strain at failure in triaxial extension
γ_f^{DSS}	Shear strain at failure in direct simple shear
γ_d	Partial factor for safety class
$\underline{\varepsilon}^e$	Elastic strain tensor
$\underline{\varepsilon}^p$	Plastic strain tensor
κ^*	Modified swelling index
λ	Magnitude of plastic strains
λ^*	Modified compression index
$\lambda_{c\varphi}$	Factor in drained slope stability evaluation
μ_q	Correction factor for additional loads at top of slope

μ_t	Correction factor for occurrence of cracks in weathered dry crust
μ_w	Correction factor for water in the excavation
μ'_w	Correction factor for drained slope stability analysis
ρ	Saturated density
ρ_w	Water density
σ	Total stress
σ'	Effective stress
σ'_v	Effective vertical stress
σ'_{vp}	Average of vertical effective stress and pre-consolidation pressure
σ'_h	Effective horizontal stress
σ'_p	Pre-consolidation pressure
$\sigma_{1,2,3}$	Principal stresses
$\underline{\sigma}$	Stress tensor
τ	Shear strength
τ_0	Initial shear strength
ϕ'	Friction angle
ψ	Dilatancy angle

Roman uppercase letters

D^e	Elastic stiffness matrix
E	Young's modulus
E_u	Undrained Young's modulus
E'	Drained Young's modulus
E_{comp}	Stiffness modulus for composite material
E_{LCC}	Stiffness modulus of lime-cement columns
E_{soil}	Stiffness modulus of unimproved soil
E_{oed}	Tangent stiffness modulus
E_{oed}^{ref}	Reference tangent stiffness modulus
E_{ur}	Unloading/reloading stiffness modulus
E_{ur}^{ref}	Reference unloading/reloading stiffness modulus
E_{50}	Secant stiffness modulus
E_{50}^{ref}	Reference secant stiffness modulus
E^{ref}	Reference stiffness modulus
F_c	Undrained factor of safety

$F_{c\varphi}$	Drained factor of safety
G_0	Specific gravity
G_{ur}	Unloading/reloading shear modulus
G_{stb}	Favourable load
G_{kj}	Permanent unfavourable load
H	Excavation depth
H_w	Total height of water
H'_w	Intrinsic groundwater table
K_0	Lateral earth pressure coefficient
K_0^{NC}	Lateral earth pressure coefficient at normally consolidated state
M_0	Swedish confined modulus prior yield
M_L	Swedish confined modulus post-yield
M^*	Aspect ratio
N_0	Ratio in undrained slope stability evaluation
N_{cf}	Stability factor for drained slope stability evaluation
P_e	Correction factor for drained slope stability
P_d	Correction factor for undrained slope stability
R	Resisting shear force
X_{min}	Left vertical boundary
X_{max}	Right vertical boundary
Y_{min}	Bottom horizontal boundary
Y_{max}	Top horizontal boundary

Roman lowercase letters

a	Distance between excavation bottom and underlying frictional material
a_s	Area replacement ratio
c'	Effective cohesion
c_u	Undrained shear strength
c_{crit}	Critical shear strength
$c_{u,comp}$	Undrained shear strength of composite material
$c_{u,LCC}$	Undrained shear strength of lime-cement columns
$c_{u,soil}$	Undrained shear strength of unimproved soil
d	Lime-cement column diameter
e_0	Initial void ratio

f	Yield surface
f_c	Cap yield surface
g	Plastic potential
i	Hydraulic gradient
i_c	Critical hydraulic gradient
k_{comp}	Permeability of composite material
k_{LCC}	Permeability of lime-cement columns
k_{soil}	Permeability of unimproved soil
m	Modulus exponent
p	Mean principal stress
p'	Mean principal effective stress
p'_0	Size of the yield surface in the Soft Soil model
p'_p	Size of the yield surface in the Hardening Soil model
p_{ref}	Reference pressure
q	Deviator stress
q_l	Additional load at top of slope
q_r/q_a	Failure ratio
s_{col}	Column spacing
s_{row}	Row spacing
$s_{u,ref}$	Reference undrained shear strength
s_u^A	Plane-strain active shear strength
$s_{u,inc}^A$	Increase of plane-strain active shear strength with depth
$s_{u,ref}^A$	Reference plane-strain active shear strength
s_u^P	Plane-strain passive shear strength
s_u^{DSS}	Plane-strain direct simple shear strength
$s_u^{C,TX}$	Plane-strain triaxial compressive shear strength
u	Pore pressure
u_y	Vertical displacement
v	Poisson’s ratio
v_u	Undrained Poisson’s ratio
v_{ur}	Unloading/reloading Poisson’s ratio
v'	Drained Poisson’s ratio
w_L	Liquid limit
w_N	Water content

y_{ref} Reference depth

1 Introduction

In the following chapter, the background, aim and objectives, limitations and methodology of the thesis are presented.

1.1 Background

Within geotechnical engineering, there has historically been an extensive use of analytical calculation methodologies which are based on a framework of standards. The standards aim to incorporate conditions which are arduous or too difficult to implement analytically. Regarding hydraulic bottom-heave, partial factors are implemented to conservatively assess the probability of hydraulic bottom-heave occurring in deep excavations. However, in recent years, there has been an increase in the use of numerical analyses to determine the likelihood of hydraulic bottom-heave failure as numerical analyses provide more detailed information on e.g., water propagation, deformations and stress mobilization in excavations. The thesis investigates the discrepancies between the analytical and numerical calculation methodologies, and studies how possible measures, specifically lime-cement columns, may decrease the risk of hydraulic bottom-heave. Additionally, the thesis investigates how 3D effects are considered in 2D plane-strain design of an excavation. The analyses are based on available data retrieved from a case study provided by AFRY: underpass road 2970 in Hasslerör, Sweden.

1.2 Aim & Objectives

The aim of the thesis is to highlight the differences in analytical and numerical analyses of hydraulic bottom-heave in an excavation. Furthermore, the thesis strives to establish if and how lime-cement columns can be implemented to reduce the risk of hydraulic bottom-heave and to increase stability of an excavation. In addition, the thesis aims to incorporate 3D effects in 2D plane-strain design.

In essence, the following objectives are set for the thesis:

- Evaluate the factor of safety with regards to slope stability and hydraulic bottom-heave failure with analytical and numerical calculation methodologies and assess the suitability of the methods applied.
- Highlight the differences between the results of the analytical and numerical calculation methodologies and its consequences.
- Investigate differences between constitutive models in numerical analyses.
- Establish key input parameters in the numerical analyses through a sensitivity analysis.
- Determine if and how lime-cement columns can be implemented to reduce the effects of hydraulic bottom-heave.

1.3 Limitations

To delimit the scope of the thesis, the following limitations are necessary:

- Numerical analyses in the thesis are delimited to the finite element software Plaxis 2D. Licenses for Plaxis 3D are unavailable and 3D analyses requires an extensive addition of input data.
- As no triaxial tests have been performed on soil samples from the site of the case study, empirical estimations are applied to several input parameters.
- The case study is delimited to a selection of boreholes. The boreholes may not fully represent the true soil characteristics at the studied excavation.
- The lime-cement columns are wished in place with no consideration of installation effects.

1.4 Methodology

Firstly, a literature study is conducted in which relevant information and theory is compiled. The literature study is comprised of undrained & drained characteristics, hydraulic bottom-heave, lime-cement columns, 3D to 2D plane-strain and FEM & constitutive models.

Secondly, the case study provided by AFRY is reviewed with respect to hydrogeology, soil stratification and geotechnical parameters. Further, an in-depth derivation of input parameters for all constitutive models is conducted. Subsequently, analyses are performed analytically with an approach according to the current Swedish design guidelines TK GEO 13 followed by a total safety approach. Additionally, slope stability is evaluated in undrained and drained conditions according to the direct method. Numerical analyses are thereafter conducted using the finite element software Plaxis 2D. Several input parameters are also verified with the SoilTest tool in Plaxis 2D prior to conducting numerical analyses. Key input parameters and their sensitivity to the output results are then examined and discussed.

The results between the analytical and numerical analyses are subsequently compared, and any differences are elaborated along with its consequences. Additionally, the adverse or favourable effects of lime-cement columns with respect to hydraulic bottom-heave are investigated in the analyses. Lastly, the impact of selecting different constitutive models is investigated.

2 Literature study

The contents of the literature study are as following; undrained & drained characteristics, hydraulic bottom-heave, lime-cement columns, 3D to 2D plane-strain, FEM & constitutive models.

2.1 Undrained & drained characteristics

The most common failure mechanism in soils is based on shear stress development (Eslami, Moshfeghi, Molaabasi, & Eslami, 2019). Failure occurs when the shear stress induced in the soil exceeds the available shear strength (Knappett & Craig, 2012). In terms of clay, the shear strength depends on the drainage conditions. In undrained conditions, generated excess pore pressures are not allowed to dissipate from the soil. This is a characteristic short-term behaviour. As no volume change occurs in the clay during undrained conditions, the shear strength of the soil is constant regardless of the applied normal stress, see equation 2.1.

$$\tau = c_u \tag{2.1}$$

The emerging undrained shear strength of clay is dependent on a set of factors constituting e.g., the overconsolidation ratio, stress history and void ratio (Strózyk & Tankiewicz, 2014). For instance, several studies have concluded that the undrained shear strength increases with higher overconsolidation ratios (Ahmed & Agaiby, 2020; Strózyk & Tankiewicz, 2014). Additionally, the undrained shear strength is influenced by the applied strain rate (Day, 2000; Larsson, 2008). During rapid shearing a pronounced peak shear strength arises, possibly overestimating the shear strength in field conditions. This phenomenon is particularly evident in overconsolidated clays where interlocking effects of the grains yield unrealistically high shear strengths at low strain rates. Furthermore, the selected stress path and effective stress level in e.g., triaxial testing will also impact the undrained shear strength (Ahmed & Agaiby, 2020).

Contrarily to short-term characteristics of clay, the excess pore pressure is allowed to dissipate in long-term conditions, characterized as a drained response (Knappett & Craig, 2012). In drained conditions an effective cohesion, c', and friction angle, ϕ', is introduced at the applied normal stress, see equation 2.2.

$$\tau = c' + \sigma' \cdot \tan(\phi') \tag{2.2}$$

It should be addressed that the most stable condition in an excavation is the short-term condition since the unloading of the soil causes negative pore pressures near the excavation (Read & Beale, 2014). As the negative pore pressures are progressively increased over time, the stability of an excavation could be compromised since the drained shear strength may be inadequate in the new state of equilibrium.

2.2 Hydraulic bottom-heave

Hydraulic bottom-heave is a critical failure mode in deep excavations where a highly permeable frictional material is underlying a layer of less permeable cohesive soil or clay (Kullingsjö, 2007). The failure mode traditionally constitutes a high safety margin as the failure mechanism occurs both rapidly and with great destructive force (Pane, Cecconi, & Napoli, 2015). A visualization of the failure mode is presented in Figure 2.1.

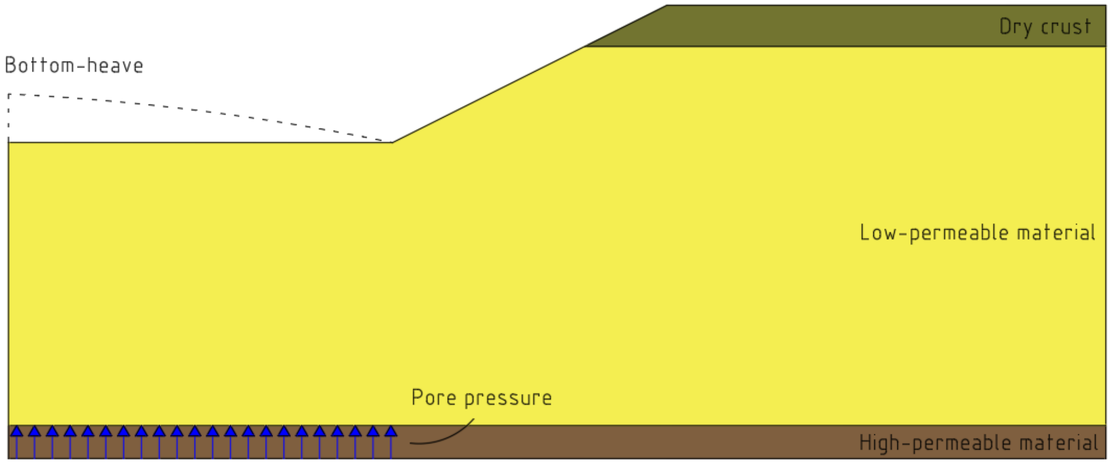

Figure 2.1 Visualization of hydraulic bottom-heave.

Failure due to hydraulic bottom-heave develops because of upward seepage forces exceeding the available in-situ effective stress level (Pane et al., 2015; Wudtke, 2008). Traditionally, the limit state against hydraulic bottom-heave is described by a critical hydraulic gradient characterized by the following relationship, see equation 2.3 (Pane et al., 2015). Thus, the critical hydraulic gradient, i_c, is governed by the effective unit weight of the soil, γ', and the unit weight of water, γ_w.

$$i_c = \frac{\gamma'}{\gamma_w} \tag{2.3}$$

Hydraulic bottom-heave failure is initiated when the hydraulic gradient, i, at an arbitrary point equals the critical hydraulic gradient, i_c. Consequently, the factor of safety, *FOS*, constitutes the ratio between the two gradients, see equation 2.4.

$$FOS = \frac{i_c}{i} \tag{2.4}$$

However, the critical gradient approach is often adjusted to strictly incorporate the ratio between the overburden soil mass and an underlying pore pressure in a frictional material, see equation 2.5 (Sällfors, 2013). Note that the factor a constitutes the distance between the excavation bottom and the underlying frictional material.

$$FOS = \frac{a \cdot \gamma}{u} \tag{2.5}$$

It is evident that the determination of the factor of safety in limit state only considers the unit weight of the soil as a stabilizing influence (Wudtke & Witt, 2013). However, additional margin for safety exists in cohesive soils such as clay as the available shear strength is ignored (Wudtke, 2008).

2.3 Lime-cement columns

In areas of predominantly sensitive clay, ground improvement techniques such e.g., lime-cement columns, are often a necessity to increase both short- and long-term stability. In Sweden, the current implementation of lime-cement columns in the passive zone of an excavation is limited in comparison to international applications, where lime-cement columns are established practice (Ignat, Larsson, & Baker, 2014; O'Rourke & O'Donnell, 1997; Yang, Tan, & Leung, 2011). The Swedish design guidelines TK GEO 13 facilitate the use of lime-cement columns as a measure for settlement reduction or embankment stabilization (Trafikverket, 2016a). There is however a demand to expand the applicability of lime-cement columns in excavations, such as in the passive zone which is subjected to extensive unloading and lateral loading conditions (Ignat, 2018). Lime-cement columns is a favourable ground improvement method in comparison to alternative measures since it is flexible to design, cost- and time efficient and consumes low amounts of both material and energy (EuroSoilStab, 2002). The influencing factors and several case studies of lime-cement column implementation in the passive zone is presented in the following sections.

2.3.1 Influencing factors

The composition and implementation of lime-cement columns in Sweden are under regulation by the Swedish Transport Administration (Trafikverket, 2016a). The allowed cement classes in the Swedish design guidelines include CEM I and CEM II. The selected cement class influences the overall strength of the lime-cement columns. Further, the presence of organic content in a to-be stabilized soil requires additional consideration in aggregate selection as it lowers the predicted outcome strength (Carlsten, 1996). For soils with considerable amounts of organic contents, exceeding 6 percent, lime-cement columns have been shown to not increase overall strength and should thus be avoided.

During installation of lime-cement columns in rows, a degree of overlap arises between each column (Ignat, 2018). The quality requirements of the overlap zone are crucial to avoid the occurrence of local failure mechanisms in the passive zone. Furthermore, the overall strength of the lime-cement columns greatly depend on the quality of the surrounding soil as the load should be carried mutually (Ignat, Baker, Larsson, & Liedberg, 2015). Therefore, it is of utmost importance to ensure that pile type behaviour in the lime-cement columns is avoided as the interaction between the stabilized soil and the unstabilized soil is lost (EuroSoilStab, 2002).

During installation of lime-cement columns, significant lateral shear strains arise due to the volume expansion induced by the binder which in turn generates excess pore pressures (Karlsrud, Eggen, Nerland, & Haugen, 2015). Installation of vertical drains in-between column rows significantly reduces the generated excess pore pressures, increasing the strength of the soil.

Furthermore, the installation of lime-cement columns temporarily reduces the bearing capacity of the soil (EuroSoilStab, 2002). The negative impact is caused by the exothermic chemical reactions during installation (British Standards, 2005; Kitazume & Terashi, 2013). Additionally, drilling with a rotational mixing tool causes soil disturbance, which may compromise overall stability (British Standards, 2005). An appropriate rotational speed, torque and velocity of the slurry delivery must be selected partly to minimize soil disturbance and partly to achieve sufficient homogeneity in the stabilized soil.

The curing time of the lime-cement columns significantly impacts the shear strength of the stabilized soil (Åhnberg et al., 1995; EuroSoilStab, 2002). The strength of the columns may reach acceptable values after only one month of curing but will develop over the course of several years. This highlights the importance of an appropriate construction schedule with sufficient curing time.

According to Moseley & Kirsch (2004), the permeability of lime-cement stabilized soil decreases with an increased curing time and confining pressure. Additionally, clay lumps emerge during the curing process which creates irregularities in the lime-cement columns (Carlsten, 1996). The irregularities allow for drainage of water and increases overall permeability.

2.3.2 Implementation in the passive zone

Several case studies regarding the implementation of lime-cement columns in the passive zone of an excavation has been conducted in Norway (Karlsrud et al., 2015). One of the remarkable results include differences between laboratory mixed specimens and field retrieved samples, where field samples exhibit up to 5 times higher strengths in triaxial testing. The contributary effects of curing conditions, greater lateral compression and higher temperatures in-situ are highlighted as key factors to explain the differences in generated strength. Additionally, the study concludes that the amount of binder significantly affects the predicted strength in laboratory mixed specimens, whilst it has negligible influence in field conditions. Furthermore, it is stated that the differences in strength from undrained and drained triaxial testing are insignificant.

In Sweden, a detailed triaxial testing programme has been conducted to verify the determination of drained strength parameters in the passive zone (Ignat, 2018). Results from the triaxial testing of lime-cement improved soils suggest an effective cohesion, c', of 32 kPa and a friction angle, ϕ', of 33 degrees in a passive zone stress regime. Contrarily, the Swedish design guidelines states that no effective cohesion is allowed in the passive zone. To overcome the limitation of the guidelines in effective stress-based models, an effective cohesion, c', equal to the undrained shear strength, c_u, may be adopted.

A recent study of lime-cement column implementation in the passive zone was conducted in the project E02-Centralen, Gothenburg (Yannie, Björkman, Isaksson, & Bergström, 2020). Yannie et al., (2020) points out that the Swedish design guidelines are inappropriate for implementation of lime-cement columns in the passive zone of an excavation. In the study, the strength parameters of the lime-cement columns are restricted to a maximum value of 100 kPa in accordance with the Swedish design guidelines (Trafikverket, 2016a; Yannie et al., 2020). However, Karlsrud et al., (2015) conclude that such a design strength limit is overly conservative and suggest an increase by a factor of up to 6 provided thorough inspections are conducted both during and after installation.

The results of the E02-centralen project indicate that the stiffness of lime-cement columns is strongly dependent on the execution of the installation procedure (Yannie et al., 2020). It was found that minor discrepancies and layers of clay within the columns has a major impact. Furthermore, the effective cohesion in the passive zone of the stabilized soil significantly exceeds the values as proposed by the Swedish design guidelines. The study at E02-Centralen was accepted by the Swedish Transport Administration provided that the lime-cement columns were configured in lattices or double rows (Yannie et al., 2020). Furthermore, the British Standards (2005) implies that rows of columns are an appropriate configuration in the passive zone.

2.4 3D to 2D plane-strain

The configuration of lime-cement columns in 3D space requires conversion to a 2D plane-strain model to facilitate analyses in Plaxis 2D. In accordance with the Swedish design guidelines, TK GEO 13, lime-cement improved soil should be modelled as a composite rigid body with weighted strength- and stiffness parameters (Trafikverket, 2016a). 2D modelling of the composite material requires implementation of an area replacement ratio, a_s, which is dependent on the configuration of the lime-cement columns. For rows of lime-cement columns with overlap and a column diameter, d, equal to or smaller than 0.6 metres, the area replacement ratio is determined according to equation 2.6, where, s_{row}, constitutes the centre- to centre spacing of the column rows (Larsson, 2006).

$$a_s = 0.87 \cdot \frac{d}{s_{row}} \tag{2.6}$$

A visualization of a general lime-cement column row configuration is presented in Figure 2.2.

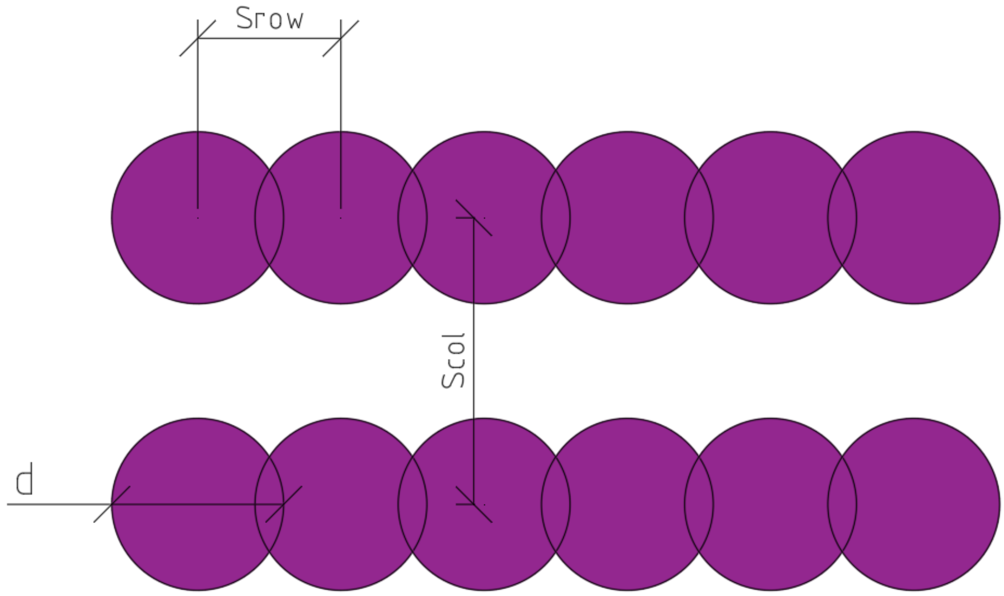

Figure 2.2 Lime-cement column row configuration with notations.

The representative weighted undrained shear strength of the composite material is determined according to equation 2.7 by incorporating the area replacement ratio (Adams, 2011; Smith, 2005; Trafikverket, 2016a).

$$c_{u,comp} = a_s \cdot c_{u,LCC} + (1 - a_s) \cdot c_{u,soil} \tag{2.7}$$

Analogously, the Young's modulus of the composite material is weighted according to equation 2.8 (Adams, 2011). Thereby, the stress-strain response of both the lime-cement columns and the surrounding clay is captured.

$$E_{comp} = a_s \cdot E_{LCC} + (1 - a_s) \cdot E_{soil} \tag{2.8}$$

Additionally, the permeability of the composite material is derived in an equal manner, see equation 2.9 (Trafikverket, 2016b). Note that the permeability of the lime-cement columns, k_{LCC}, equals to $500 \cdot k_{soil}$ in accordance with the Swedish design guidelines.

$$k_{comp} = a_s \cdot k_{LCC} + (1 - a_s) \cdot k_{soil} \tag{2.9}$$

2.5 FEM & constitutive models

Conventionally, geotechnical boundary value problems have been solved with simplified analytical calculation methodologies or empirical approximations often based on cumulative experience (Potts & Zdravković, 1999). These approximations may be satisfactory in a limited number of applications where the soil behaviour is somewhat represented by an elastic response to incremental strains (Wood, 2017). However, when a boundary value problem is characterised by non-linear behaviour or other more complex constraints, numerical approximations are often a necessity. A commonly applied finite element software by practising geotechnical engineers is Plaxis 2D (Karstunen & Amavasai, 2017).

Constitutive models are applied within soil mechanics to realistically capture the expected stress- strain relationship of a soil element (Kempfert & Gebreselassie, 2006). However, real soil behaviour is not perfectly elastic nor perfectly plastic and many of its properties are dependent on the applied stress path. According to Karstunen & Amavasai (2017), "the idea of constitutive modelling is to have a mathematical formulation that enables us to do predictions for the soil response under any arbitrary stress path, based on a single set of model constants" (p.6).

In essence, there exists numerous constitutive models of varying complexity which range from linear-elastic, elasto-plastic to more advanced formulations such as e.g., hypoplasticity (Kempfert & Gebreselassie, 2006). The simplest constitutive model, corresponding to a perfectly linear-elastic model, has its origin from Hooke's law of where the link between applied stress increments and elastic strains are related by a stiffness matrix, D^e, see equation 2.10 (Kempfert & Gebreselassie, 2006; Wood, 2017). In more advanced constitutive models described by e.g., elasto-plastic stress- strain relationships, the strain is divided into elastic and plastic strain components (Wood, 2017).

$$d\underline{\sigma} = D^e \cdot d\underline{\varepsilon}^e \tag{2.10}$$

The yield surface describes the interface between elastic and plastic strains where hardening laws governs its development (Karstunen & Amavasai, 2017). Equation 2.11 describes the direction of plastic strain and its corresponding magnitude (Kempfert & Gebreselassie, 2006; Wood, 2017).

$$d\underline{\varepsilon}^p = d\lambda \cdot \frac{\partial g}{\partial \underline{\sigma}} \tag{2.11}$$

In constitutive modelling, flow rules are required to define the size of the incremental strain components, denoted plastic flow (Karstunen & Amavasai, 2017). Flow rules are defined by either associate flow, where the incremental plastic strain is assumed to be orthogonal to the yield surface, or by non-associate flow, where additional plastic potential surfaces are defined. Therefore, in non-associate flow, plastic strains may develop well before the peak strength.

2.5.1 Mohr-Coulomb model

The Mohr-Coulomb model is a simple elastic perfectly plastic constitutive model (Potts & Zdravković, 1999; Wood, 2017). The failure envelope is based on the Coulomb failure criterion which is described according to equation 2.12.

$$\tau = c' + \sigma' \cdot \tan(\phi') \tag{2.12}$$

The simplicity of the constitutive model is due to the small number of parameters required. The stiffness is governed by two material parameters which are the Young's modulus, E, and the Poisson's ratio, v (Potts & Zdravković, 1999). The strength parameters constitute of the effective cohesion, c', the friction angle, ϕ', and the dilatancy angle, ψ. The plastic strains are represented both in terms of non-associated and associated flow (Karstunen & Amavasai, 2017).

The Mohr-Coulomb model has a significant number of limitations. Firstly, the intermediate stress, σ_2, is not considered which may lead to misleading results in problems where the intermediate stress governs the soil behaviour (Jiang & Xie, 2011). Further, the Mohr-Coulomb yield surface is an irregular hexagon in the space of principal stresses (Jiang & Xie, 2011; Potts & Zdravković, 1999). The irregular shape of the yield surface renders problems with convergence. In addition, the Mohr-Coulomb model overpredicts the plastic volumetric strains in comparison to true soil behaviour as there is no constraint that ceases dilation once it is initiated (Potts & Zdravković, 1999). Since the stiffness is formulated by one stiffness modulus, it should not be applied in problems where e.g., the unloading/reloading stiffness governs the soil response. Also, the Mohr-Coulomb model does not incorporate anisotropy of soil (Karstunen & Amavasai, 2017).

Regardless, the Mohr-Coulomb model is easy to implement in practice and is often applied as a first order estimate of a boundary value problem. As previously mentioned, the Swedish design guidelines recommend an elastic-perfectly plastic model to describe the stress- strain response of lime-cement columns (Trafikverket, 2016a).

2.5.2 Soft Soil model

The Soft Soil model is a constitutive model which incorporates stress- dependent stiffness (Plaxis, 2019). Additionally, the model has the ability to both consider and memorize the pre-consolidation pressure. The model is constrained to the Mohr-Coulomb failure envelope to avoid predictions of unrealistically high initial K_0 values (Karstunen & Amavasai, 2017). The yield surface of the Soft Soil model is shaped as an ellipsoid and has been formulated according to equation 2.13.

$$f = \frac{q^2}{(M^*)^2} + p'(p' - p_0') \tag{2.13}$$

Where, M^*, describes the aspect ratio of the ellipsoid and does not correlate with the critical state of the soil (Karstunen & Amavasai, 2017). The aspect ratio is derived based on the lateral earth pressure coefficient at normally consolidated state, K_0^{NC}, which is often determined based on Jaky's formula with the critical state friction angle in compression. The size of the yield surface, $p_0{}'$, changes throughout the analysis, where its magnitude depends on the input of OCR or the pre- overburden pressure, POP. The plastic strain increments are constrained to associated flow at the cap surface and non-associated flow at the Mohr-Coulomb failure envelope. The Plaxis manual states that the input parameters should be effective input parameters (Plaxis, 2019). Also, the stress path of the emerging undrained shear strength needs to be validated. In a p-q space, the yield surfaces of the Soft Soil model are illustrated accordingly, see Figure 2.3 (Karstunen & Amavasai, 2017).

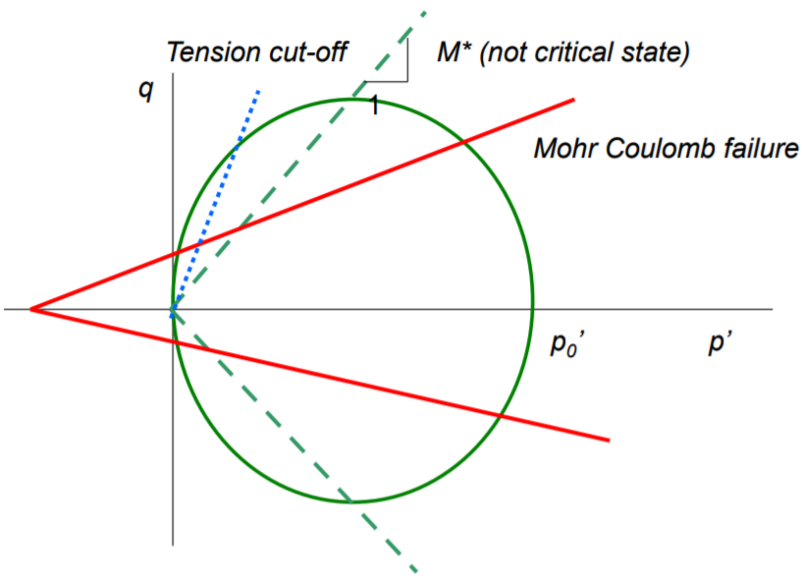

Figure 2.3 The Soft Soil model and the included yield surfaces (*Karstunen & Amavasai, 2017*).

The main input parameters of the Soft Soil model include the modified compression index, λ^*, modified swelling index, κ^*, effective cohesion, c', friction angle, ϕ', and the dilatancy angle, ψ (Plaxis, 2019). Additionally, the model incorporates input parameters such as the unloading/reloading Poisson's ratio, ν_{ur}, and the lateral earth pressure coefficient at normally consolidated state, K_0^{NC}. The modified compression index, λ^*, and modified swelling index, κ^*, are determined according to equations 2.14 and 2.15, which correlate the stiffness parameters to data from CRS tests often applied in Sweden (Hernvall, 2021). It should be noted that σ'_{vp} corresponds to the average of the vertical effective stress and the pre-consolidation pressure.

$$\lambda^* \approx \frac{1.1 \cdot \sigma'_p}{M_L} \tag{2.14}$$

$$k^* \approx \frac{2 \cdot \sigma'_{vp}}{M_0} \tag{2.15}$$

The Soft Soil model is subjected to several limitations. Firstly, the model is purely isotropic and does not consider anisotropic stress states (Plaxis, 2019). Karstunen & Amavasai (2017) states that the constraint of the Mohr-Coulomb failure envelope often contributes to misleading predictions in deep excavations, where the failure mechanism is developed too early. More advanced models may therefore be adopted to achieve more realistic results. The Soft Soil model does not incorporate creep-rate effects, which may negatively influence long-term analyses (Plaxis, 2019). Lastly, no strain softening effects are accounted for since the Mohr-Coulomb failure envelope restricts its development (Karstunen & Amavasai, 2017).

2.5.3 Hardening Soil model

The Hardening Soil model is an advanced constitutive model which similarly to the Soft Soil model accounts for stress- strain dependency of the soil stiffness (Plaxis, 2019). However, by considering a shear hardening cone as a function of plastic shear strains, the model overcomes certain limitations of the Soft Soil model (Karstunen & Amavasai, 2017). The model includes a cap yield surface of which the tangent stiffness modulus, E_{oed}, is governing the magnitude of plastic strains at the cap surface and the secant stiffness modulus, E_{50}, determines the level of plastic strains at the shear yield surface. The plastic shear strains are limited by the Mohr-Coulomb failure criterion. The size of the yield surface on the p-axis is derived from the input OCR or POP whilst the height of the ellipse on the q-axis depends on the aspect ratio, M^* (Plaxis, 2019). The aspect ratio is derived based on K_0^{NC}, preferably estimated with Jaky's formula. The yield surfaces in the Hardening Soil model is visualized in Figure 2.4 (Karstunen & Amavasai, 2017).

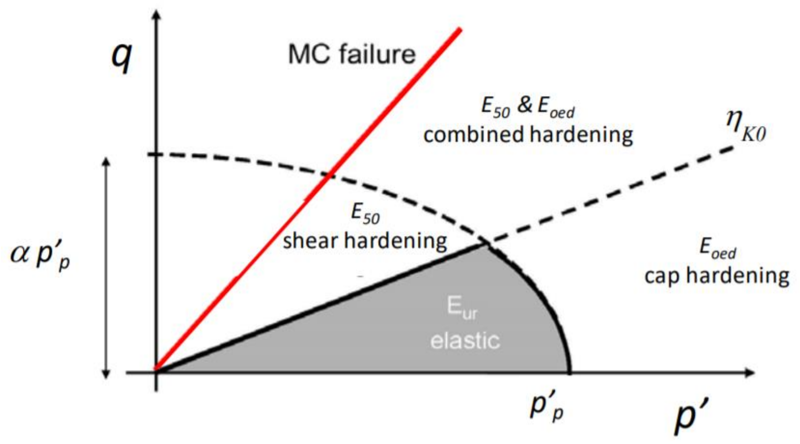

Figure 2.4 The Hardening Soil model and the included yield surfaces (Karstunen & Amavasai, 2017).

The cap yield surface is defined in accordance with equation 2.16 (Plaxis, 2019). It should be noted that the Hardening Soil model includes associated flow at the cap and non-associated flow at the Mohr-Coulomb failure criterion and at the shear hardening cone.

$$f_c = \frac{q^2}{(M^*)^2} + (p')^2 - {p'}_p^2 \tag{2.16}$$

The reference stiffnesses are defined with respect to the reference pressure, p_{ref}, and the modulus exponent, m, see equation 2.17. The reference pressure is by default set to 100 kPa (Plaxis, 2019; Schanz, Vermeer, & Bonnier, 1999). The $c'\cot(\phi')$ term governs the magnitude of tensile strength. Further, the Hardening Soil model includes a dilatancy cut-off which is activated when the maximum void ratio of the soil is reached (Plaxis, 2019).

$$E_i' = E_i^{ref} \left(\frac{\sigma_i' + c' \cdot \cot(\phi')}{p_{ref} + c' \cdot \cot(\phi')} \right)^m \tag{2.17}$$

Similarly to previously presented constitutive models, the Hardening Soil model has several drawbacks. Firstly, the implementation of reference stiffnesses impedes the ability to interpret and accurately relate the derived reference stiffnesses with values from accumulated experience (Karstunen & Amavasai, 2017). The Hardening Soil model is also not suitable for soft clays since the modulus exponent, m, for sensitive clays in Sweden exceeds the maximum allowed input value. Additionally, a traditional laboratory in Sweden does not possess the necessary equipment to capture the required input parameters. Consequently, the Soft Soil model should be applied instead in cases where input data is scarce. Likewise to the Soft Soil model, the Hardening Soil model tend to be conservative in triaxial extension and may therefore be inappropriate for deep excavation problems, especially regarding bottom-heave. Lastly, the Hardening Soil model does not include the effects of soil anisotropy (Plaxis, 2019).

2.5.4 NGI-ADP model

NGI-ADP is a complex constitutive model developed by Grimstad, Andresen & Jostad at the Norwegian Geotechnical Institute (Grimstad, Andresen, & Jostad, 2012). The model incorporates anisotropy and is applied for short-term analyses since it consists of undrained strength- and stiffness input parameters (Plaxis, 2019). The Plaxis manual (2019) states that the model is suitable for problems involving deformation analysis and ultimate bearing capacity. The benefits of the model include a distinction between the undrained shear strength in the active, direct simple shear and passive zone.

The NGI-ADP constitutive model requires a significant amount of input parameters (Plaxis, 2019). The stiffness parameters are comprised of the ratio of unloading/reloading shear modulus over plane-strain active shear strength, G_{ur}/s_u^A, the shear strain at failure in triaxial compression, γ_f^C, triaxial extension, γ_f^E, and in direct simple shear, γ_f^{DSS}. The strength parameters consist of the reference plane-strain active shear strength, $s_{u,ref}^A$, the ratio of triaxial compressive shear strength over plane-strain active shear strength, $s_u^{C,TX}/s_u^A$, the reference depth, y_{ref}, the increase of shear strength with depth, $s_{u,inc}^A$, the ratio of plane-strain passive shear strength over plane-strain active shear strength, s_u^P/s_u^A, the initial mobilization, τ_0/s_u^A, and the ratio of direct simple shear strength over plane-strain active shear strength, s_u^{DSS}/s_u^A. Lastly, an undrained Poisson's ratio, ν_u , is required. However, the extensive parameter requirement is simplified with empirical correlations and default values. The shear strain at failure in triaxial compression, triaxial extension and in direct simple shear are according to Plaxis (2019) typically reported in the range of 0.5 – 4 %, 3 – 8 % and 2 – 8 % respectively.

Similarly, to the antecedent constitutive models, the NGI-ADP model has several limitations. Firstly, the model is unable to capture long-term behaviour due to its formulation by undrained parameters. Additionally, the NGI-ADP model should not be applied for heavily overconsolidated clays (Plaxis, 2019). This restricts the use of the model to normally to near normally consolidated clay formations. Finally, the NGI-ADP model does not update the undrained shear strengths with respect to load history (Plaxis, 2018).

3 Case study

In the following sections, a case study of underpass road 2970 in Hasslerör, Sweden is presented. The case study is provided by AFRY and is investigated to relate lime-cement column implementation with regards to hydraulic bottom-heave. The case study is described in detail with respect to background, hydrogeology, soil stratification and geotechnical parameters.

3.1 Background

As a part of the Swedish national plan for development of the transportation system between 2014 and 2025, highway E20, a critical communication link between major cities in Sweden, is currently undergoing planning and development (Trafikverket, 2020). The current state of highway E20 is inadequate since level crossing intersections between local roads and the highway are frequent along the route. Other issues include high traffic loads, heavy traffic and a low-speed limit in many areas.

An area of particular concern is underpass road 2970 situated in Hasslerör northeast of Mariestad. A critical cross-section is situated where the underpass reaches its maximum depth, see the yellow line in Figure 3.1. The geotechnical conditions provide a challenge in the design of the excavation for the underpass. The area consists of sensitive and partly quick clay overlying a water-bearing layer of frictional material. A nearby aquifer situated in Hasslerör induces high pore pressures which travels in the frictional material to the site due to differences in hydraulic gradients. The clay of a limited thickness in combination with high underlying pore pressures undermine the stability of the planned excavation. Thus, extensive mitigation measures are required to ensure short- and long-term stability.

Figure 3.1 Planned infrastructure in Hasslerör, along with the location of the critical cross-section.

Figure 3.2 presents the boreholes relevant to the critical cross-section. The radius of the area of interest is approximately 360 metres and is selected to delimit the extent of boreholes and to facilitate a local assessment of the soil conditions in proximity to the critical cross-section.

Figure 3.2 Boreholes within the area of interest for the critical cross-section.

3.2 Hydrogeology

The hydrogeological conditions at the site are strongly influenced by a nearby formation of gravel and sand which was deposited during the last glaciation (Trafikverket, 2020). Throughout the community of Hasslerör there is a continuous deposit of the frictional material, visualized in green in Figure 3.3 (SGU, 2021).

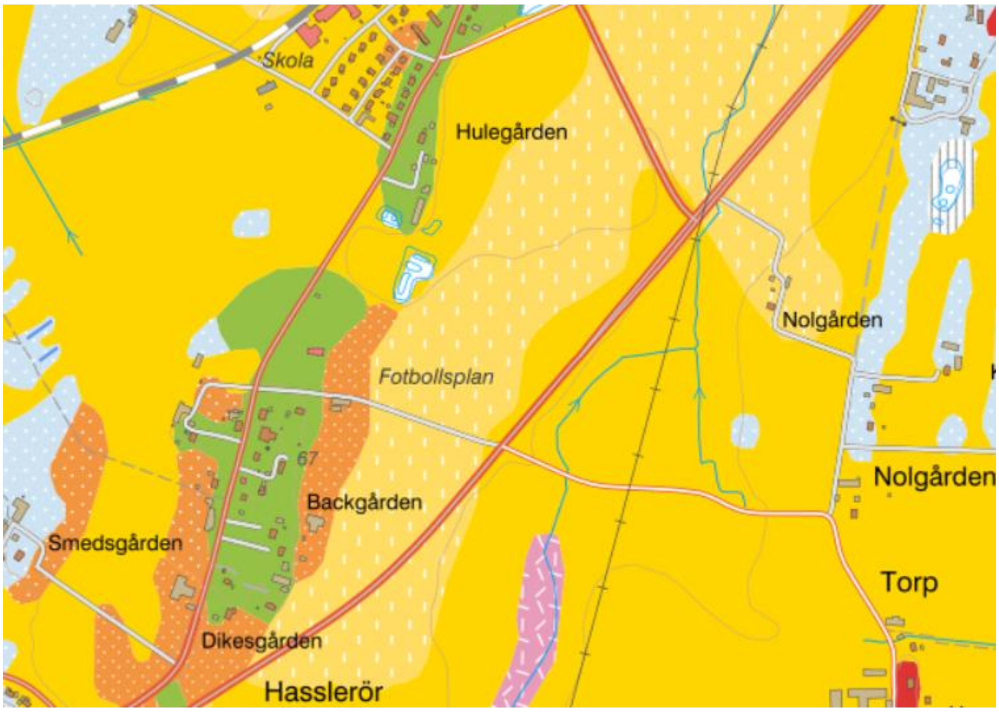

Figure 3.3   Soil map of Hasslerör (SGU, 2021).

At the location of underpass road 2970, the frictional material is underlying a layer of glacial clay (Trafikverket, 2020). Performed groundwater level measurements have established a groundwater level of 0 – 2 metres below the ground surface. Therefore, the groundwater level is selected as the average value of 1 metre below the ground surface at the critical cross-section. Furthermore, the aquifer situated in Hasslerör induce a pore pressure in the underlying frictional material which corresponds to a theoretical groundwater level of 1.3 metres above the ground surface. The pore pressure constitutes a value of 166 kPa at the top of the underlying frictional material. The induced artesian pressure at the critical cross-section increases the predicted risk of hydraulic bottom-heave failure.

Additionally, many researchers and organisations emphasize that future climate change will lead to an increased quantity of precipitation in Sweden (Livsmedelverket, 2021; Naturvårdsverket, 2020; SMHI, 2012). The likelihood of recurring cloudbursts will increase, and groundwater levels are projected to elevate throughout the country, excluding the south-east part of Sweden (Livsmedelverket, 2021). Consequently, it would be reasonable to assume that the already high artesian pressure at the underpass road 2970 will escalate over time.

3.3 Soil stratification

As mentioned previously, the critical cross-section of the underpass road 2970 is located where the depth of the excavation reaches its maximum. Three boreholes are in proximity to the critical cross-section and is therefore of most relevance to derive the soil stratification of the model. Among these one of the boreholes constitutes the minimum clay thickness, and thus, yields the minimum resisting forces against failure due to hydraulic bottom-heave. However, as one should not solely rely on the interpretation from a single borehole, an average soil stratification between the three boreholes is selected. An illustration of the soil stratification is presented in Figure 3.4.

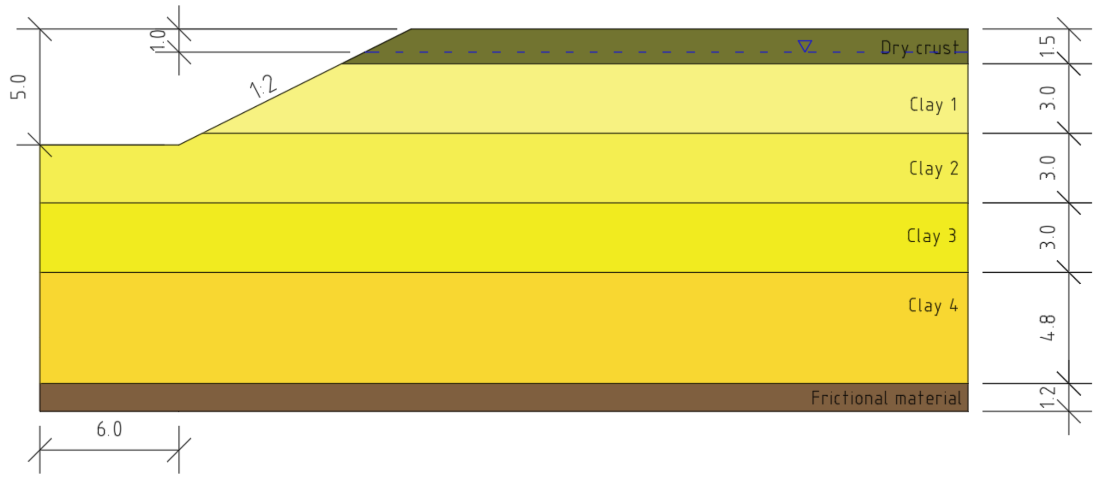

Figure 3.4 Soil stratification of the cross-section without lime-cement columns.

The lime-cement columns are installed below the dry crust down to a depth of 13.3 metres. The columns extend 20 metres outwards from the centre of the excavation. Figure 3.5 present the soil stratification of the critical cross-section with the implementation of lime-cement columns.

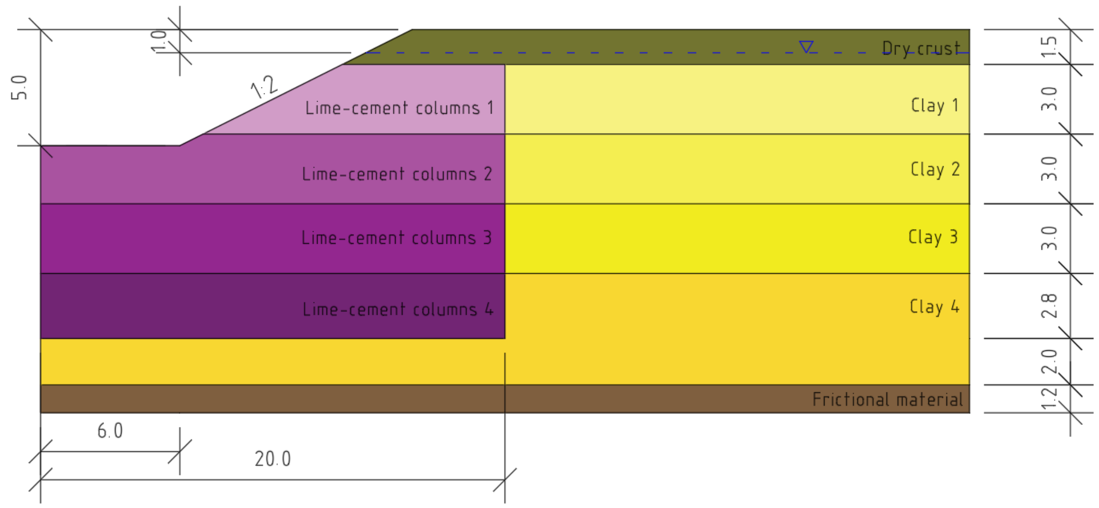

Figure 3.5 Soil stratification of the cross-section with lime-cement columns.

3.4 Geotechnical parameters

Analytical and numerical analyses require several parameters that are either derived from laboratory tests or based on empirical relations. As triaxial laboratory tests have not been conducted, many of the geotechnical parameters rely on empirical relationships. Parameters derived from laboratory tests are based on boreholes located in proximity to the critical cross-section.

The clay is divided into four layers as illustrated in Figure 3.4, Section 3.3, of which the strength- and stiffness parameters are derived from the centre of each layer at depths of 3, 6, 9 and 12.9 metres. The strength- and stiffness parameters of the lime-cement columns are derived analogously. The division of the clay and lime-cement column layers is performed to avoid under- or overestimation of material parameters.

The laboratory data is comprised of the following parameters: liquid limit, water content, density, sensitivity, permeability, undrained shear strength and the Swedish confined moduli prior and post-yield. Figure 3.6 presents the saturated density of the clay within the area of the critical cross-section. Through evaluation of the raw data, a trend of representative saturated density is established. The trend is selected conservatively, motivated by borehole B25 and the fact that a lower saturated density results in less resisting forces against hydraulic bottom-heave failure. The saturated density is set to 16.3 kN/m^3 for all clay layers.

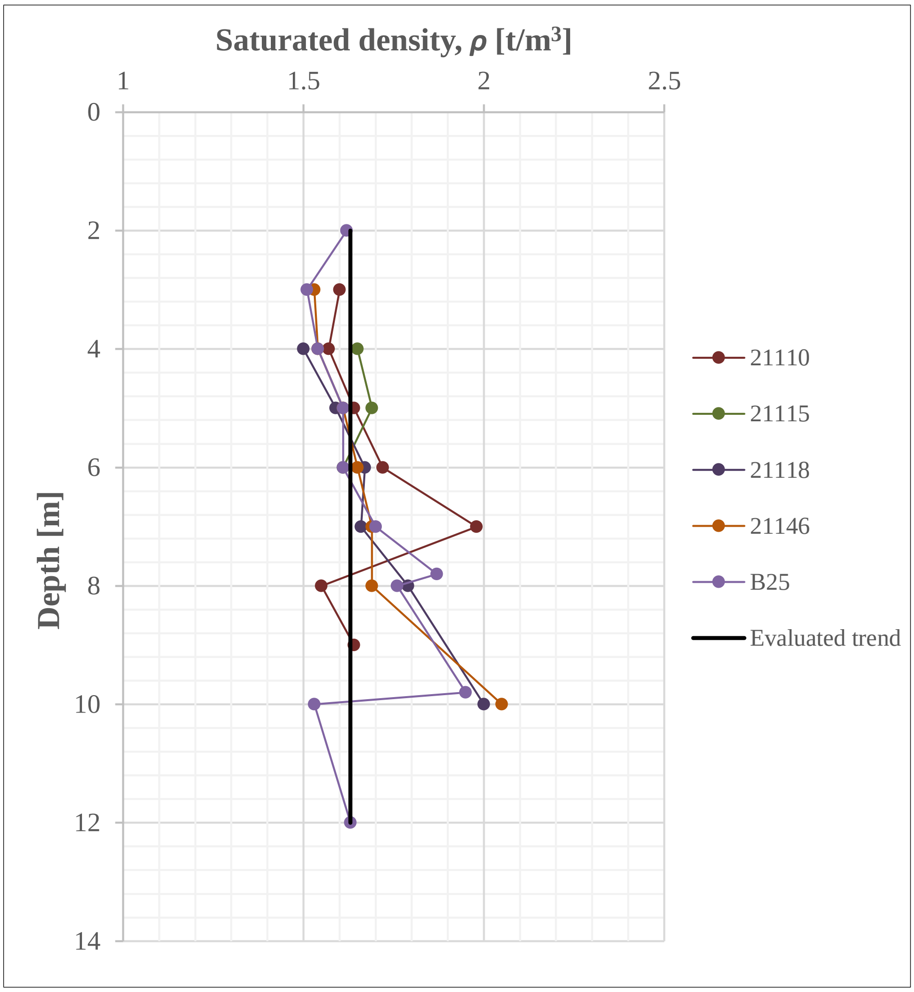

Figure 3.6 Saturated density of the clay and the evaluated trend.

Pore pressure measurements in the area are scarce and thus assumptions regarding the pore pressure distribution with depth is necessary. Precipitation, plants and other environmental impacts are assumed to influence the pore pressure distribution near the ground surface. Consequently, the soil beneath the ground surface is characterised by a hydrostatic increase in pore pressure of 10 kPa/m to a depth of 5 metres. Below the depth of 5 metres, an increase of 12.23 kPa/m is required to attain a pore pressure of 166 kPa at the top of the frictional material. Figure 3.7 presents the distribution of in-situ vertical effective stresses as a result of the applied pore pressure distribution and the unit weights of the soils. The evaluated trend of the pre-consolidation pressure is also presented.

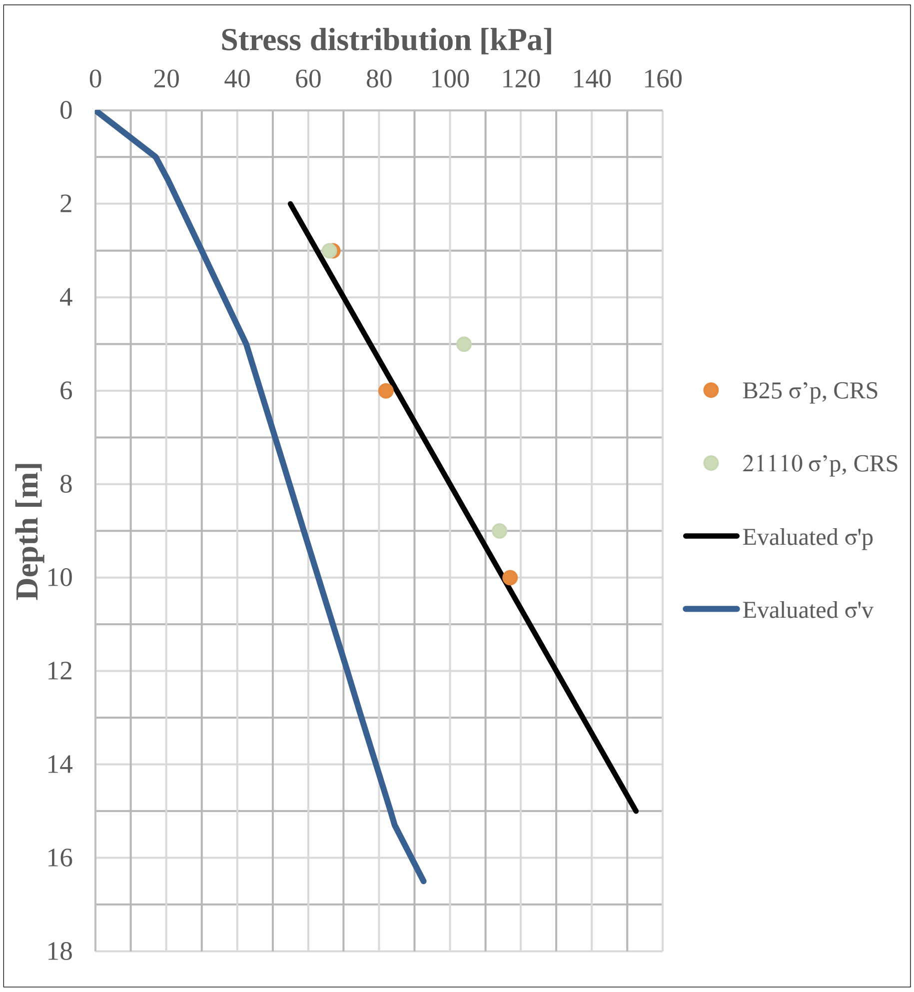

Figure 3.7 Stress distribution of the vertical effective stresses and the evaluated trend of the pre-consolidation pressure.

Figure 3.8 illustrates the undrained shear strength obtained from CPT, fall cone tests and field vane tests along with an evaluated trend of the undrained shear strength. The evaluated undrained shear strength of the clay layer is verified with borehole 21012, of which a direct shear test was performed. A conservative evaluation of the undrained shear strength is applied, slightly below the values from the direct shear tests displayed as green triangles.

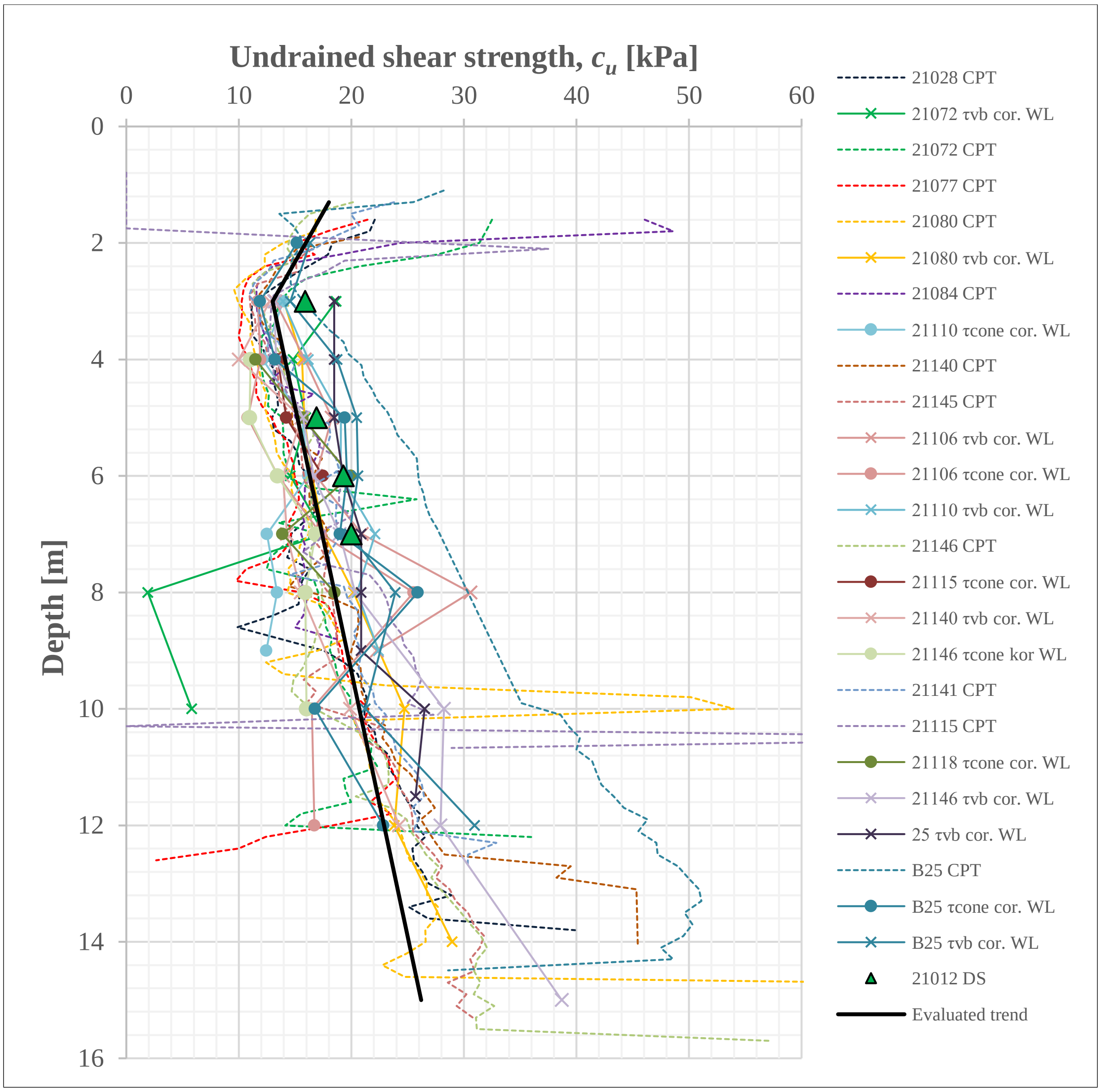

Figure 3.8 Undrained shear strength of the clay obtained from CPT, field vane tests, fall cone tests, direct shear tests and the evaluated trend.

Figures illustrating the raw data and evaluated trends for water content, liquid limit, sensitivity and permeability are presented in Figure A.1 – Figure A.4, Appendix A. Furthermore, evaluated trends for the Swedish confined moduli prior and post-yield, M_0, and M_L, are presented in Figure A.5 and Figure A.6, Appendix A.

The initial void ratio, e_0, of the clay is determined from the liquid limit, w_L, density of water, ρ_w, density of clay, ρ, and the specific gravity, G_0, see equation 3.1 (Knappett & Craig, 2012). The specific gravity is set to 2.65.

$$e_0 = G_0 \cdot (1 + w_L) \cdot \frac{\rho_w}{\rho} - 1 \tag{3.1}$$

The lateral earth pressure coefficient, K_0, for the clay layer depends on the overconsolidation ratio, OCR. For slightly overconsolidated clay, the lateral earth pressure coefficient is evaluated according to equation 3.2 (Mayne & Kulhawy, 1982).

$$K_0 = 1 - \sin(\phi') \cdot OCR^{\sin(\phi')} \tag{3.2}$$

For the lime-cement columns, the lateral earth pressure coefficient, K_0, is determined according to Jaky's formula, see equation 3.3.

$$K_0 = 1 - \sin(\phi') \tag{3.3}$$

In a study conducted by Alén et al., (2006), it was concluded that lime-cement columns can be considered as highly overconsolidated clay. Therefore, an initial overconsolidation ratio of 5 is assumed.

3.4.1 Mohr-Coulomb model

The Mohr-Coulomb constitutive model is comprised of input strength- and stiffness parameters as established in Section 2.5.1. All parameters require empirical correlation as no triaxial test have been performed. For clay in undrained conditions, the undrained Young's modulus, E_u, is based on the empirical relationship with the undrained shear strength, c_u, see equation 3.4 (Trafikverket, 2016b).

$$E_u = 250 \cdot c_u \tag{3.4}$$

Comparatively, in drained conditions, the drained Young's modulus, E', is derived according to equation 3.5, which utilize Hooke's law (Plaxis, 2019).

$$E' = \frac{2 \cdot (1 + v')}{3} \cdot E_u \tag{3.5}$$

The undrained Young's modulus of the lime-cement columns is derived according to equation 3.6, which is based on the critical shear strength, c_{crit} (Trafikverket, 2016b). The Swedish design guidelines restrict the critical undrained shear strength to a maximum of 100 kPa, although this value was not exceeded in the available unconfined compression tests for a mixture of 90 kg/m^3 and a curing time between 7 - 21 days. The drained Young's modulus, E', is derived according to equation 3.5 similarly to the clay.

$$E_u = 13 \cdot c_{crit}^{1.6} \tag{3.6}$$

In clay, the undrained Poisson's ratio, v_u, is equal to 0.5. However, in numerical analyses it should be selected slightly below, preferably 0.495, to avoid numerical issues (Plaxis, 2019; Trafikverket, 2016b). The drained Poisson's ratio, v', corresponds to a value of 0.2, which is often applied in Scandinavian clays. Comparatively, the drained Poisson's ratio for the lime-cement columns is set to 0.33 (Alén et al., 2006).

The effective cohesion, c', of the clay is determined according to equation 3.7, as proposed in TR GEO 13 (Trafikverket, 2016b).

$$c' = 0.1 \cdot c_u \tag{3.7}$$

For the lime-cement columns, equation 3.8, applicable for the direct shear zone, is used to determine the effective cohesion according to recommendations in TK GEO 13 (Trafikverket, 2016a).

$$c' = 0.15 \cdot c_{crit} \tag{3.8}$$

For clay, the friction angle, ϕ', is determined according to TR GEO 13, which recommend a friction angle of 30 degrees (Trafikverket, 2016b). For lime-cement columns, the friction angle is instead based on TK GEO 13, constituting an angle of 32 degrees (Trafikverket, 2016a). Furthermore, clay usually constitutes small to no dilatancy (Plaxis, 2019). Hence, the dilatancy angle, ψ, is assumed equal to zero. This assumption also applies for the lime-cement columns.

Due to lack of information regarding both the dry crust and the frictional material of the critical cross-section, their strength- and stiffness parameters must be assumed. The Young's modulus of the dry crust is assumed slightly stiffer compared to the first clay layer. The drained Poisson's ratio was set equal to the clay layers, i.e., 0.2. The effective cohesion of the dry crust is derived analogously to the clay. However, in numerical analyses the effective cohesion is set to 10 kPa to avoid numerical issues. The friction angle of the dry crust was set equal to the clay layers, i.e., 30 degrees.

The frictional material is modelled with strength- and stiffness parameters from a study conducted by Hernvall (2021). The values from the case study are applied since no information is available regarding the parameters of the underlying frictional material. The Young's modulus of the frictional material is set to 40 000 kPa and the drained Poisson's ratio is set to 0.2. The effective cohesion is 2 kPa and the friction angle is set to 40 degrees.

3.4.2 Soft Soil model

Similarly to the Mohr-Coulomb constitutive model, the Soft Soil model requires triaxial laboratory tests of soil samples to determine its strength- and stiffness parameters. Hence, for several input parameters, use of empirical correlations in accordance with the Swedish design guidelines is necessary.

The stiffness parameters of the Soft Soil model which constitutes the modified compression index, λ^*, and the modified swelling index, κ^*, are derived with empirical correlations according to equation 3.9 and 3.10 (Hernvall, 2021). The parameters are based on the Swedish confined moduli prior and post-yield, derived from performed CRS tests. It should be noted that the Swedish confined modulus prior yield, M_0, should be increased by a factor of 3 – 5 from evaluated CRS tests to more accurately represent field conditions (Olsson, 2010). Figure A.7 and Figure A.8 in Appendix A illustrate the evaluated trends of the modified compression index, λ^*, and the modified swelling index, κ^*.

$$\kappa^* = \frac{2 \cdot \sigma'_{vp}}{M_0} \tag{3.9}$$

$$\lambda^* = \frac{1.1 \cdot \sigma'_p}{M_L} \tag{3.10}$$

Likewise to the Mohr-Coulomb model, the effective cohesion, *c'*, is determined using equation 3.7, Section 3.4.1. Furthermore, the friction angle, ϕ', and the dilatancy angle, ψ, is empirically based and thus remain the same as in the Mohr-Coulomb model.

Additionally, the Soft Soil model constitutes of advanced strength parameters which include the unloading/reloading Poisson's ratio, v_{ur}, and the lateral earth pressure coefficient at normally consolidated state, K_0^{NC}. The unloading/reloading Poisson's ratio, v_{ur}, is equal to 0.15 as per the default value stated in the Plaxis manual (Plaxis, 2019). The lateral earth pressure coefficient at normally consolidated state is determined according to Jaky's formula, see equation 3.11.

$$K_0^{NC} = 1 - \sin(\phi') \tag{3.11}$$

3.4.3 Hardening Soil model

The Hardening Soil model is a more advanced model and thus requires additional input parameters, see Section 2.5.3. Unlike the Mohr-Coulomb and Soft Soil constitutive models, the Hardening Soil model constitutes of several additional stiffness moduli, namely the reference secant stiffness modulus, E_{50}^{ref}, reference tangent stiffness modulus, E_{oed}^{ref}, and reference unloading/reloading stiffness modulus, E_{ur}^{ref}. It should be noted that all stiffness moduli are dependent on a reference pressure, p_{ref}, which by default is assumed equal to the atmospheric pressure of 100 kPa. The modulus exponent, *m*, is set to the maximum allowed value of 1 for the clay (Karstunen & Amavasai, 2017). Contrarily, the modulus exponent for the lime-cement columns, *m*, is set equal to 0.7 based on a case study in Enköping where the soil conditions are similar to the critical cross-section in Hasslerör (Ignat, Baker, Karstunen, Liedberg, & Larsson, 2020).

Firstly, the reference secant stiffness modulus, E_{50}^{ref}, is derived according to equation 3.12. The effective horizontal stress, σ_h', is determined by the in-situ effective vertical stress, σ_v', and the K_0 value for the clay and the lime-cement columns respectively.

$$E'_{50} = E_{50}^{ref} \cdot \left(\frac{\sigma_h' + c' \cdot \cot(\phi')}{p_{ref} + c' \cdot \cot(\phi')} \right)^m \tag{3.12}$$

Secondly, the reference tangent stiffness modulus of the clay, E_{oed}^{ref}, is determined according to equation 3.13 based on the drained tangent stiffness modulus, E_{oed}', and the vertical effective stress, σ_v'. The drained tangent stiffness modulus corresponds to the Swedish confined modulus post-yield, M_L, and the vertical effective stress is set equal to the pre-consolidation pressure (Karstunen & Amavasai, 2017). The tangent stiffness modulus of the lime-cement columns is derived from correlations from the case study in Enköping (Ignat et al., 2020). In the case study, it was deduced that the reference tangent stiffness modulus had a minor impact and thus it is set equal to the secant tangent modulus.

$$E'_{oed} = E_{oed}^{ref} \cdot \left(\frac{\sigma_v' + c' \cdot \cot(\phi')}{p_{ref} + c' \cdot \cot(\phi')} \right)^m \tag{3.13}$$

Moreover, the reference unloading/reloading stiffness modulus, E_{ur}^{ref}, is empirically set to three times the reference secant stiffness modulus, E_{50}^{ref}. This correlation is also based on the case study in Enköping (Ignat et al., 2020).

The effective cohesion, c', friction angle, ϕ', and dilatancy angle, ψ, is determined similarly to the Mohr-Coulomb and Soft Soil constitutive models and thus remain equal. Furthermore, the lateral earth coefficient at normally consolidated state, K_0^{NC}, is determined in accordance with Jaky's formula, see equation 3.11, Section 3.4.2. Additional parameters including the unloading/reloading Poisson's ratio, ν_{ur}' and the failure ratio, q_r/q_a, are based on default values as proposed by the Plaxis manual.

3.4.4 NGI-ADP model

The NGI-ADP constitutive model is comprised of several strength- and stiffness parameters which require derivation, see Section 2.5.4. The parameters are derived solely for the clay. The plane-strain active shear strength is based on equation 3.14 which empirically correlates the effective vertical stress, σ_v', and the overconsolidation ratio, OCR (Larsson et al., 2007). The factor, b, is assigned a value of 0.8.

$$s_u^A = 0.33 \cdot \sigma_v' \cdot OCR^b \tag{3.14}$$

Furthermore, the reference plane-strain active shear strength, $s_{u,ref}^A$, is determined at a reference depth, y_{ref} (Plaxis, 2019). The reference depth is defined where the plane-strain active shear strength increases linearly with depth, $s_{u,inc}^A$. The active shear strength above the reference depth corresponds to a constant value. For each respective clay layer, the reference depth is set at the top of the layer with a corresponding plane-strain active shear strength.

The plane-strain direct shear strength, s_u^{DSS}, and passive shear strength, s_u^P further require empirical correlation. Equations 3.15 and 3.16 correlate the respective shear strength parameters with the effective vertical stress, σ_v', the liquid limit, w_L, and the overconsolidation ratio, OCR (Larsson et al., 2007).

$$s_u^{DSS} = (0.125 + 0.205 \cdot w_L)/1.17 \cdot \sigma_v' \cdot OCR^b \tag{3.15}$$

$$s_u^P = (0.055 + 0.275 \cdot w_L)/1.17 \cdot \sigma_v' \cdot OCR^b \tag{3.16}$$

Figure 3.9 presents the empirically derived shear strength parameters as functions of increasing depth. The shear strength parameters coincide with the arrangement as stated in the Plaxis manual, $s_u^P < s_u^{DSS} < s_u^A$ (Plaxis, 2019).

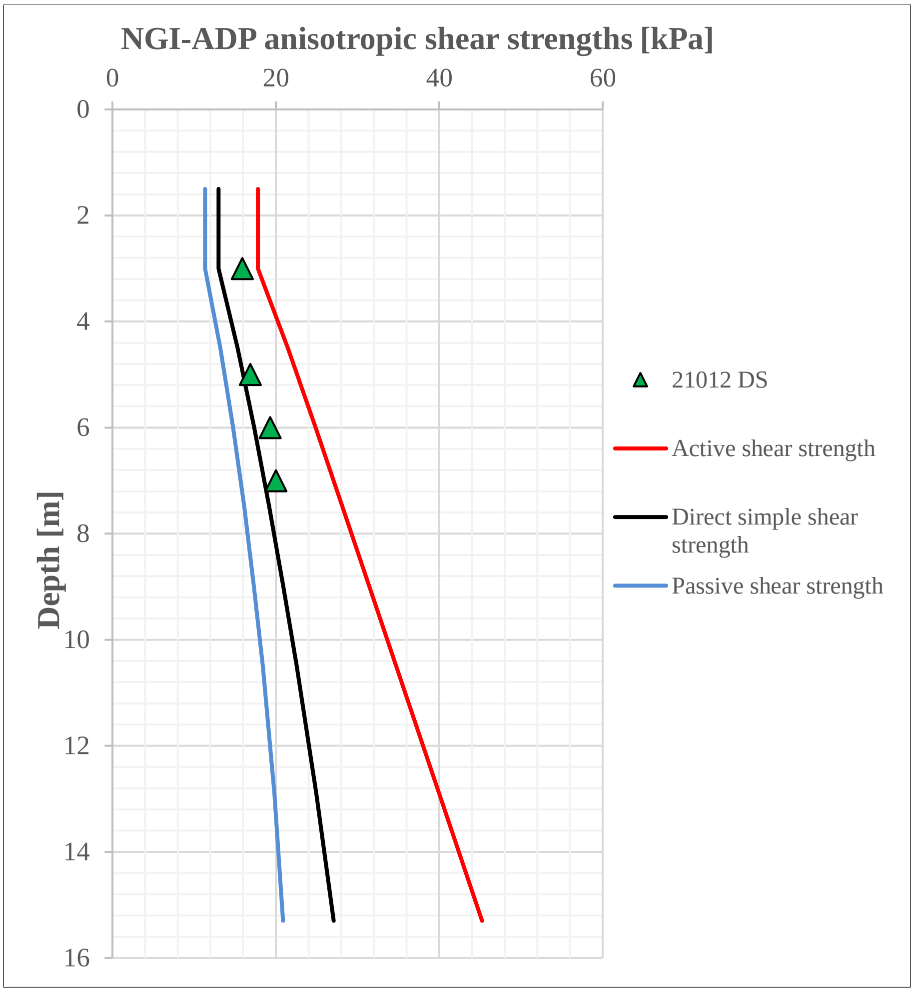

Figure 3.9 Empirically determined NGI-ADP anisotropic undrained shear strengths as a function of depth for the clay.

The ratio of unloading/reloading shear modulus over the plane-strain active shear strength, G_{ur}/s_u^A, is evaluated from an initial shear modulus provided from conducted laboratory tests. The shear strain at failure in triaxial compression, γ_f^C, direct simple shear, γ_f^{DSS}, and triaxial extension, γ_f^E, is initially assumed 2 %, 3 % and 4 % respectively. Additionally, the ratio of triaxial compressive shear strength over plane-strain active shear strength, $s_u^{C,TX}/s_u^A$ is assigned a default value of 0.99 (Plaxis, 2019). Since the NGI-ADP model is based on total stress analysis, an undrained Poisson's ratio of 0.495 is assigned.

As the clay is slightly overconsolidated, the default value of initial mobilization over plane-strain active shear strength, τ_0/s_u^A, of 0.7 should not be applied. Instead, the ratio of initial mobilization is evaluated according to equation 3.17, which correlates the in-situ vertical effective stress, σ_v', and the lateral earth pressure coefficient, K_0, in accordance with the Plaxis manual (Plaxis, 2019).

$$\tau_0/s_u^A = -0.5 \cdot (1 - K_0) \cdot \sigma_v'/s_u^A \tag{3.17}$$

3.4.5 Composite material

The varying properties of the composite material depends on the area replacement ratio, a_s, related to the configuration of the lime-cement columns, see Section 2.4. For rows of lime-cement columns with a diameter equal to or smaller than 0.6 metres, the centre-to centre distance between rows, s_{row}, should range between 1 to 1.6 metres (Larsson, 2006). In accordance with a study on lime-cement column implementation in the passive zone conducted by Ignat et al., (2015), a centre-to centre distance of 1 metre between rows is selected to ensure sufficient interaction between the lime-cement columns and the surrounding clay. Furthermore, a centre- to centre distance between individual lime-cement columns, s_{col}, of 0.5 metres is selected. The lime-cement column diameter, d, is set to 0.6 metres as recommended in TK GEO 13 (Trafikverket, 2016a). Figure 3.10 present the lime-cement column layout along with corresponding dimensions.

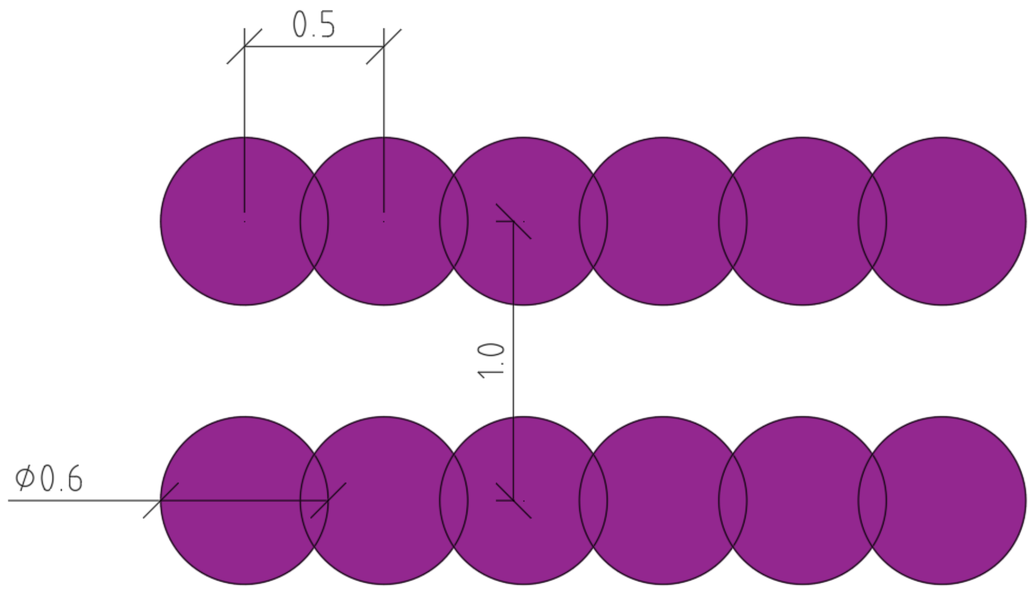

Figure 3.10 Lime-cement column row configuration as a composite material with its corresponding dimensions.

The permeability and the strength- and stiffness parameters of the composite material is derived in accordance with Section 2.4. Remaining material parameters is comprised of characteristic values for lime-cement columns established in Sections 3.4.1 and 3.4.3.

4 Analytical analysis

The analytical analysis of hydraulic bottom-heave is divided into two methodologies to demonstrate different approaches of evaluation. Firstly, an analytical calculation methodology involving partial factors according to Swedish design guidelines, TK GEO 13, is presented. Secondly, a total safety method to determine the factor of safety is introduced.

Additionally, drained and undrained slope stability analyses are conducted in accordance with the direct method (Sällfors, 2013). The purpose of the analytical analyses is to act as a reference point when studying the results obtained from the numerical analyses which incorporate additional effects such as soil deformations, shear mobilization and localization of the slip surface.

4.1 TK GEO 13 method

The equilibrium condition for hydraulic bottom-heave is expressed in accordance with TK GEO 13, see equation 4.1. The favourable load, G_{stb}, and the unfavourable load, G_{kj}, are reduced and increased respectively by partial factors (Trafikverket, 2016a).

$$1.0 \cdot \left(1.1 \cdot \gamma_d \cdot G_{kj}\right) \leq 0.9 \cdot G_{stb} + R \tag{4.1}$$

The partial factor γ_d , depends on the selected safety class of an excavation (Trafikverket, 2016a). For areas of predominantly sensitive or quick clay, safety class 3 should be applied, which constitutes a partial factor γ_d, equal to 1.0. Furthermore, to conservatively determine the factor of safety against hydraulic bottom-heave, the resisting shear force, R, is disregarded. Thus, the equilibrium condition for hydraulic bottom-heave is expressed according to equation 4.2.

$$1.0 \cdot 1.1 \cdot G_{kj} \leq 0.9 \cdot G_{stb} \tag{4.2}$$

Hence, the factor of safety, *FOS*, is formulated as the ratio between the resisting forces, G_{stb}, and the driving forces, G_{kj}, according to equation 4.3 with corresponding partial factors.

$$FOS = \frac{0.9 \cdot G_{stb}}{1.0 \cdot 1.1 \cdot G_{kj}} \tag{4.3}$$

4.2 Total safety method

The total safety method incorporates characteristic values where unfavourable and favourable loads are neither increased nor decreased with partial factors. The total safety method comprises of the ratio between the overburden soil mass and the induced pore pressure in a frictional material layer underlying clay, see equation 4.4 (Sällfors, 2013).

$$FOS = \frac{a \cdot \gamma}{u} \tag{4.4}$$

Where, a, constitutes the depth between the bottom of the excavation and the underlying frictional material, γ, is the saturated unit weight of the clay layer and u, is the pore pressure underneath the clay layer.

4.3 Undrained slope stability

The direct method is a simplified approach to evaluate the factor of safety in undrained conditions and is a function of the slope geometry and characteristic strength values (Sällfors, 2013). The methodology considers additional loads at the top of the slope, q_l, unit weight, γ, and thickness of the soil within the slope, H, water in the excavation expressed in unit weight, γ_w, and the total height of the water body, H_w. Furthermore, correction factors are introduced for additional loads at the top of the slope, μ_q, water in the excavation, μ_w, and the occurrence of cracks in the weathered dry crust, μ_t. The correction factor, P_d, incorporating these aspects is formulated according to equation 4.5 (Sällfors, 2013).

$$P_d = \frac{\gamma \cdot H - \gamma_w \cdot H_w(+q_l)}{\mu_q \cdot \mu_w \cdot \mu_t} \tag{4.5}$$

Thereafter the undrained factor of safety, F_c, is formulated with regards to the undrained shear strength, c_u, the correction factor, P_d, and N_0, which is a function of the slope inclination, β, and the ratio between the distance from the excavation bottom to the frictional material and the height of the slope, see equation 4.6.

$$F_c = N_0 \cdot \frac{c_u}{P_d} \tag{4.6}$$

The Swedish design guidelines state that a minimum allowed factor of safety of 1.65 is required for sites categorized as safety class 3 (Trafikverket, 2016a). The site of the critical cross-section is characterized in safety class 3 due to the occurrence of sensitive and quick clay.

4.4 Drained slope stability

Slope stability analysis with the direct method in drained conditions is more advanced since it requires consideration of an intrinsic groundwater table, H'_w (Sällfors, 2013). Analogously to the undrained slope stability analysis with the direct method, a correction factor, P_e, is introduced, see equation 4.7. Similarly to the determination of P_d, a correction factor, μ'_w, is applied which is determined graphically.

$$P_e = \frac{\gamma \cdot H - \gamma_w \cdot H'_w\ (+q_l)}{\mu'_w} \tag{4.7}$$

Subsequently, the correction factor, P_e, is inserted into the following equation along with the friction angle, ϕ', and the effective cohesion, c', see equation 4.8 (Sällfors, 2013).

$$\lambda_{c\varphi} = \frac{P_e \cdot \tan(\phi')}{c'} \tag{4.8}$$

The factor $\lambda_{c\varphi}$, along with the inclination of the slope, β, yields a stability factor denoted N_{cf}, which is obtained by a graphical solution. Consequently, the drained factor of safety, $F_{c\varphi}$, is then determined by the N_{cf} factor, effective cohesion, c', and the P_d factor, see equation 4.9 (Sällfors, 2013).

$$F_{c\varphi} = N_{cf} \cdot \frac{c'}{P_d} \tag{4.9}$$

As a reference point, the Swedish design guidelines states a minimum allowed drained factor of safety of 1.4 in safety class 3 (Trafikverket, 2016a).

5 Numerical analysis

The numerical analyses are divided into four scenarios to emphasize the differences in constitutive models and the impact of lime-cement columns. In all scenarios, the dry crust and frictional material constitutes of the Mohr-Coulomb model since they are granular materials. Table 5.1 presents a compilation of the constitutive models applied in each scenario.

Table 5.1 Scenarios applied in the numerical analyses of the excavation.

Scenarios				
Scenario	**Dry crust**	**Clay**	**Composite material**	**Frictional material**
Scenario 1	Mohr-Coulomb	Soft soil	-	Mohr-Coulomb
Scenario 2	Mohr-Coulomb	Soft soil	Mohr-Coulomb	Mohr-Coulomb
Scenario 3	Mohr-Coulomb	Soft soil	Hardening Soil	Mohr-Coulomb
Scenario 4	Mohr-Coulomb	NGI-ADP	-	Mohr-Coulomb

5.1 Model configuration

The geometric model in all numerical analyses is based on the critical cross-section as presented in Figure 3.4 and Figure 3.5, Section 3.3. The width of the model is determined to minimize deformations at the vertical boundaries. Upon iteration, the model width is set to 80 metres. Furthermore, symmetry is applied to alleviate the modelling procedure and reduce the computational time. Figure 5.1 presents the model configuration without implementation of lime-cement columns which applies for Scenario 1 and 4.

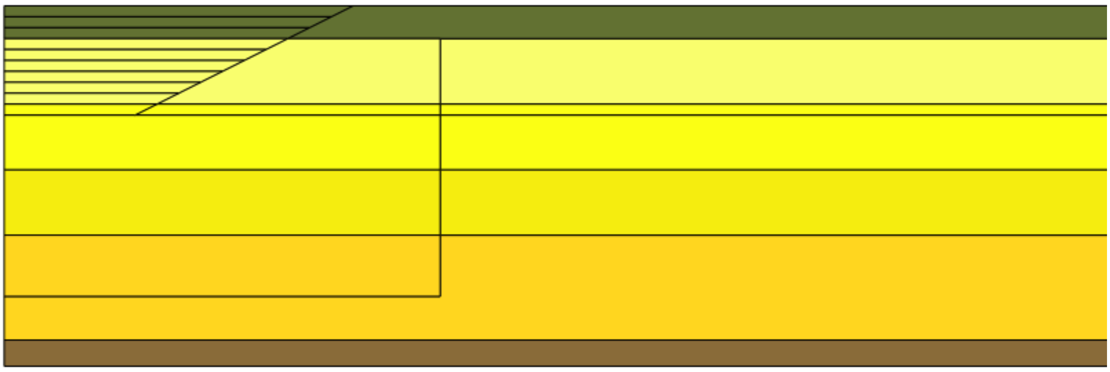

Figure 5.1 Plaxis model configuration without the implementation of lime-cement columns (Scenario 1 and 4).

Figure 5.2 presents the model configuration with implementation of the lime-cement columns which applies for Scenario 2 and 3.

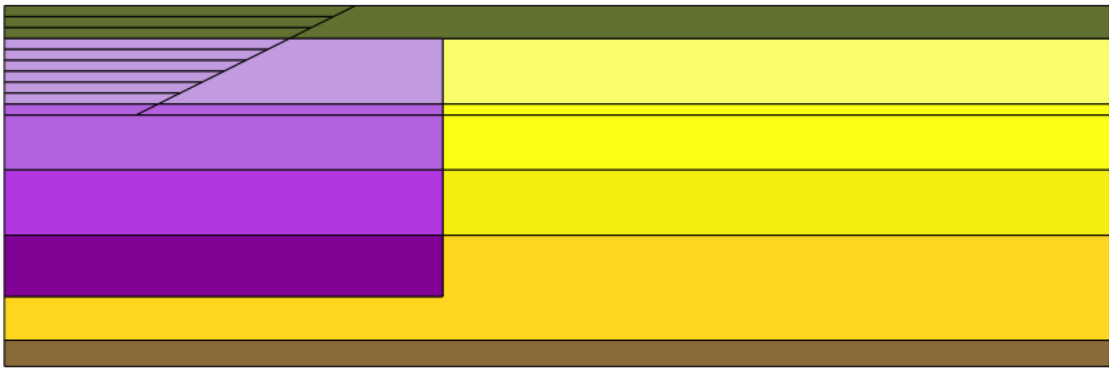

Figure 5.2 Plaxis model configuration with implementation of the lime-cement columns (Scenario 2 and 3).

The excavation is modelled with 15-noded triangular elements. The initial stresses are generated by the K_0-procedure since both the ground surface and groundwater table are horizontal in the initial phase. The excavation is kept dry during all excavation stages. Table 5.2 present the boundary conditions of the model with regards to deformation and groundwater flow.

Table 5.2 Boundary conditions in the numerical model.

Boundary conditions		
Boundary	**Deformations**	**Groundwater flow**
X_{min}	Horizontally fixed	Closed
X_{max}	Horizontally fixed	Open
Y_{min}	Fully fixed	Closed
Y_{max}	Free	Open

The selection of drainage type in the different material sets have a major impact on the results of the numerical analyses. Undrained (A) is selected when both undrained and drained material behaviour is of interest and is applicable to advanced constitutive models which are based on effective strength- and stiffness parameters. Examples of such models are the Soft Soil and Hardening Soil model. Undrained (B) is selected for undrained analyses where a reference undrained shear strength is implemented which restricts the possible shear mobilization. Undrained (B) is adopted for the Mohr-Coulomb constitutive model. In the NGI-ADP model, which is suited for short-term analysis, undrained (C) is adopted with undrained strength- and stiffness parameters. The dry crust and frictional material are modelled as drained due to their high permeability in contrast to the clay and composite material.

The groundwater table is initially set to 1 metre below the ground surface as determined in Section 3.2. The pore pressure is assumed to increase hydrostatically by 10 kPa/m to a depth of 5 metres to allow for infiltration of precipitation and other environmental effects. The artesian pressure of 166 kPa is induced in the frictional material by defining a linear increase of 12.23 kPa/m in pore pressure from a depth of 5 metres to the top of the frictional material at a depth of 15.3 metres. Figure 5.3 illustrates the water conditions of all soil layers at the initial stage of the construction sequence.

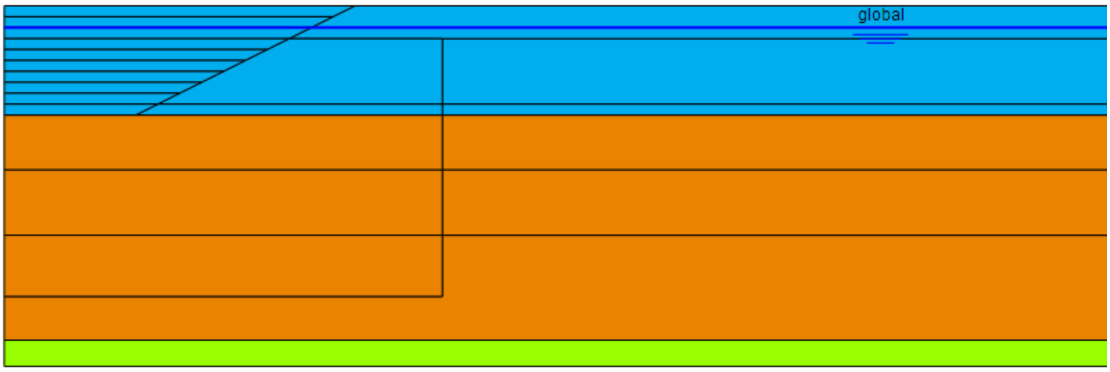

Figure 5.3 *Plaxis model water conditions in the initial phase. Blue corresponds to the global water level (hydrostatic), orange corresponds to interpolation and green corresponds to the user defined artesian pressure.*

Additionally, local lowering of the groundwater table is required in the excavation to allow for an increased stability during the construction stage. To avoid numerical modelling issues and to capture the drawdown behaviour near the excavation more realistically, each lowered groundwater table will follow the principal layout as depicted in Figure 5.4.

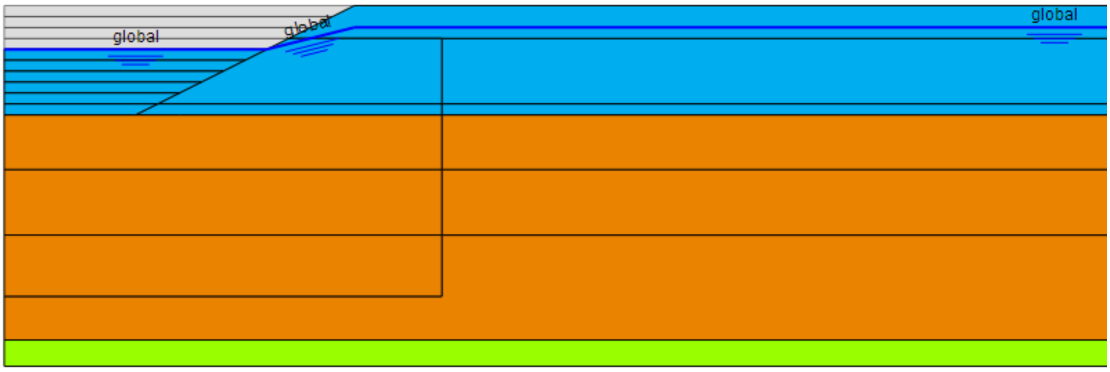

Figure 5.4 *Plaxis model local groundwater lowering conditions at the excavation site for the excavation phase at a depth of 2 metres.*

In long-term analyses the groundwater table is lowered by 1 metre below the excavation bottom to simulate a steady- state groundwater table. Figure 5.5 displays the principal layout of the final long-term consolidation phase which applies to Scenario 1 and 3.

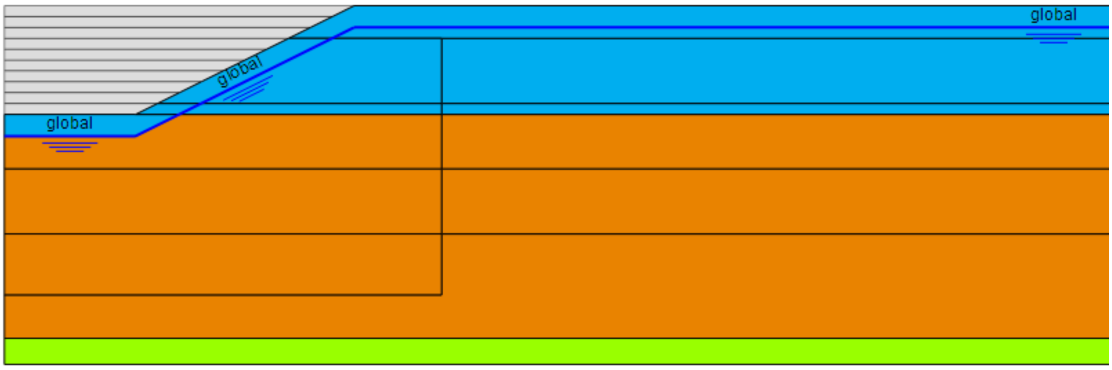

Figure 5.5 *Plaxis model local groundwater lowering conditions at the excavation site for the long-term slope stability analyses.*

The excavation is modelled with a very fine mesh with additional local mesh refinements in the area where the composite material is implemented, see Figure 5.6. Mesh refinement is applied to ensure that the results are accurately captured in proximity to the excavation.

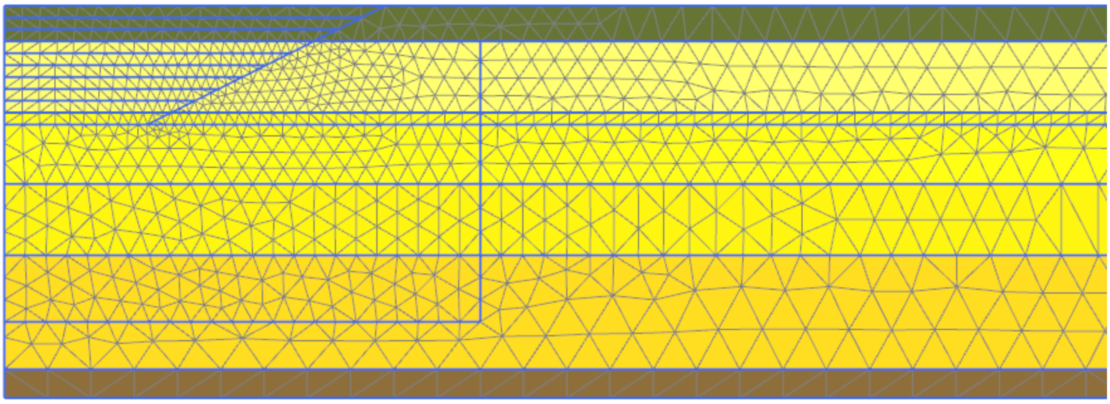

Figure 5.6 *Plaxis model initial mesh corresponding to a very fine mesh with three local mesh refinements in proximity to the excavation.*

To ensure that convergence is fulfilled, a mesh sensitivity analysis is conducted where the long-term factor of safety in Scenario 1 is studied for a varying number of elements, see Figure 5.7. As evident in the figure, convergence is reached at roughly 2 500 elements. Therefore, the very fine mesh with local mesh refinements corresponding to 2 482 elements is applied to all scenarios.

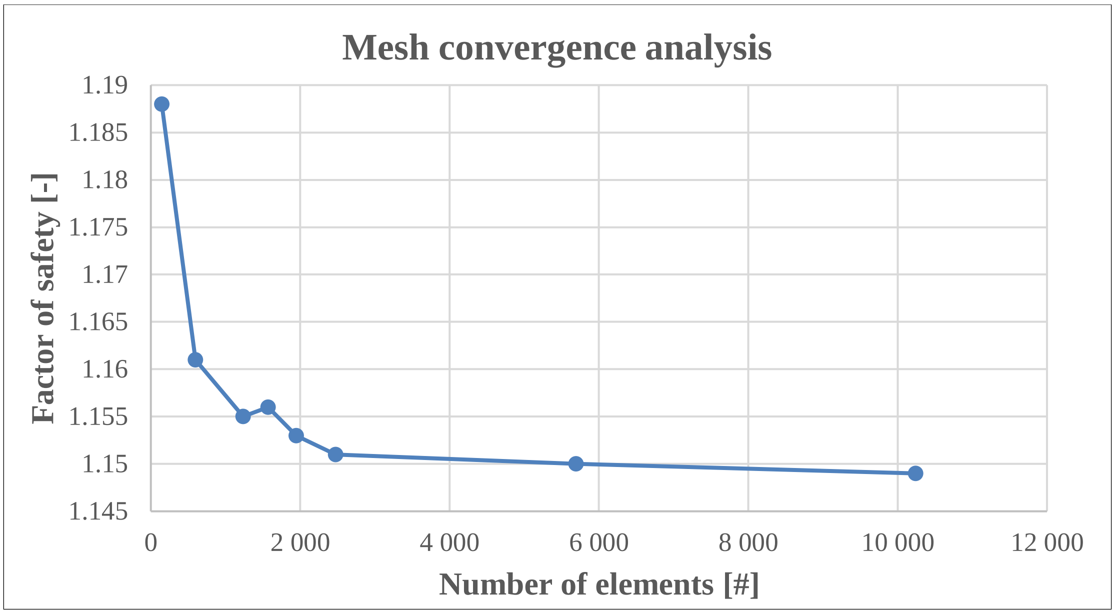

Figure 5.7 Mesh convergence analysis of long-term factor of safety with increasing number of elements.

The excavation is divided into 0.5 metres excavation stages to obtain sufficient slope stability throughout the construction sequence. Each excavation stage constitutes a period of 15 days to allow for some stabilization of negative pore pressures. Following two excavation stages, the groundwater level in the excavation is lowered by 1 metre with a corresponding time of 30 days which subsequently is followed by additional excavation stages. The pattern is repeated until the excavation bottom is reached. In scenarios incorporating the composite material, an installation phase in which the lime-cement columns are wished in place is implemented following the initial phase. A detailed description of the construction stages for each scenario is presented in Table C.1 - Table C.4, Appendix CC.

5.2 Parameter verification

Since the undrained shear strength of clay is an emerging strength property, the undrained shear strength in compression, direct shear and extension requires verification for the Soft Soil model. The input undrained shear strengths of the NGI-ADP model also require verification. Plaxis 2D built-in tool, SoilTest, is applied with the in-situ stress state as depicted in Figure 3.7, Section 3.4. Figure 5.8 illustrates the undrained shear strength as predicted by the Soft Soil and NGI-ADP model in consolidated undrained anisotropic compression, direct shear, and consolidated undrained anisotropic extension.

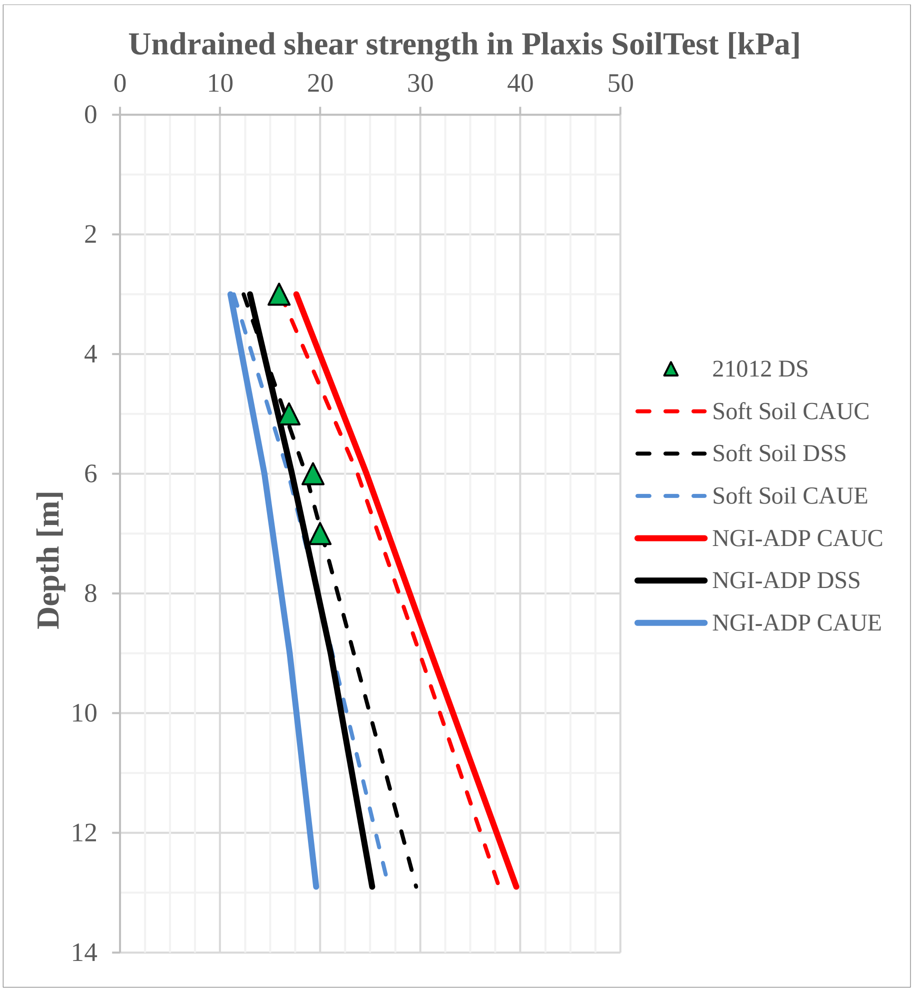

Figure 5.8 Predicted undrained shear strength in Plaxis SoilTest for the Soft Soil and NGI-ADP model.

As evident, the undrained shear strength of the NGI-ADP model generally constitutes a lower value in direct shear and triaxial extension. The slight difference in undrained shear strength is explained by the influence of anisotropy and the application of empirical correlations incorporating the liquid limit, w_L, see equations 3.14 - 3.16, Section 3.4.4.

Furthermore, the predictions of the pre-consolidation pressure, horizontal and vertical stresses in the boundary value problem are verified in the Soft Soil model, see Figure 5.9. The K_0 values are evaluated in accordance with equation 3.2, Section 3.4.

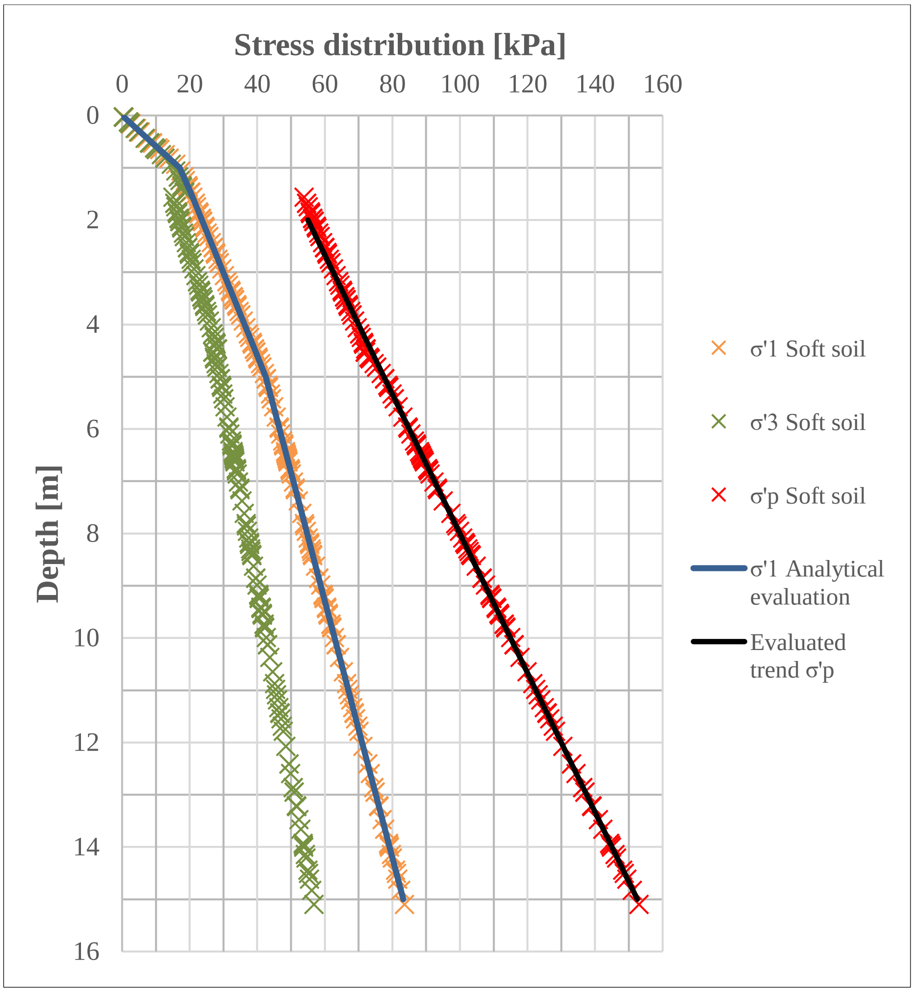

Figure 5.9 Verification of the horizontal and vertical stresses along with the predicted pre-consolidation pressure of the Soft Soil model.

Evidently, the predicted stress state of the Soft Soil model correlates with the analytical evaluation of the effective vertical stresses and pre-consolidation pressure. Thereby, the Soft Soil model predicts a realistic stress state in the initial phase by the K_0-procedure. It should be noted that the input stress state of the NGI-ADP model is verified as well with satisfactory results.

6 Results

In the following chapter, the results of the analytical and numerical analyses are presented separately along with a sensitivity analysis on the model and material input parameters associated with the numerical analyses.

6.1 Analytical analysis

The following sections presents the results of the analytical analyses of hydraulic bottom-heave by the TK GEO 13 method and the total safety method. Further, the results of slope stability evaluation in short- and long-term conditions by the direct method is presented.

6.1.1 TK GEO 13 method

The calculation procedure of the factor of safety, *FOS*, with the TK GEO 13 method is based on Section 4.1. The analysis is conducted for safety class 3 with input parameters established in Sections 3.3 and 3.4.

The unfavourable load, G_{kj}, in the equilibrium of hydraulic bottom-heave is the artesian pore pressure of 166 kPa acting at the top of the frictional material The artesian pore pressure is derived in accordance with equation 6.1 based on the distance between the theoretical artesian groundwater level at 1.3 metres above the ground surface and the top of the frictional material at the depth of 15.3 metres multiplied by the unit weight of water.

$$G_{kj} = 10 \cdot (1.3 + 15.3) = 166 \text{ kPa} \tag{6.1}$$

The favourable load, G_{stb}, affects the equilibrium by the overburden unit weight of the clay, 16.3 kN/m^3. The stabilizing influence is obtained by multiplying the unit weight with the distance between the excavation bottom and the frictional material, see equation 6.2.

$$G_{stb} = 16.3 \cdot (15.3 - 5) = 167.9 \text{ kPa} \tag{6.2}$$

Consequently, the factor of safety, *FOS*, is obtained by the ratio between resisting and driving forces and their corresponding partial coefficients according to equation 6.3.

$$FOS = \frac{0.9 \cdot G_{stb}}{1.0 \cdot 1.1 \cdot G_{kj}} = \frac{0.9 \cdot 167.9}{1.0 \cdot 1.1 \cdot 166} = 0.83 < 1 \tag{6.3}$$

As evident, the equilibrium condition as stated in the Swedish design guidelines is not satisfied and therefore stabilizing measures are required.

6.1.2 Total safety method

Evaluation of the factor of safety, *FOS*, by the total safety method is established in Section 4.2. As previously stated, the total safety method does not incorporate partial coefficients on favourable and unfavourable loads. Therefore, the equilibrium is solely dependent on the favourable load divided by the artesian pore pressure according to equation 6.4.

$$FOS = \frac{167.9}{166} = 1.01 > 1 \tag{6.4}$$

It should be addressed that the total safety approach predicts sufficient resisting forces in comparison to the TK GEO 13 method. Hence, no stabilizing measures are required according to the total safety method, although stability is barely fulfilled.

6.1.3 Undrained slope stability

The result of the undrained slope stability by the direct method as established in Section 4.3 is presented below. Inserting the characteristic values of the critical cross-section yields the following value of the correction factor, P_d, see equation 6.5. Note that no additional loads at the top of the slope, q_l, nor external water loads, $\gamma_w \cdot H_w$, are considered.

$$P_d = \frac{\gamma \cdot H - \gamma_w \cdot H_w(+q_l)}{\mu_q \cdot \mu_w \cdot \mu_t} = \frac{(17 \cdot 1.5 + 16.3 \cdot 3.5)}{1} = 82.6 \text{ kPa} \tag{6.5}$$

By applying the correction factor, P_d, and the inclination of the slope, β, in a graphical solution, the stability factor, N_0, equal to 5.65 is obtained. In order to consider the impact of the dry crust, a weighted undrained shear strength is evaluated according to equation 6.6.

$$c_u = \frac{c_{u,clay} \cdot H_{clay} + c_{u,crust} \cdot H_{crust}}{H_{clay} + H_{crust}} = \frac{(13 \cdot 3 + 16.3 \cdot 0.5) + 18 \cdot 1.5}{5} = 14.8 \text{ kPa} \tag{6.6}$$

Lastly, the undrained factor of safety, F_c, is evaluated according to equation 6.7.

$$F_c = N_0 \cdot \frac{c_u}{P_d} = 5.65 \cdot \frac{14.8}{82.6} = 1.01 \tag{6.7}$$

The resulting undrained factor of safety of 1.01 is significantly lower in comparison to 1.65 as stated in the Swedish design guidelines (Trafikverket, 2016a). Mitigation measures are therefore required to achieve an adequate factor of safety.

6.1.4 Drained slope stability

The result of the drained slope stability analysis by the direct method as established in Section 4.4 is presented below. Firstly, the correction factor, P_e, is determined according to equation 6.8 with no additional loads at the top of the slope. Note that the correction factor of the intrinsic water table, μ'_w, is determined by a graphical solution.

$$P_e = \frac{\gamma \cdot H - \gamma_w \cdot H'_w\ (+q_l)}{\mu'_w} = \frac{(17 \cdot 1.5 + 16.3 \cdot 3.5) - (10 \cdot 4)}{0.97} = 43.9 \text{ kPa} \tag{6.8}$$

Subsequently, the value of P_e is inserted along with the friction angle, ϕ', and the effective cohesion, c'. Analogously to the undrained shear strength, the effective cohesion is weighted with respect to the influencing dry crust. The weighted effective cohesion is calculated according to equation 6.9. Each respective effective cohesion, c'_{clay} and c'_{crust}, is determined according to the Swedish design guidelines, see equation 3.7, Section 3.4.1.

$$c' = \frac{c'_{clay} \cdot H_{clay} + c'_{crust} \cdot H_{crust}}{H_{clay} + H_{crust}} = \frac{(1.3 \cdot 3 + 1.6 \cdot 0.5) + 1.8 \cdot 1.5}{5} = 1.48 \text{ kPa} \quad (6.9)$$

The factor $\lambda_{c\varphi}$, equal to 17.1 along with the inclination of the slope in a graphical solution yields a stability factor in drained conditions, N_{cf}, of 47. By inserting the stability factor, N_{cf}, along with the weighted effective cohesion, c', and the factor P_d, the factor of safety in drained conditions, $F_{c\varphi}$, is obtained, see equation 6.10.

$$F_{c\varphi} = N_{cf} \cdot \frac{c'}{P_d} = 47 \cdot \frac{1.48}{82.6} = 0.84 \quad (6.10)$$

The drained factor of safety of 0.84 is significantly lower than the allowed factor of 1.40 (Trafikverket, 2016a).

6.2 Numerical analysis

The results of the numerical analyses of Scenario 1 - 4, which include the factor of safety, slip surface and the vertical displacements at the bottom of the excavation are presented in the following sections. The progressive build-up and dissipation of negative pore pressures are also presented for Scenario 1 and 3.

6.2.1 Scenario 1

In Scenario 1, which is an analysis implicitly formulated by effective stresses, the build-up and dissipation of negative pore pressures should follow the theory as mentioned in Section 2.1. The excess pore pressures as a function of time are illustrated in Figure 6.1 for the depths 6, 9 and 12.9 metres which corresponds to the centre of clay layer 2, 3 and 4 along the symmetry line. Detailed overviews of the input parameters are presented in Table B.1 and Table B.2**,** Appendix B.

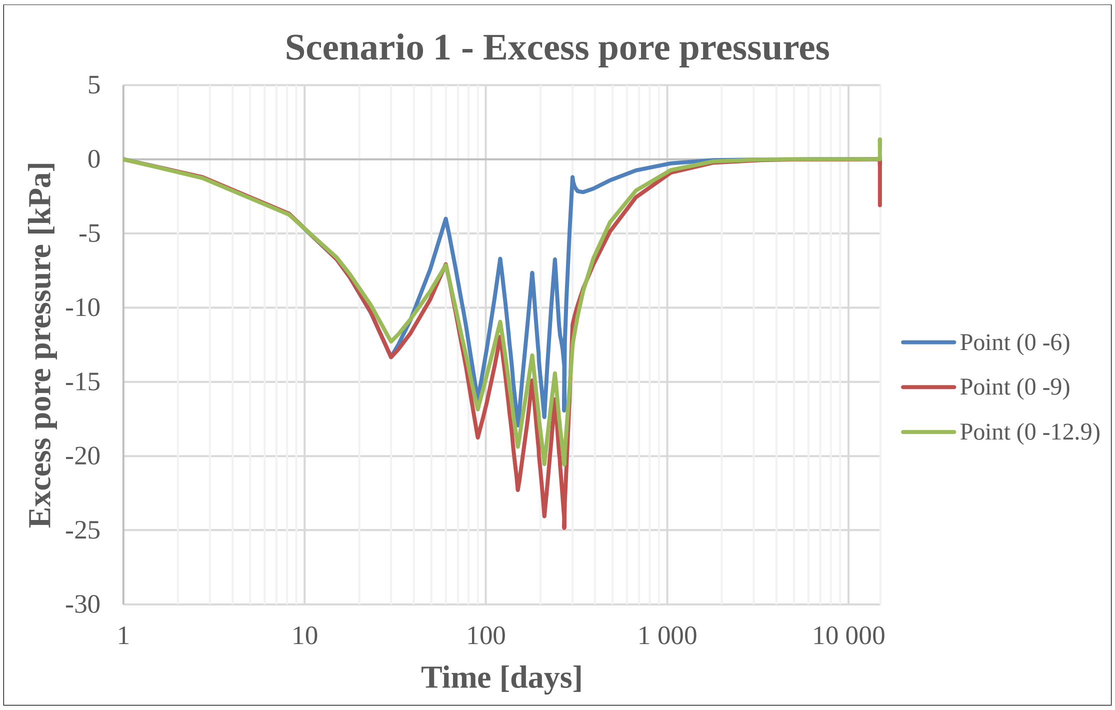

Figure 6.1 Distribution of excess pore pressures as a function of time in logarithmic scale for Scenario 1.

The resulting excess pore pressures is subjected to oscillations caused by the consecutive lowering of the groundwater table in the excavation. As evident in the figure, negative excess pore pressures are generated during the construction sequence of the excavation and dissipates during steady state conditions. The results comply with the theory and is thus considered reasonable.

The short-term factor of safety which is determined by phi-c reduction after the final excavation stage constitutes a value of 1.33. The predicted short-term factor of safety does not satisfy the requirement of 1.65 as mentioned in the Swedish design guidelines. Figure 6.2 illustrates the predicted short-term slip surface in incremental displacements for the phi-c reduction phase.

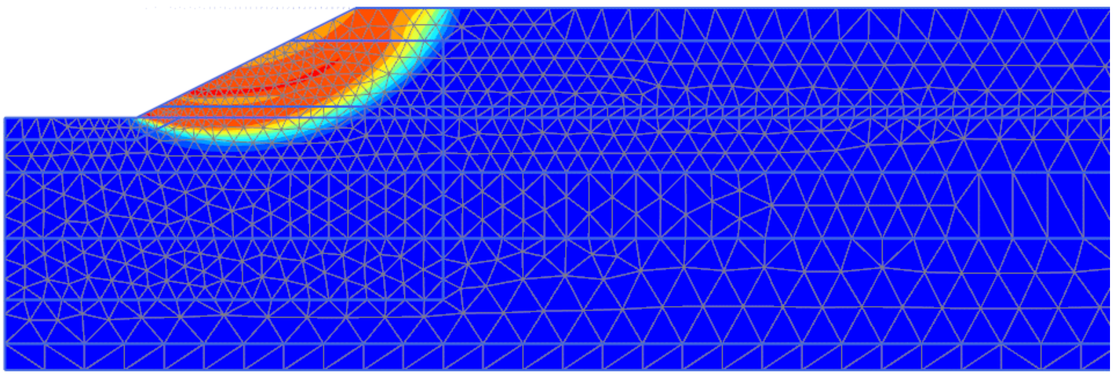

Figure 6.2 Scenario 1 short-term slip surface in incremental displacements for a phi-c reduction.

Furthermore, Figure 6.3 presents the long-term slip surface in incremental displacements for a phi-c reduction after a consolidation period of 40 years. The resulting factor of safety corresponds to a value of 1.15. The factor of safety in long-term conditions is lower in comparison to short-term which complies with the expected behaviour.

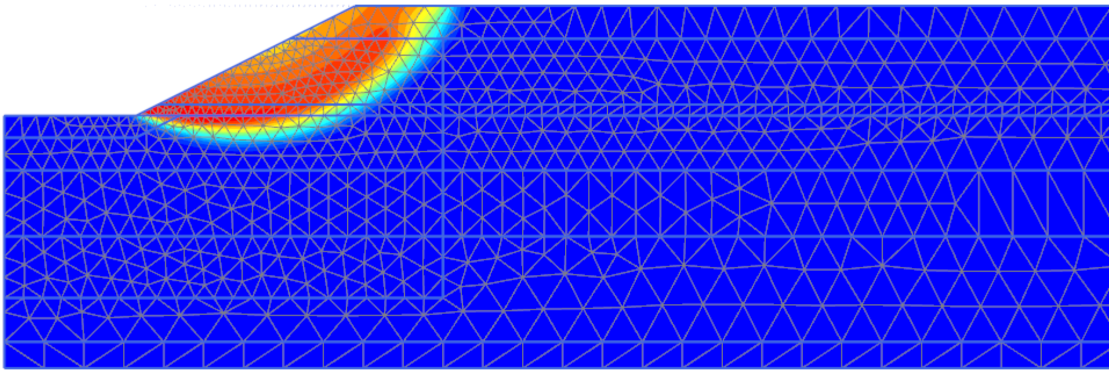

Figure 6.3 Scenario 1 long-term slip surface in incremental displacements for a phi-c reduction.

The predicted heave at the excavation bottom is presented in Figure 6.4 as vertical displacements, u_y, by the distance from the symmetry line. The maximum bottom-heave corresponds to 62.1 mm after the final excavation stage and 80.2 mm after a consolidation period of 40 years.

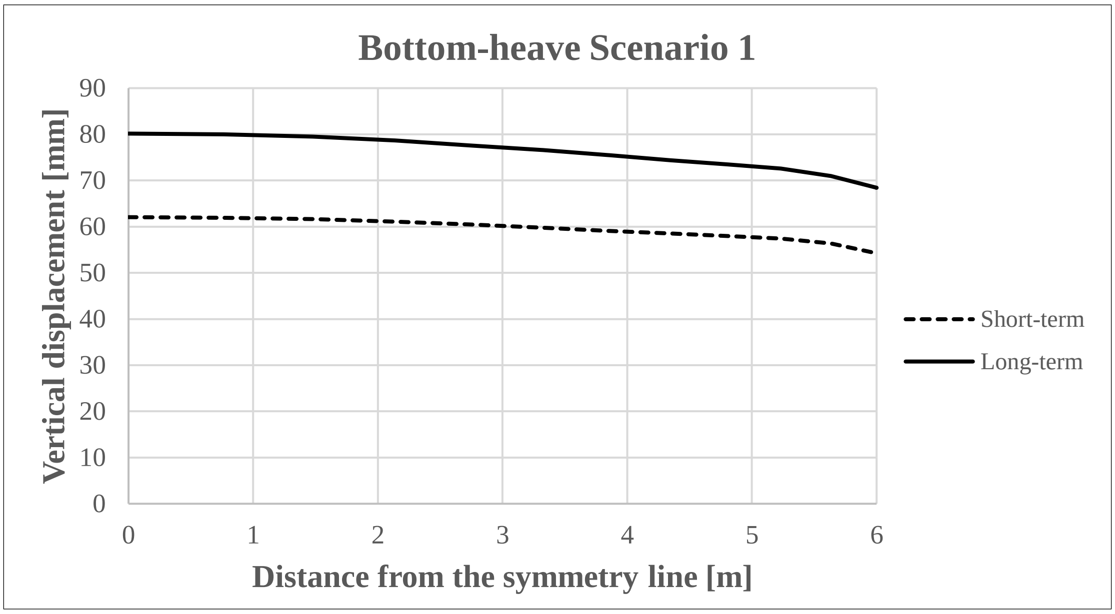

Figure 6.4 Predicted bottom-heave for Scenario 1 in short- and long-term conditions.

6.2.2 Scenario 2

The results of Scenario 2 which introduces lime-cement columns are presented below. The results are based on material input parameters presented in Table B.1 and Table B.3**,** Appendix B**.** As the composite material is modelled with Mohr-Coulomb

Undrained (B), characteristic long-term behaviour of the slope cannot be realistically captured. Therefore, only short-term analysis is of particular interest. The short-term slip surface in incremental displacements for a phi-c reduction after the final excavation stage is illustrated in Figure 6.5. The short-term factor of safety amounts to a value of 2.42.

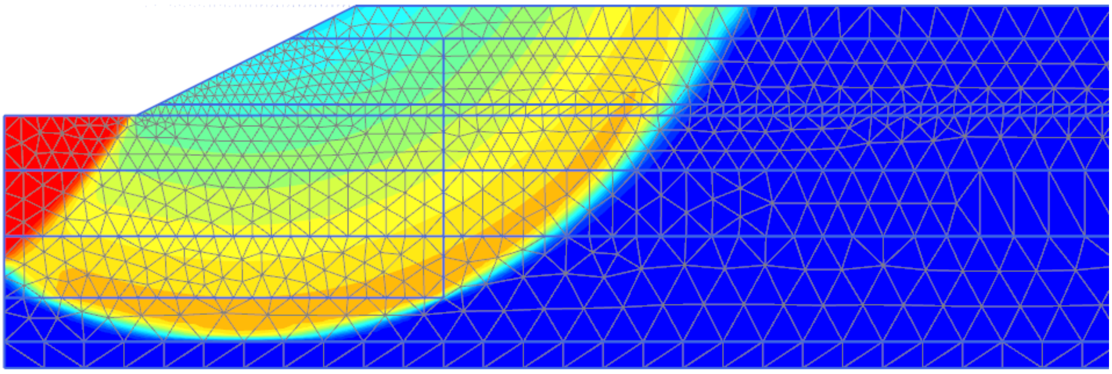

Figure 6.5 Scenario 2 short-term slip surface in incremental displacements for a phi-c reduction.

In comparison to Scenario 1, the slip surface constitutes a significantly different behaviour, extending below the composite material. The global slip surface is caused by the large difference in shear strength between the clay and the implemented composite material. The resulting factor of safety, 2.42, also differ significantly from Scenario 1, highlighting the pronounced stabilizing effect of the lime-cement columns.

The predicted bottom-heave should be lower in contrast to Scenario 1 since the composite material constitutes a higher stiffness. Figure 6.6 visualize the predicted heave at the bottom of the excavation. The maximum vertical displacement constitutes a value of 55.3 mm, which is a slight reduction in comparison to Scenario 1.

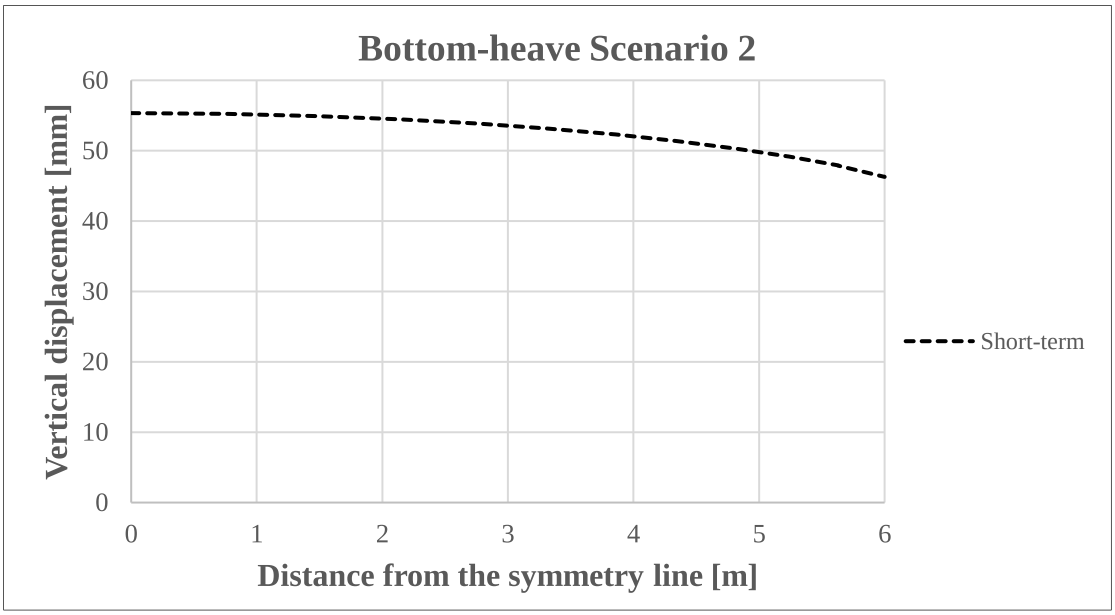

Figure 6.6 Predicted bottom-heave for Scenario 2 in short-term conditions.

Consequently, the implementation of the composite material reduces the predicted bottom-heave. However, the reduction of vertical displacements is minimal in contrast to the increase in factor of safety. The minimal difference in vertical displacements may be explained by the limited formulation of stiffness parameters in the Mohr-Coulomb model.

6.2.3 Scenario 3

Scenario 3 introduces lime-cement columns modelled with the Hardening Soil model. The input parameters of the analysis are presented in Table B.1 and Table B.4, Appendix B. As both the clay and composite material is formulated by effective parameters, the model is able to accurately capture the generation and dissipation of excess pore pressures over time. Figure 6.7 illustrates the successive generation of excess pore pressures as each excavation stage is executed.

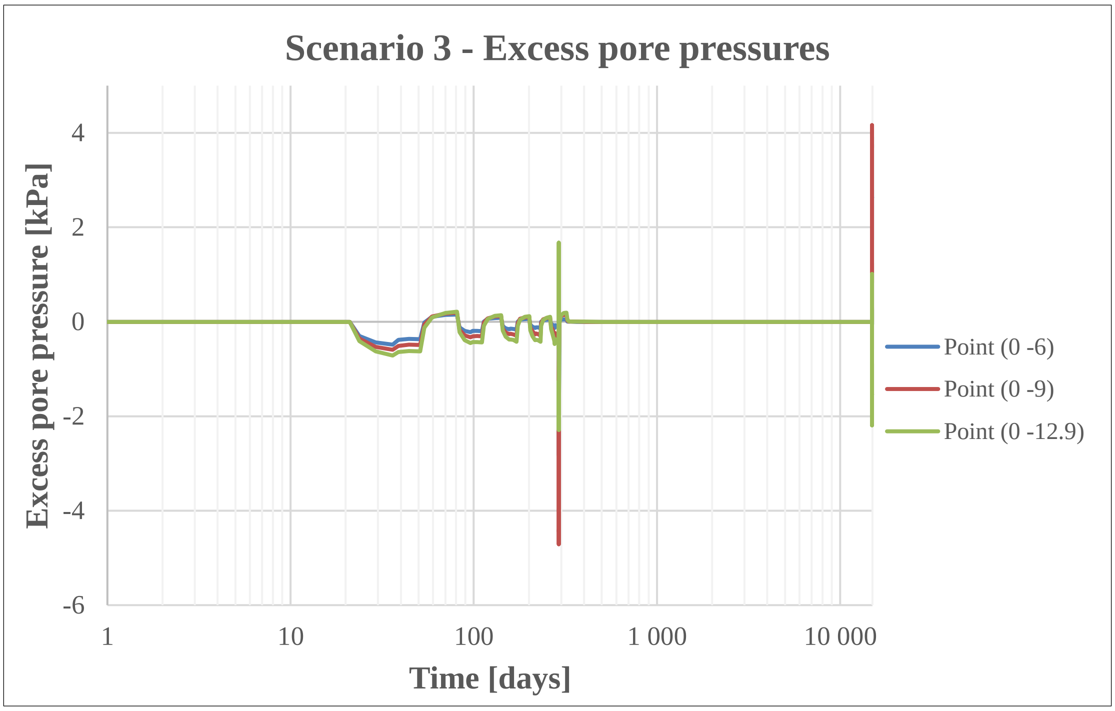

Figure 6.7 Distribution of excess pore pressures as a function of time in logarithmic scale for Scenario 3.

The build-up of negative pore pressures is significantly lower in comparison to Scenario 1, which may be explained by the higher permeability of the composite material. Note that the drastic oscillations at 300 days and 14 600 days are consequences of phi-c reduction phases.

The short-term factor of safety amounts to a value of 1.54. Figure 6.8 presents the resulting short-term slip surface in incremental displacements for a phi-c reduction after the final excavation stage.

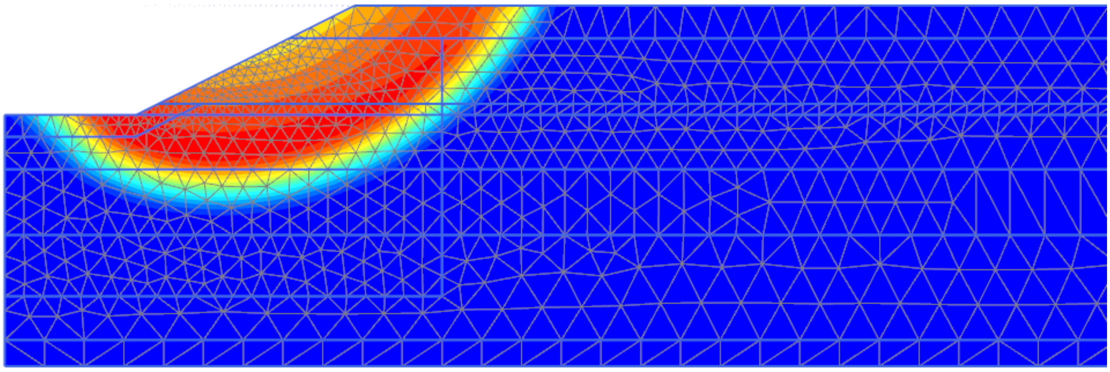

Figure 6.8 Scenario 3 short-term slip surface in incremental displacements for a phi-c reduction.

The resulting short-term factor of safety is significantly lower in comparison to Scenario 2. This might be explained by the conservative selection of drained strength parameters in accordance with the Swedish design guidelines. Furthermore, the location of the slip surface differs considerably in comparison to Scenario 2.

Steady state analysis of the excavation yields a long-term factor of safety equal to 1.69. Figure 6.9 visualize the long-term slip surface in incremental displacements for a phi-c reduction after a consolidation period of 40 years.

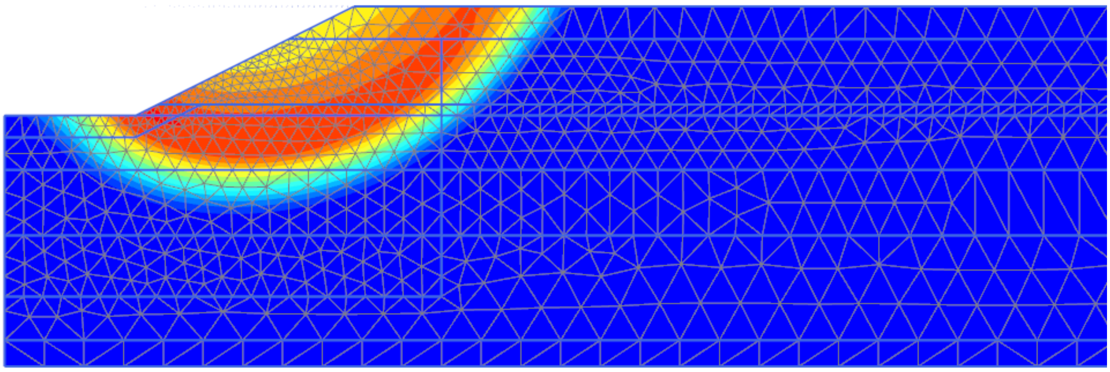

Figure 6.9 Scenario 3 long-term slip surface in incremental displacements for a phi-c reduction.

As evident, the long-term analysis yields favourable results, as it increases the resulting factor of safety from 1.54 to 1.69. This further implies the conservative nature of short-term analysis with the Hardening Soil model.

The maximum vertical displacement amount to 52.6 mm after the final excavation stage and 49.5 mm after a consolidation period of 40 years. Figure 6.10 illustrates the predicted bottom-heave.

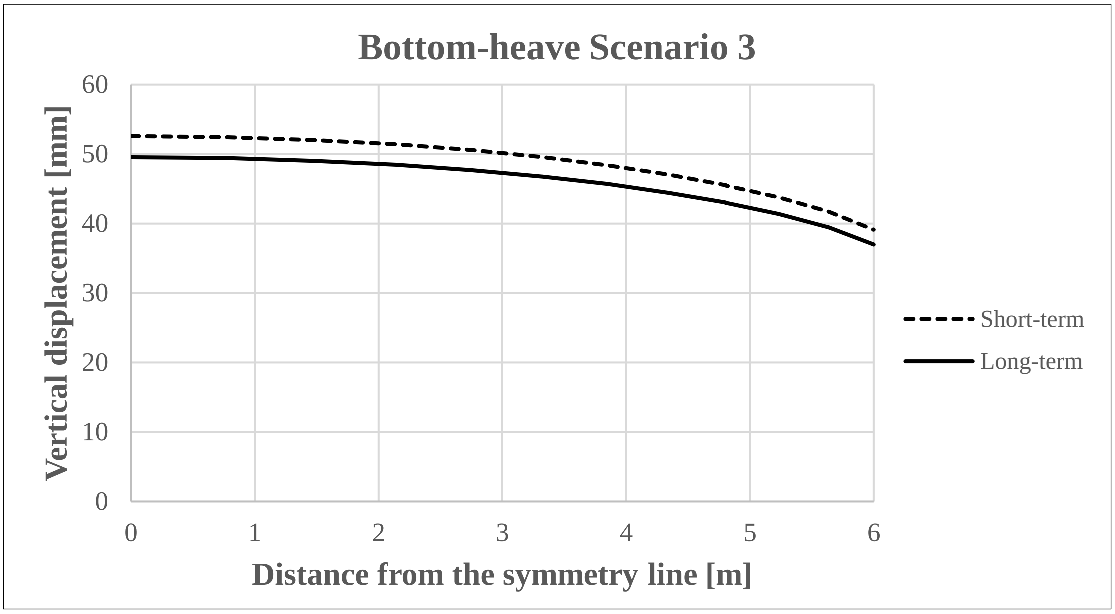

Figure 6.10 Predicted bottom-heave for Scenario 3 in short- and long-term conditions.

The predicted vertical displacements are reduced in Scenario 3 compared to Scenario 2. The combined effect of different stiffness moduli in virgin compression, oedometric- and unloading/reloading stress regimes in the Hardening Soil model are likely contributing to the reduced vertical displacements at the bottom of the excavation.

6.2.4 Scenario 4

Scenario 4, which incorporates the NGI-ADP model formulated by undrained (C) should only be applied for an undrained analysis. The results are based on input data compiled in Table B.1 and Table B.5, Appendix B. Figure 6.11 illustrates the undrained slip surface in incremental displacements for a phi-c reduction after the final excavation stage. The resulting undrained factor of safety amounts to a value of 1.39.

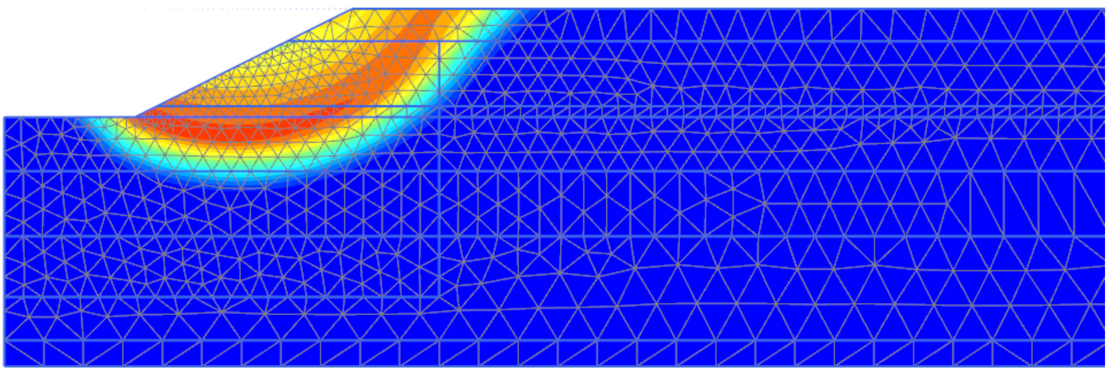

Figure 6.11 Scenario 4 undrained slip surface in incremental displacements for a phi-c reduction.

The predicted undrained factor of safety exceeds the value of 1.33 from Scenario 1. Since Scenario 4 incorporates anisotropy in its formulation, the predicted factor of safety should be lower in comparison to Scenario 1. However, as Scenario 4 does not allow for consolidation, the analysis may be an upper bound solution, overestimating the factor of safety in comparison to Scenario 1. This may be unrealistic, as time-dependent consolidation will have an impact during the construction sequence.

The predicted vertical displacements at the bottom of the excavation in Scenario 4 is visualized in Figure 6.12. The maximum vertical displacement constitutes a value of 42.5 mm.

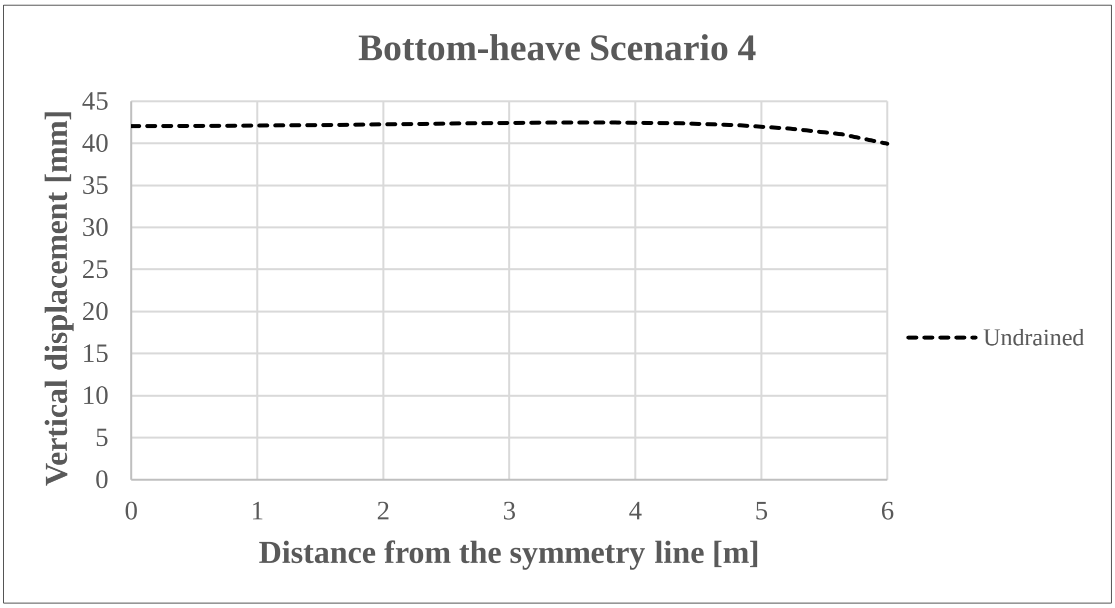

Figure 6.12 Predicted bottom-heave for Scenario 4 in undrained conditions.

The maximum vertical displacement is significantly lower in comparison to remaining scenarios, likely explained by the undrained plastic analysis type. As a result of the time-dependency of Scenario 1, 2 and 3, comparisons between Scenario 4 and the remaining scenarios are erroneous. However, Scenario 4 still implies that mitigation measures are required since the undrained factor of safety from the Swedish design guidelines, 1.65, is not fulfilled.

6.3 Sensitivity analysis

In the following sections, several key input parameters of the numerical model are studied in a sensitivity analysis. The sensitivity analysis constitutes of groundwater conditions, stiffness parameters, strength parameters and the selection of calculation type.

6.3.1 Groundwater conditions

Firstly, the effect of an increased artesian pressure is studied. The sensitivity is studied with regards to the factor of safety, FOS, and maximum vertical displacements, $u_{y,max}$, at the bottom of the excavation. The analysis is conducted with an artesian pressure in the frictional material ranging between 166 kPa, 180 kPa and 190 kPa. The results of the analyses are presented in Table 6.1 and Figure D.1 - Figure D.2, Appendix D. The increase in artesian pressure requires further mesh refinements within the zone of the composite material to achieve adequate convergence.

Table 6.1 Sensitivity analysis of variation in induced artesian pressure within the interval of 166 kPa – 190 kPa conducted in Scenario 1.

Artesian pressure Scenario 1			
Scenario 1	**Short-term**	**Long-term**	**Rate of change (%)**
Original 166 [kPa/m]			
$u_{y,max}$ [mm]	62.1	80.2	-
FOS [-]	1.33	1.15	-
180 [kPa/m]			
$u_{y,max}$ [mm]	69.9	Failure	+ 12.6 % / -
FOS [-]	1.32	Failure	- 0.8 % / -
190 [kPa/m]			
$u_{y,max}$ [mm]	124.6	Failure	+ 100.6 % / -
FOS [-]	1.13	Failure	- 15 % / -

As expected, the factor of safety decreases with an increasing artesian pressure which is a result of the reduction in vertical effective stresses. Furthermore, the vertical displacements, u_y, increases as the artesian pressure is amplified. In the interval of 180 – 190 kPa, a transition from a local stability slip surface into a global slip surface occurs because of the emerging artesian pressure, see Figure D.1 - Figure D.2, Appendix D.

An increase in artesian pressure of 166 kPa, 180 kPa and 190 kPa is also applied in Scenario 2 to facilitate a direct comparison with Scenario 1. The factor of safety and maximum vertical displacement are presented in Table 6.2 and in Figure D.3 – Figure D.4, Appendix D.

Table 6.2 Sensitivity analysis of variation in induced artesian pressure within the interval of 166 kPa – 190 kPa conducted in Scenario 2.

Artesian pressure Scenario 2		
Scenario 2	**Short-term**	**Rate of change (%)**
Original 166 [kPa/m]		
$u_{y,max}$ [mm]	55.3	-
FOS [-]	2.42	-
180 [kPa/m]		
$u_{y,max}$ [mm]	61.7	+ 11.6 %
FOS [-]	2.16	- 10.7 %
190 [kPa/m]		
$u_{y,max}$ [mm]	91.5	+ 65.5 %
FOS [-]	1.92	- 20.7 %

Similarly to Scenario 1, the factor of safety decreases with an increase in artesian pressure. The deformations also increase although the rate of change is lower in comparison to Scenario 1, most notable in the interval of 180 - 190 kPa. This implies that the composite material reduces the deformations at the excavation bottom as the artesian pressure is increased. Additionally, the factor of safety obtained with 190 kPa of artesian pressure exceeds the design guidelines as presented in TK GEO 13 for undrained slope stability. Therefore, the composite material acts as a satisfactory mitigation measure.

Secondly, the sensitivity of the groundwater table in steady state conditions is studied between depths of 5.5 metres and 7 metres. The groundwater table is altered in both Scenario 1 and 3 since they are applicable as long-term simulations. Table 6.3 presents the results of the groundwater table sensitivity analysis.

Table 6.3 Sensitivity analysis of variation in depth of the steady state groundwater table within the interval of 5.5 metres – 7 metres conducted in Scenario 1 and 3.

Groundwater table			
	Scenario 1 Long-term	**Scenario 3 Long-term**	**Rate of change (%)**
Original 6 [m] GW-table			
$u_{y,max}$ [mm]	80.2	49.5	-
FOS [-]	1.15	1.69	-
5.5 [m] GW-table			
$u_{y,max}$ [mm]	(3484)	51.3	(+ 4244 %) / + 3.4 %
FOS [-]	1.00	1.61	- 13 % / - 4.7 %
7 [m] GW-table			
$u_{y,max}$ [mm]	66.6	46.7	- 17 % / - 5.7 %
FOS [-]	1.22	1.81	+ 6.1 % / + 7.1 %

As evident, the groundwater table in steady state analysis significantly influence the stability of the excavation. As failure occur at a groundwater level of 5.5 metres, a steady state groundwater level equal to or below 6 metres is required to obtain sufficient long-term stability.

6.3.2 Stiffness parameters

Furthermore, the sensitivity of stiffness parameters in a local area at the bottom of the excavation is studied. The influence area constitutes the width of the excavation and a depth of 1 metre below the excavation bottom. Variation in the modified swelling index, κ^*, by a factor of 2 – 5 is applied within the influence area. The results of the sensitivity analysis are presented in Table 6.4.

Table 6.4 Sensitivity analysis of a local increase in stiffness by a factor 2 – 5 within the influence area conducted in Scenario 1.

Influence of modified swelling index, κ^*			
Scenario 1	**Short-term**	**Long-term**	**Rate of change (%)**
Original κ^*			
$u_{y,max}$ [mm]	62.1	80.2	-
FOS [-]	1.33	1.15	-
$\boldsymbol{\kappa^*/2}$			
$u_{y,max}$ [mm]	60	76.6	- 3.4 % / - 4.5 %
FOS [-]	1.34	1.15	+ 0.8 % / -
$\boldsymbol{\kappa^*/5}$			
$u_{y,max}$ [mm]	59.5	74.6	-4.2 % / - 7 %
FOS [-]	1.35	1.15	+ 1.5 % / -

The results indicate that the variation in modified swelling index within the influence area yields a negligible increase in factor of safety and a slight decrease in the maximum vertical displacement at the excavation bottom.

Additionally, a similar procedure is performed in Scenario 2 where the drained Young's modulus, E', of the lime-cement columns is increased by a factor of 2 – 5 within the established influence area. The results of the analysis are presented in Table 6.5.

Table 6.5 Sensitivity analysis of a local increase in drained Young's modulus by a factor of 2 – 5 of the lime-cement columns within the influence area conducted in Scenario 2.

Influence of drained Young's modulus, E'		
Scenario 2	**Short-term**	**Rate of change (%)**
Original E'		
$u_{y,max}$ [mm]	55.3	-
FOS [-]	2.42	-
$\boldsymbol{2 \cdot E'}$		
$u_{y,max}$ [mm]	54.0	- 2.4 %
FOS [-]	2.42	-
$\boldsymbol{5 \cdot E'}$		
$u_{y,max}$ [mm]	53.3	- 3.6 %
FOS [-]	2.42	-

The increase in drained Young's modulus yields minimal differences in maximum vertical displacement at the excavation bottom. The predicted factor of safety is unaffected. It should be noted that the assumed influence area could be under- or overestimated which affects the accuracy of the results.

A sensitivity analysis of Scenario 4 is also performed to highlight the impact of the selected stiffness parameters in an undrained model, see Table 6.6. The ratio of unloading/reloading shear modulus over plane-strain active shear strength, G_{ur}/s_u^A, is set to a constant value of 200 causing a stiffer material response. Moreover, the shear strain at failure in triaxial compression, γ_f^C, triaxial extension, γ_f^E, and direct simple shear, γ_f^{DSS}, are altered to 5 %, 7 % and 6 % respectively to allow for larger strain mobilization.

Table 6.6 Sensitivity analysis of an increase in NGI-ADP stiffness parameters conducted in Scenario 4.

Influence of G_{ur}/s_u^A and γ_f^C, γ_f^E, γ_f^{DSS}		
Scenario 4	**Short-term**	**Rate of change (%)**
Original G_{ur}/s_u^A and γ_f^C, γ_f^E, γ_f^{DSS}		
$u_{y,max}$ [mm]	42.5	-
FOS [-]	1.39	-
G_{ur}/s_u^A = 200 and original γ_f^C, γ_f^E, γ_f^{DSS}		
$u_{y,max}$ [mm]	24.4	- 42.6 %
FOS [-]	1.39	-
Original G_{ur}/s_u^A and $\gamma_f^C = 5$ %, $\gamma_f^E = 7$ %, $\gamma_f^{DSS} = 6$ %		
$u_{y,max}$ [mm]	49.2	+ 15.8 %
FOS [-]	1.38	- 0.7 %

As expected, the results indicate that a stiffer material response will yield lower deformations and an allowance of larger shear strains will yield the opposite. The influence on the factor of safety is negligible and thus not a point of concern.

6.3.3 Strength parameters

The sensitivity of the assumed effective cohesion of the dry crust is studied with a variation between 2 – 10 kPa. The variation in effective cohesion yields negligible differences in the predicted factor of safety and thus, it can be concluded that the initially assumed value of 10 kPa is valid for the numerical analyses. A low value of the effective cohesion yields unrealistic slip surfaces in the dry crust in Scenario 2 which further motivates the applied value of 10 kPa in the numerical analyses.

A variation in the reference undrained shear strength, $s_{u,ref}$, of the composite material is studied in Scenario 2, where an increase and decrease of 30 % is applied. The results of the analysis are presented in Table 6.7.

Table 6.7 Sensitivity analysis of an increase and decrease in the undrained shear strength of the lime-cement columns conducted in Scenario 2.

Influence of reference undrained shear strength, $s_{u.ref}$		
Scenario 2	**Short-term**	**Rate of change (%)**
Original $s_{u,ref}$		
$u_{y,max}$ [mm]	55.3	-
FOS [-]	2.42	-
30 % decrease $s_{u,ref}$		
$u_{y,max}$ [mm]	55.3	-
FOS [-]	2.08	- 14 %
30 % increase $s_{u,ref}$		
$u_{y,max}$ [mm]	55.3	-
FOS [-]	2.75	+ 13.6 %

The variation by 30 % in reference undrained shear strength yields a difference of roughly 14 % in the factor of safety. However, variations of 30 % in undrained shear strength are unrealistic. It should be noted that the predicted maximum vertical displacement is unaffected.

Additionally, variation in the effective cohesion, c', of the composite material with the Hardening Soil model is studied. The analysis is conducted based on Karlsrud et al., (2015) statement regarding the conservative selection of critical shear strength of lime-cement columns. In Sweden, the critical shear strength of lime-cement columns is limited to 100 kPa according to the Swedish design guidelines. The effects of an increase in critical shear strength by a factor of 3 and 6 is studied with regards to the effective cohesion. The effective cohesion is evaluated in accordance with the Swedish design guidelines, see equation 3.8, Section 3.4.1. The sensitivity analysis investigates the impact of varying the effective cohesion on the resulting factor of safety and maximum vertical displacement. The results of the sensitivity analysis are presented in Table 6.8.

Table 6.8 *Sensitivity analysis of an increase in the effective cohesion of the lime-cement columns conducted in Scenario 3.*

Influence of effective cohesion			
Scenario 3	**Short-term**	**Long-term**	**Rate of change (%)**
Original $\boldsymbol{c'}$			
$u_{y,max}$ [mm]	52.6	49.5	-
FOS [-]	1.54	1.69	-
$\boldsymbol{c' = 0.15 \cdot (3 \cdot c_{crit})}$			
$u_{y,max}$ [mm]	35.8	33.8	- 31.9 % / -31.7 %
FOS [-]	2.11	2.19	+ 37.0 % / + 29.6 %
$\boldsymbol{c' = 0.15 \cdot (6 \cdot c_{crit})}$			
$u_{y,max}$ [mm]	31.5	29.9	- 40.1 % / - 39.6 %
FOS [-]	2.57	2.65	+ 66.9 % / + 56.8 %

The results indicate a significant increase in the factor of safety and a decrease in the maximum vertical displacement at the excavation bottom with an increase in effective cohesion, c', in the composite material. Furthermore, by applying a large effective cohesion, c', the resulting factor of safety converges towards the Mohr-Coulomb solution, which suggests that the initially assumed cohesion is overly conservative according to the design guideline from TK GEO 13.

6.3.4 Calculation type

To study the effects on the selection of calculation type, a sensitivity analysis with variation in the consolidation period and calculation type is performed. The sensitivity analysis is conducted in Scenario 1. The results of the analysis are presented in Table 6.9**.**

Table 6.9 Sensitivity analysis of the influence of calculation type with a variation between consolidation and plastic analysis and variation in the consolidation period conducted in Scenario 1.

Influence of calculation type			
Scenario 1	**Short-term**	**Long-term**	**Rate of change (%)**
Original calculation type			
$u_{y,max}$ [mm]	62.1	80.2	-
FOS [-]	1.33	1.15	-
Plastic calculation type			
$u_{y,max}$ [mm]	31.1	-	- 49.9 % / -
FOS [-]	1.56	-	+ 17.3 % / -
Consolidation calculation type (2*days during construction)			
$u_{y,max}$ [mm]	73.1	83	+ 17.7 % / + 3.5 %
FOS [-]	1.23	1.11	- 7.5 % / - 3.5 %

As evident, the calculation type significantly influences the predicted factor of safety and the resulting maximum vertical displacement at the excavation bottom. The results partly explain the discrepancies between Scenario 1 and 4 and emphasises the importance of selecting an appropriate construction schedule and calculation type.

7 Discussion

In the following chapter, the results of the analytical and numerical analyses are discussed in detail. Furthermore, sources of errors are presented along with recommendations for further studies.

7.1 Analytical and numerical analyses

The analytical and numerical analyses of the excavation provided several topics of discussion. Firstly, the time investment required to perform each respective analysis differentiated monumentally. The numerical analyses require both an in-depth material parameter derivation and the consideration of aspects involving e.g., construction sequence and fluctuating groundwater conditions. Additionally, the set-up of a reliable numerical model is critical and thorough investigation of output parameters is necessary to ensure realistic and trustworthy results. In comparison, the analytical analyses, both with regards to failure caused by hydraulic bottom-heave and slope stability, require significantly less time and effort, but might seem overly simplified. However, the analytical analyses provide an early-stage estimation of the limit equilibrium of an excavation and could consequently be of guidance in numerical modelling. The analytical analyses will also indicate whether a detailed numerical analysis is necessary to perform. The results of the analytical analyses are summarized and presented in Table 7.1.

Table 7.1 Resulting factor of safety for each conducted analytical analysis.

Analytical analyses	
	Factor of safety, *FOS* [-]
Hydraulic bottom-heave	
TK GEO 13 method	0.83
Total safety method	1.01
Slope stability	
Undrained slope stability	1.01
Drained slope stability	0.84

The analytical analyses indicate that mitigation measures are required to achieve a satisfactory factor of safety in short- and long-term conditions. Consequently, the analytical analyses emphasise the need for detailed numerical analyses to both capture the complex nature of the excavation and to evaluate the suitability of a mitigation measure. A compiled table of the resulting factor of safety and vertical displacement of the numerical analyses is presented in Table 7.2.

Table 7.2 Resulting factor of safety and maximum vertical displacement for each conducted numerical analysis.

Numerical analyses		
	Factor of safety, *FOS* [-]	**Vertical displacement, $u_{y,max}$ [mm]**
Scenario 1		
Short-term	1.33	62.1
Long-term	1.15	80.2
Scenario 2		
Short-term	2.42	55.3
Long-term	-	-
Scenario 3		
Short-term	1.54	52.6
Long-term	1.69	49.5
Scenario 4		
Undrained	1.39	42.5
Long-term	-	-

Similarly to the analytical analyses, numerical analyses of the excavation without lime-cement column implementation indicate that mitigation measures are necessary to reach an adequate factor of safety. Implementation of lime-cement columns, specifically in Scenario 2, yield satisfactory results with regards to slope stability since the factor of safety exceeds 1.65 as stated in the Swedish design guidelines. Evidently, the lime-cement columns also mitigate the risk of hydraulic bottom-heave failure in the numerical analyses but cannot be accounted for within the current design guidelines. As established in Section 4.1, TK GEO 13 only considers the resisting forces by the overburden soil mass and thus, solely mitigation measures which increase the overburden weight are applicable, e.g., installation of a road.

The discrepancies in the results of the numerical analyses compared to the analytical analyses are explained by several factors. Firstly, the effective cohesion in the dry crust is different in the analytical and numerical analyses. A higher effective cohesion was necessary in the numerical analyses to avoid generation of unrealistic slip surfaces. Moreover, the numerical analyses consider additional effects such as the influence of OCR, stiffnesses, permeability, anisotropy and horizontal stresses. The combined influence of these factors contributes to the different predictions of the factor of safety in the numerical and analytical methodologies. Also, the analytical methodology consists of an idealized solution whereas the numerical analyses aim to realistically replicate the physical response of the excavation.

Furthermore, significant variation in the results of the numerical analyses are evident. Scenario 2 which is formulated by effective stiffness parameters and undrained strength parameters deviate from the short-term factor of safety as presented in Scenario 3. The low factor of safety in Scenario 3 is a result of the conservative evaluation of the effective cohesion in the Swedish design guidelines. This is evident from the sensitivity analysis regarding the effective cohesion, see Table 6.8, Section 6.3.3. Furthermore, the conservatively applied values of effective cohesion between 8.4 - 9.1 kPa in Scenario 3 are significantly lower in comparison to values in the passive zone from triaxial testing as reported in literature. However, it should be addressed that the excavation in this thesis includes areas with an active, direct shear and passive zone. To obtain reliable results from Scenario 3, drained triaxial testing is of essence in both compression and extension. If no triaxial tests are performed, the conservative guidelines applied in Scenario 3 may be altered to the use of zero friction angle and an effective cohesion equal to the undrained shear strength obtained from unconfined compression tests. However, such a simplification is only valid for short-term analyses, i.e., to describe an undrained response. Thus, the Hardening Soil model in Scenario 3 may be simplified to a Mohr-Coulomb model with different stiffnesses depending on the stress regime.

Although the factor of safety differs significantly between Scenario 2 and 3, the predicted deformations at the excavation bottom were similar. By comparing the secant stiffness modulus as applied in Scenario 2 and 3, displayed in Figure 7.1, it is noted that the stiffnesses are correlating. The deformations in Scenario 2 approaches Scenario 3 when applying an unloading/reloading stiffness in Scenario 2, as presented in the sensitivity analysis, see Table 6.5, Section 6.3.2. This further emphasizes an appropriate use of stiffness moduli depending on the considered stress regime.

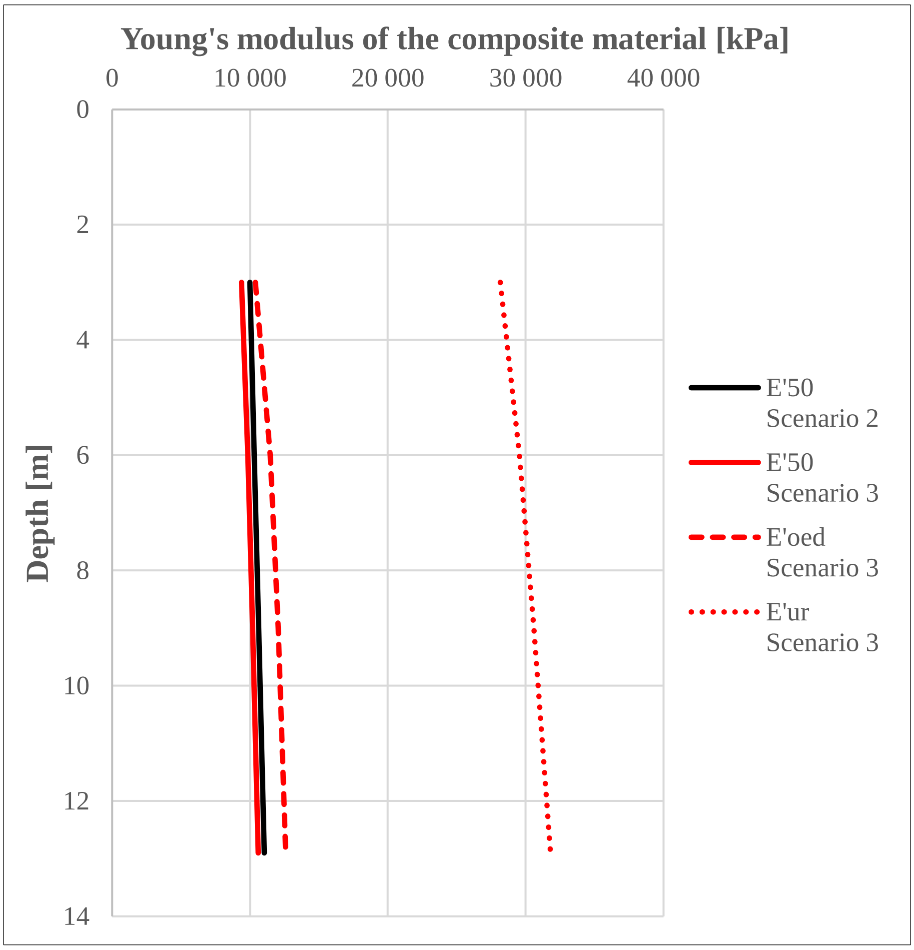

Figure 7.1 Differences in stiffness moduli of the composite material for Scenario 2 and 3.

7.2 Sources of error

Several input parameters to the performed analyses, both analytically and numerically, are derived from empirical correlations in accordance with the Swedish design guidelines. The effective cohesion and friction angle of the material sets require triaxial testing to verify the parameters as their in-situ values may diverge from the values suggested by the guidelines. Further, correlations for several stiffness parameters are applied to Scenario 3 from a case study in Enköping with similar soil conditions. Such correlations are necessary to assemble enough input data for the numerical analyses.

Moreover, the performed boreholes near the critical cross-section resemble a small proportion of the total soil volume available for testing. Therefore, certain key material parameters may be falsely determined from misrepresentative data. To bridge this issue, statistical Monte Carlo simulations may be performed to minimize the risk of outliers. An alternative and more expensive approach is to execute further in-situ testing.

The long-term solution of Scenario 3 is dependent on the steady state conditions of the groundwater table, see Table 6.3, Section 6.3.1. The applied steady state solution of the groundwater table at a depth of 6 metres were selected to obtain sufficient vertical distance from the planned road. Also, the sequential groundwater drawdown may not fully represent the field conditions. Therefore, a representative steady- state solution and drawdown are subjects for further verification with pore pressure measurements. Additionally, the hydrostatic pore pressure to a depth of 5 metres may be falsely assumed and is a subject for further validation.

3D effects are not explicitly incorporated in the analyses since they are performed in Plaxis 2D in plane-strain conditions. The assumption of plane-strain implies that the critical cross-section is applied to a large extent in an out-of-plane direction. The critical cross-section is therefore an idealized 2D solution which may differ from a solution in 3D. However, as presented in the thesis, the shortage of input data in the 2D analyses were significant. By resorting to 3D analyses additional parameters would need empirical correlations, which would further impugn the validity of the analyses.

7.3 Recommendations & further studies

Due to the time limit of the thesis, some subjects have been delimited and therefore require further studies. Execution of triaxial testing in compression and extension is of essence to verify the results presented in the thesis. By performing an accurate triaxial testing programme, advanced constitutive models such as Soft Soil Creep or Creep-SCLAY1S may be adopted. The long-term predictions of the vertical displacements at the excavation bottom in the clay will likely be more accurate with advanced models. Regarding the lime-cement columns, the selection of the drained parameters in the Hardening Soil model should be further investigated since the column strength develops over time.

Installation methods and its overall effects were not incorporated in the numerical analyses. Possible topics may include an altered composition of the lime-cement columns, influence of overlap zones, effect of organic content, exothermic reactions during installation, curing time and varying permeability as the column strength is developing. Further, other column type configurations such as variation in centre- to centre spacing, row distance and diameter of the lime-cement columns may be studied. Such a study may conclude when the block effect of the columns is lost, i.e., when the load is carried by a pile type behaviour. There is also a possibility to resort to Plaxis 3D with sufficient input parameters.

Additionally, the predicted pore pressures and displacements from the numerical models should be verified with measurements in the area. The selected undrained shear strength of the lime-cement columns also require verification in the field as stated in the Swedish design guidelines, TK GEO 13.

Finally, possible climate effects on the predicted deformations and factor of safety should be considered. The influence of prolonged heavy rainfall and its impact on the groundwater levels should not be ignored. Also, its long-term effect on the artesian pressure may be a subject for further studies.

8 Conclusions

The thesis sought out to highlight the differences between analytical and numerical determination of hydraulic bottom-heave and to establish if and how lime-cement columns could provide stability against hydraulic bottom-heave failure. Conclusively, the result of the thesis suggests that the analytical analysis should serve as a first order estimate and could consequently indicate whether advanced numerical modelling is required. The results of the analytical and numerical analyses indicate that mitigation measures are required in Hasslerör, which demonstrates the applicability of both methodologies.

Furthermore, the thesis establishes the uncertainties of numerical modelling with regards to the selection of input parameters, model configuration and constitutive models. The discrepancies in the results of the numerical analyses emphasise the importance of representative input data and accumulated knowledge of the practising geotechnical engineer. Before conducting numerical analyses, triaxial testing is of essence to produce accurate predictions. Moreover, a representative characterisation of the groundwater conditions and its time-dependent response requires consideration. Altogether, a detailed investigation programme and adequate knowledge of the engineer are crucial factors when resorting to numerical analyses.

The numerical analyses imply that lime-cement columns increase overall stability of the excavation and reduces the risk of hydraulic bottom-heave. However, the current Swedish design guidelines have been proven to be conservative regarding the selection of drained strength parameters for lime-cement columns in excavation stress regimes. Additionally, the design guidelines of hydraulic bottom-heave only accounts for the overburden soil mass as a resisting force. Therefore, the favourable effects of lime-cement columns are not incorporated within the current guidelines. The only identified mitigation measure, according to the guidelines, is to increase the overburden soil mass by e.g., construction of a road. In summary, these findings point towards further research and consequent development of the Swedish design guidelines in the evaluation and mitigation of hydraulic bottom-heave with lime-cement columns.

References

Adams, T. E. (2011). *Stability of levees and floodwalls supported by deep-mixing shear walls: Five case studies in the New Orleans area* [Doctoral thesis, Virginia Polytechnic Institute and State University]. Virginia Tech. https://vtechworks.lib.vt.edu/handle/10919/29065

Ahmed, S. M., & Agaiby, S. S. (2020). Strength and stiffness characterization of clays using Atterberg limits. *Transportation Geotechnics, 25*. doi: 10.1016/j.trgeo.2020.100420

Åhnberg, H., Ljungkrantz, C., Johansson, S.-E., Holmqvist, L., Retelius, A., & Holm, G. (1995). *Cement och kalk för djupstabilisering av jord*. Linköping: Swedish Geotechnical Institute.

Alén, C., Sällfors, G., Bengtsson, P.-E., & Baker, S. (2006). *Provbankar Riksväg 45/Nordlänken Bankar på kalkcementpelarförstärkt jord Beräkningsmodell för sättningar*. Linköping: Swedish Deep Stabilization Research Centre.

British Standards. (2005). *Execution of special geotechnical works - Deep mixing*. Brussels: Standards Policy and Strategy Committee.

Carlsten, P. (1996). Chapter 10 Lime and lime/cement columns. *Developments in Geotechnical Engineering*, *80*(C), 355–399. doi: 10.1016/S0165-1250(96)80013-7

Day, R. W. (2000). *Soil Testing Manual: Procedures, Classification Data, and Sampling Practices*. New York, NY: McGraw-Hill.

Eslami, A., Moshfeghi, S., Molaabasi, H., & Eslami, M. M. (2019). *Piezocone and Cone Penetration Test (CPTu and CPT) Applications in Foundation Engineering*. Amsterdam: Elsevier. doi: 10.1016/C2017-0-04195-2

EuroSoilStab. (2002). *Design Guide: Soft Soil Stabilisation* (1st ed.). London: IHS BRE Press.

Grimstad, G., Andresen, L., & Jostad, H. P. (2012). NGI-ADP: Anisotropic shear strength model for clay. *International Journal for Numerical and Analytical Methods in Geomechanics*, *36*(4), 483–497. doi: 10.1002/nag.1016

Hernvall, H. (2021). *Changes in undrained shear strength as a function of time under embankments*. Gothenburg: Chalmers University of Technology.

Ignat, R. (2018). *Ground Improvement by Dry Deep Mixing Lime-Cement Column Panels as Excavation Support* [Doctoral thesis, KTH Royal Institute of Technology]. DiVA. http://kth.diva-portal.org/smash/record.jsf?pid=diva2%3A1254063&dswid=-7275

Ignat, R., Baker, S., Karstunen, M., Liedberg, S., & Larsson, S. (2020). Numerical analyses of an experimental excavation supported by panels of lime-cement columns. *Computers and Geotechnics*, *118*, 103296. doi: 10.1016/j.compgeo.2019.103296

Ignat, R., Baker, S., Larsson, S., & Liedberg, S. (2015). Two- and three-dimensional analyses of excavation support with rows of dry deep mixing columns. *Computers and Geotechnics*, *66*, 16–30. doi: 10.1016/j.compgeo.2015.01.011

Ignat, R., Larsson, S., & Baker, S. (2014). Studie av 2D/3D numeriskmodellering av kalkcementpelare installerade som överlappande skivor. *Bygg & Teknik*, *106*(1), 80–83.

Jiang, H., & Xie, Y. (2011). A note on the Mohr-Coulomb and Drucker-Prager strength criteria. *Mechanics Research Communications*, *38*(4), 309–314. doi: 10.1016/j.mechrescom.2011.04.001

Karlsrud, K., Eggen, A., Nerland, Ø., & Haugen, T. (2015). Some Norwegian experiences related to use of dry-mixing methods to improve stability of excavations and natural slopes in soft clays. *Proceedings of the Deep Mixing 2015 Conference*, 87–100.

Karstunen, M., & Amavasai, A. (2017). *BEST SOIL: Soft soil modelling and parameter determination*. Gothenburg: Chalmers University of Technology.

Kempfert, H. G., & Gebreselassie, B. (2006). Excavations and foundations in soft soils. In *Excavations and Foundations in Soft Soils*. Berlin: Springer Berlin Heidelberg. doi: 10.1007/3-540-32895-5

Kitazume, M., & Terashi, M. (2013). *The Deep Mixing Method* (1st ed.). Boca Raton, FL: CRC Press. doi: 10.1201/b13873

Knappett, J., & Craig, R. F. (2012). *Craig's Soil Mechanics* (8th ed.). Boca Raton, FL: CRC Press.

Kullingsjö, A. (2007). *Effects of deep excavations in soft clay on the immediate sourroundings-Analysis of the possibility to predict deformations and reactions against the retaining system* [Doctoral thesis, Chalmers University of Technology]. Chalmers Research. https://research.chalmers.se/publication/45541

Larsson, R. (2006). *Rapport 17 Djupstabilisering med bindemedels-stabiliserade pelare och masstabilisering-En vägledning*. Linköping: Swedish Deep Stabilization Research Centre.

Larsson, R. (2008). *Jords egenskaper*. Linköping: Swedish Geotechnical Institute.

Larsson, R., Sällfors, G., Bengtsson, P.-E., Alén, C., Bergdahl, U., & Eriksson, L. (2007). *Skjuvhållfasthet - utvärdering i kohesionsjord*. Linköping: Swedish Geotechnical Institute.

Livsmedelverket. (2021). *Konsekvenser av ett förändrat klimat*. Retrieved 2021-02-15 from https://www.livsmedelsverket.se/produktion-handel--kontroll/dricksvattenproduktion/kaskad-handbok-for-klimatanpassning_dricksvattenproduktion/konsekvenser_av_ett_forandrat_klimat?AspxAutoDetectCookieSupport=1

Mayne, P. W., & Kulhawy, F. H. (1982). Ko- OCR relationships in soil. *Journal of the Geotechnical Engineering Division, ASCE*, *108*(6), 851–872. doi: 10.1061/ajgeb6.0001306

Moseley, M. P., & Kirsch, K. (2004). *Ground Improvement, Second Edition* (2nd ed.). Boca Raton, FL: CRC Press.

Naturvårdsverket. (2020). *Effekter i Sverige*. Retrieved 2021-02-15 from https://www.naturvardsverket.se/Sa-mar-miljon/Klimat-och-luft/Klimat/Klimatet-i-framtiden/Effekter-i-Sverige/

O'Rourke, T. D., & O'Donnell, C. J. (1997). Field Behavior of Excavation Stabilized by Deep Soil Mixing. *Journal of Geotechnical and Geoenvironmental Engineering, 123*(6), 516–524. doi: 10.1061/(asce)1090-0241(1997)123:6(516)

Olsson, M. (2010). *Calculating long-term settlement in soft clays - with special focus on the Gothenburg region* [Licentiate thesis, Chalmers University of Technology]. Chalmers Research. https://research.chalmers.se/publication/120809

Pane, V., Cecconi, M., & Napoli, P. (2015). Hydraulic Heave Failure in EC7: Suggestions for Verification. *Geotechnical and Geological Engineering, 33*(3), 739–750. doi: 10.1007/s10706-014-9834-8

Plaxis. (2018). *The SHANSEP NGI-ADP model 2018* [Computer software manual].

Plaxis. (2019). *Plaxis Material Models Manual 2019* [Computer software manual].

Potts, D. M., & Zdravković, L. (1999). *Finite element analysis in geotechnical engineering*. London: Thomas Telford Publishing. doi: 10.1680/feaiget.27534

Read, J., & Beale, G. (2014). *Guidelines for Evaluating Water in Pit Slope Stability* (1st ed.). Clayton, Victoria: CSIRO Publishing.

Sällfors, G. (2013). *Geoteknik: Jordmateriallära, Jordmekanik*. Gothenburg: Cremona.

Schanz, T., Vermeer, P. A., & Bonnier, P. G. (1999). The hardening soil model: Formulation and verification. *Beyond 2000 in Computational Geotechnics. Ten Years of PLAXIS International. Proceedings of the International Symposium, Amsterdam, March 1999.*, 281–296. doi: 10.1201/9781315138206-27

SGU. (2021). *Jordarter 1:25 000 - 1:100 000 [map]*. Retrieved 2021-03-02 from https://apps.sgu.se/kartvisare/kartvisare-jordarter-25-100.html?zoom=433132.3876398387,6509291.974432802,443884.4091438817,6514569.9849888235

SMHI. (2012). *Sveriges klimat har blivit varmare och blötare*. Retrieved 2021-02-15 from https://www.smhi.se/kunskapsbanken/klimat/sveriges-klimat/sveriges-klimat-har-blivit-varmare-och-blotare-1.21614

Smith, M. E. (2005). *Design of Bridging Layers in Geosynthetic-Reinforced Column-Supported Embankments* [Doctoral thesis, Virginia Polytechnic Institute and State University]. Virginia Tech. https://vtechworks.lib.vt.edu/handle/10919/28260

Strózyk, J., & Tankiewicz, M. (2014). The undrained shear strength of overconsolidated clays. *Procedia Engineering, 91*, 317–321. doi: 10.1016/j.proeng.2014.12.067

Trafikverket. (2016a). *Trafikverkets tekniska krav för geokonstruktioner TK Geo 13*. Borlänge: Trafikverket.

Trafikverket. (2016b). *Trafikverkets tekniska råd för geokonstruktioner TR Geo 13*. Borlänge: Trafikverket.

Trafikverket. (2020). *Projekterings PM, Geoteknik: E20 förbi Mariestad, delen Muggebo-Tjos*. Skövde: Trafikverket.

Wood, D. M. (2017). *Geotechnical Modelling* (1st ed.). Boca Raton, FL: CRC Press. doi: 10.1201/9781315273556

Wudtke, R.-B. (2008). Failure Mechanisms of Hydraulic Heave at Excavations. *19. Young Geotechnical Engineers' Conference (EYGEC)*, 331–338.

Wudtke, R.-B., & Witt, K.-J. (2013). Hydraulic Heave in Cohesive Soils. *18th International Conference on Soil Mechanics & Geotechnical Engineering, Vol 1*, 449–452.

Yang, H., Tan, T. S., & Leung, C. F. (2011). Mass behaviour of embedded improved soil raft in an excavation. *Proceedings of the Institution of Civil Engineers - Geotechnical Engineering*, *164*(1), 11–25. doi: 10.1680/geng.9.00078

Yannie, J., Björkman, T., Isaksson, J., & Bergström, A. (2020). KC-pelare i passivzon - Nyheten på det geotekniska smörgåsbordet, E02 - Centralen Västlänken. *Grundläggningsdagen*, 57–67.

A. Parameter derivation

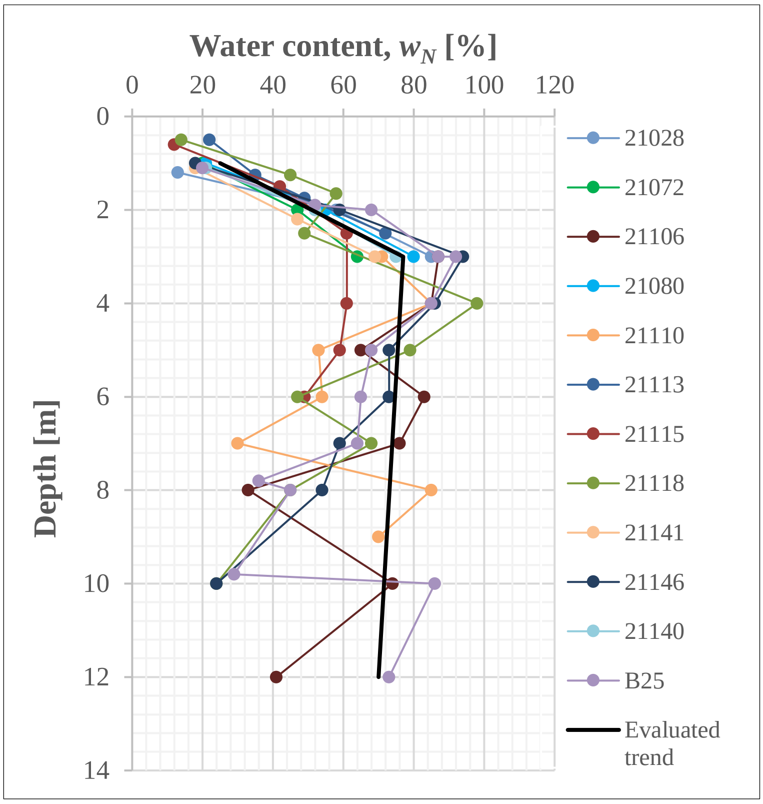

Figure A.1 Measured water content and the evaluated trend as a function of depth.

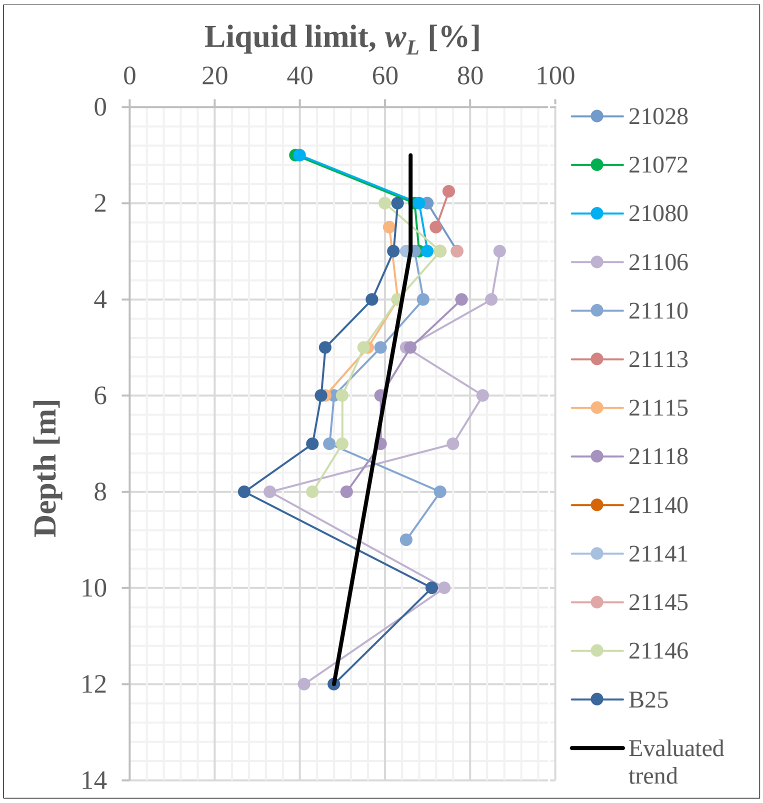

Figure A.2 Measured liquid limit and the evaluated trend as a function of depth.

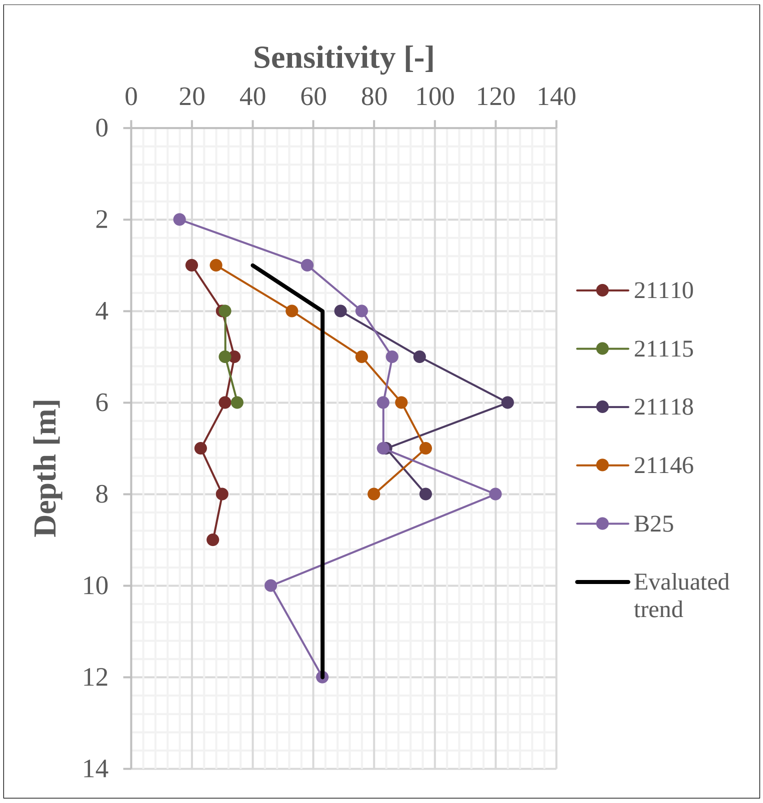

Figure A.3 Measured sensitivity and the evaluated trend as a function of depth.

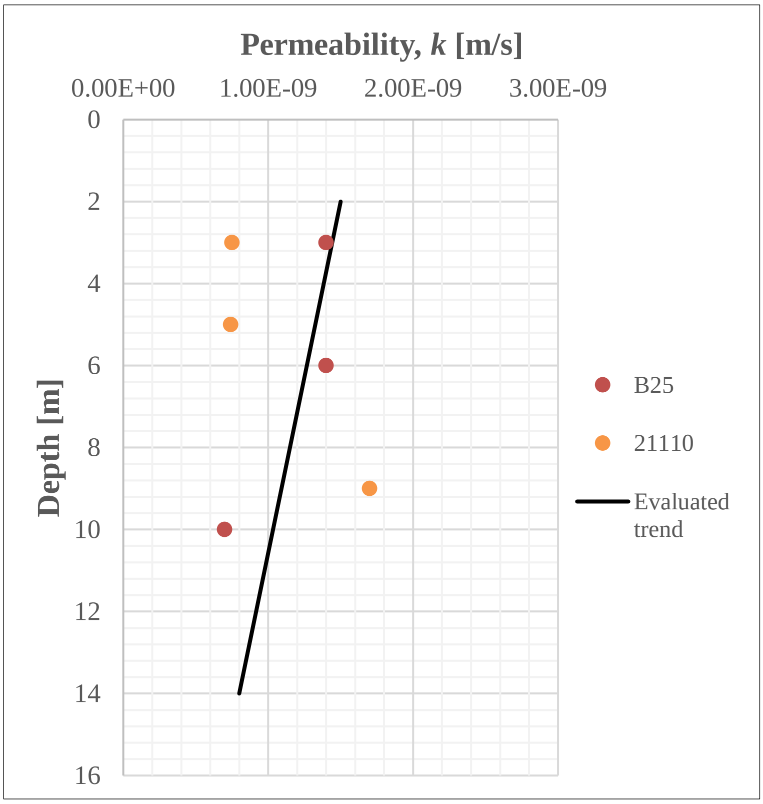

Figure A.4 Measured permeability and the evaluated trend as a function of depth.

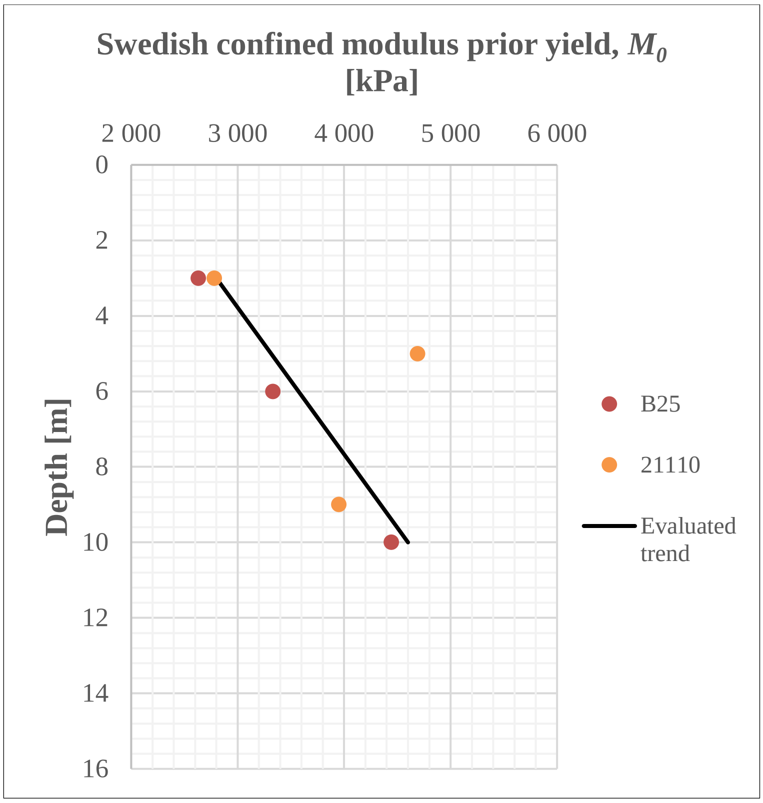

Figure A.5 Evaluated Swedish confined modulus prior yield and the evaluated trend as a function of depth.

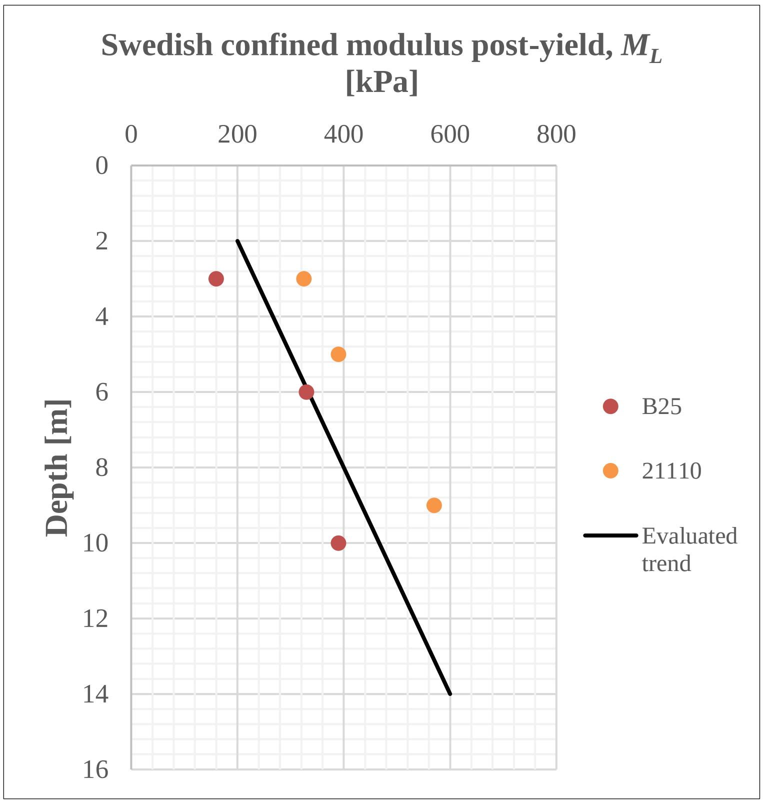

Figure A.6 Evaluated Swedish confined modulus post-yield and the evaluated trend as a function of depth.

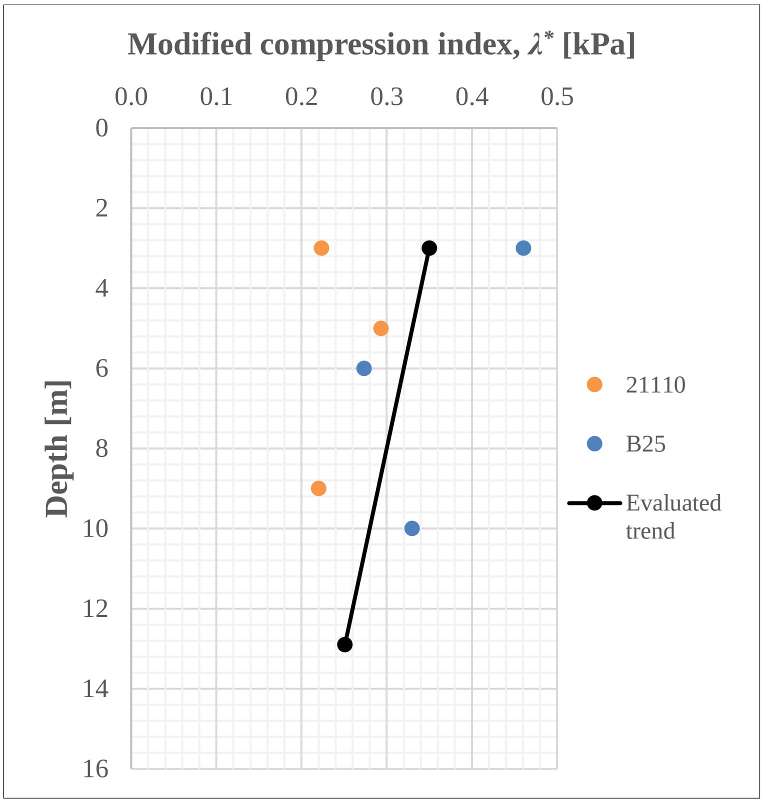

Figure A.7 Evaluated modified compression index and the evaluated trend as a function of depth.

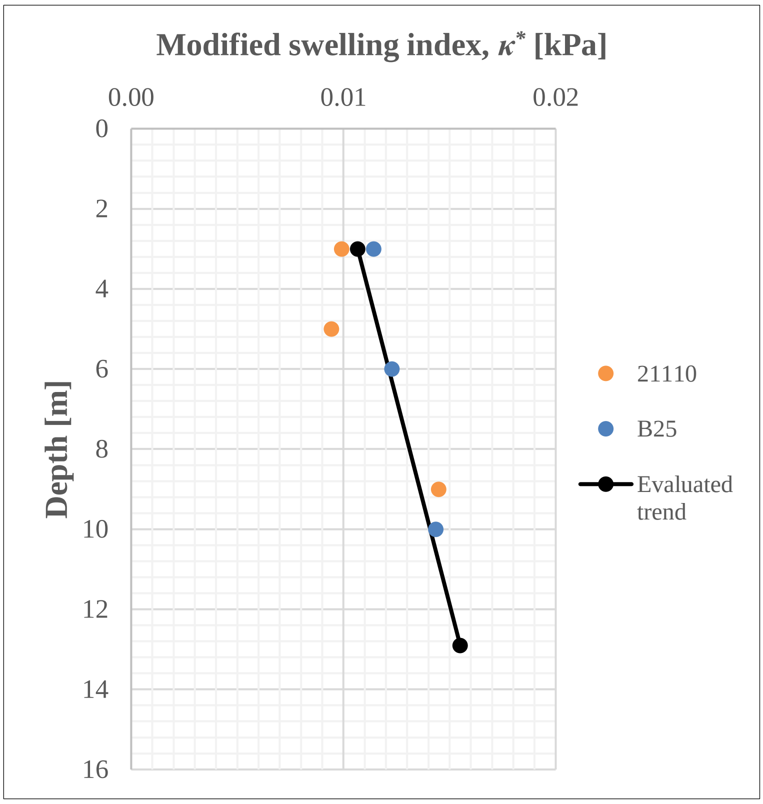

Figure A.8 Evaluated modified swelling index and the evaluated trend as a function of depth.

B. Input parameters

Table B.1 Dry crust and frictional material input parameters for all scenarios.

All scenarios				
Parameter	**Symbol**	**Unit**	**Dry crust**	**Frictional material**
General				
Material model	Model	-	Mohr-Coulomb	Mohr-Coulomb
Type of behaviour	Type	-	Drained	Drained
Dry weight	γ_{unsat}	[kN/m^3]	17	19
Wet weight	γ_{sat}	[kN/m^3]	17	19
Parameters				
Drained Young's modulus	E'	[kPa]	4000	40000
Drained Poisson's ratio	ν'	-	0.2	0.2
Effective reference cohesion	c'_{ref}	[kPa]	10	2
Friction angle	φ'	[°]	30	40
Dilatancy angle	ψ	[°]	0	0
Groundwater				
Horizontal permeability	k_x	[m/day]	8.640E-3	43.2
Vertical permeability	k_y	[m/day]	8.640E-3	43.2
Initial void ratio	e_{init}	-	-	-
Change of permeability	c_k	-	1E+15	1E+15
Interfaces				
Interface strength	-	-	Rigid	Rigid
Interface reduction strength	R_{inter}	-	1	1
Initial				
K_0 determination	-	-	Automatic	Automatic
Lateral earth pressure coefficient	$K_{0,x}$	-	0.5	0.36
Overconsolidation ratio	*OCR*	-	-	-
Pre-overburden pressure	*POP*	-	-	-

Table B.2 Clay material input parameters for Scenario 1.

Scenario 1						
Parameter	**Symbol**	**Unit**	**Clay 1**	**Clay 2**	**Clay 3**	**Clay 4**
General						
Material model	Model	-	Soft Soil	Soft Soil	Soft Soil	Soft Soil
Type of behaviour	Type	-	Undrained (A)	Undrained (A)	Undrained (A)	Undrained (A)
Dry weight	γ_{unsat}	[kN/m^3]	16.3	16.3	16.3	16.3
Wet weight	γ_{sat}	[kN/m^3]	16.3	16.3	16.3	16.3
Parameters						
Modified compression index	λ^*	-	0.35	0.32	0.29	0.251
Modified swelling index	κ^*	-	0.0107	0.0121	0.0136	0.0155
Effective cohesion	c'	[kPa]	1.3	1.6	2.0	2.4
Friction angle	φ'	[°]	30	30	30	30
Dilatancy angle	ψ	[°]	0	0	0	0
Unloading/reloading Poisson's ratio	v'_{ur}	-	0.15	0.15	0.15	0.15
Groundwater						
Horizontal permeability	k_x	[m/day]	0.1250E-3	0.1100E-3	0.09450E-3	0.0750E-3
Vertical permeability	k_y	[m/day]	0.1250E-3	0.1100E-3	0.09450E-3	0.0750E-3
Initial void ratio	e_{init}	-	1.88	1.84	1.80	1.75
Change of permeability	c_k	-	1E+15	1E+15	1E+15	1E+15
Interfaces						
Interface strength	-	-	Rigid	Rigid	Rigid	Rigid
Interface reduction strength	R_{inter}	-	1	1	1	1
Initial						
K_0 determination	-	-	Manual	Manual	Manual	Manual
Lateral earth pressure coefficient	$K_{0,x}$	-	0.72	0.68	0.68	0.68
Overconsolidation ratio	OCR	-	-	1.82	1.83	1.83
Pre-overburden pressure	POP	-	33	-	-	-

Table B.3 Clay and Composite material input parameters for Scenario 2.

Scenario 2										
Parameter	**Symbol**	**Unit**	**Clay 1**	**Clay 2**	**Clay 3**	**Clay 4**	**Composite 1**	**Composite 2**	**Composite 3**	**Composite 4**
General										
Material model	Model	-	Soft Soil	Soft Soil	Soft Soil	Soft Soil	Mohr-Coulomb	Mohr-Coulomb	Mohr-Coulomb	Mohr-Coulomb
Type of behaviour	Type	-	Undrained (A)	Undrained (A)	Undrained (A)	Undrained (A)	Undrained (B)	Undrained (B)	Undrained (B)	Undrained (B)
Dry weight	γ_{unsat}	[kN/m^3]	16.3	16.3	16.3	16.3	16.3	16.3	16.3	16.3
Wet weight	γ_{sat}	[kN/m^3]	16.3	16.3	16.3	16.3	16.3	16.3	16.3	16.3
Parameters										
Modified compression index	λ^*	-	0.35	0.32	0.29	0.251	-	-	-	-
Modified swelling index	κ^*	-	0.0107	0.0121	0.0136	0.0155	-	-	-	-
Drained Young's modulus	E'	[kPa]	-	-	-	-	9998	10314	10629	11040
Drained Poisson's ratio	ν'	-	-	-	-	-	0.33	0.33	0.33	0.33
Effective cohesion	c'	[kPa]	1.3	1.6	2.0	2.4	-	-	-	-
Friction angle	φ'	[°]	30	30	30	30	-	-	-	-
Reference undrained shear strength	$s_{u,ref}$	[kPa]	-	-	-	-	56	57	59	61
Dilatancy angle	ψ	[°]	0	0	0	0	-	-	-	-
Unloading/reloading Poisson's ratio	ν'_{ur}	-	0.15	0.15	0.15	0.15	-	-	-	-
Groundwater										
Horizontal permeability	k_x	[m/day]	0.1250E-3	0.1100E-3	0.09450E-3	0.0750E-3	0.03250	0.02850	0.02460	0.01950
Vertical permeability	k_y	[m/day]	0.1250E-3	0.1100E-3	0.09450E-3	0.0750E-3	0.03250	0.02850	0.02460	0.01950
Initial void ratio	e_{init}	-	1.88	1.84	1.80	1.75	-	-	-	-
Change of permeability	c_k	-	1E+15	1E+15	1E+15	1E+15	1E+15	1E+15	1E+15	1E+15
Interfaces										
Interface strength	-	-	Rigid	Rigid	Rigid	Rigid	Rigid	Rigid	Rigid	Rigid
Interface reduction strength	R_{inter}	-	1	1	1	1	1	1	1	1
Initial										
K_0 determination	-	-	Manual	Manual	Manual	Manual	Manual	Manual	Manual	Manual
Lateral earth pressure coefficient	$K_{0,x}$	-	0.72	0.68	0.68	0.68	0.47	0.47	0.47	0.47
Overconsolidation ratio	OCR	-	-	1.82	1.83	1.83	-	-	-	-
Pre-overburden pressure	POP	-	33	-	-	-	-	-	-	-

Table B.4 Clay and Composite material input parameters for Scenario 3.

Scenario 3										
Parameter	**Symbol**	**Unit**	**Clay 1**	**Clay 2**	**Clay 3**	**Clay 4**	**Composite 1**	**Composite 2**	**Composite 3**	**Composite 4**
General										
Material model	Model	-	Soft Soil	Soft Soil	Soft Soil	Soft Soil	Hardening Soil	Hardening Soil	Hardening Soil	Hardening Soil
Type of behaviour	Type	-	Undrained (A)	Undrained (A)	Undrained (A)	Undrained (A)	Undrained (A)	Undrained (A)	Undrained (A)	Undrained (A)
Dry weight	γ_{unsat}	[kN/m^3]	16.3	16.3	16.3	16.3	16.3	16.3	16.3	16.3
Wet weight	γ_{sat}	[kN/m^3]	16.3	16.3	16.3	16.3	16.3	16.3	16.3	16.3
Parameters										
Modified compression index	λ^*	-	0.35	0.32	0.29	0.251	-	-	-	-
Modified swelling index	κ^*	-	0.0107	0.0121	0.0136	0.0155	-	-	-	-
Secant Young's modulus	E_{50}^{ref}	[kPa]	-	-	-	-	25652	22409	20792	19152
Tangent Young's modulus	E_{oed}^{ref}	[kPa]	-	-	-	-	20503	17955	16520	15018
Unloading/reloading Young's modulus	E_{ur}^{ref}	[kPa]	-	-	-	-	76957	67228	62375	57455
Power for stress-level dependency of stiffness	m	-	-	-	-	-	0.7	0.7	0.7	0.7
Effective reference cohesion	c'_{ref}	-	-	-	-	-	8.4	8.6	8.8	9.1
Effective cohesion	c'	[kPa]	1.3	1.6	2.0	2.4	-	-	-	-
Friction angle	φ'	[°]	30	30	30	30	32	32	32	32
Dilatancy angle	ψ	[°]	0	0	0	0	0	0	0	0
Unloading/reloading Poisson's ratio	v'_{ur}	-	0.15	0.15	0.15	0.15	0.2	0.2	0.2	0.2
Groundwater										
Horizontal permeability	k_x	[m/day]	0.1250E-3	0.1100E-3	0.09450E-3	0.0750E-3	0.03250	0.02850	0.02460	0.01950
Vertical permeability	k_y	[m/day]	0.1250E-3	0.1100E-3	0.09450E-3	0.0750E-3	0.03250	0.02850	0.02460	0.01950
Initial void ratio	e_{init}	-	1.88	1.84	1.80	1.75	-	-	-	-
Change of permeability	c_k	-	1E+15	1E+15	1E+15	1E+15	1E+15	1E+15	1E+15	1E+15
Interfaces										
Interface strength	-	-	Rigid	Rigid	Rigid	Rigid	Rigid	Rigid	Rigid	Rigid
Interface reduction strength	R_{inter}	-	1	1	1	1	1	1	1	1
Initial										
K_0 determination	-	-	Manual	Manual	Manual	Manual	Manual	Manual	Manual	Manual
Lateral earth pressure coefficient	$K_{0,x}$	-	0.72	0.68	0.68	0.68	0.47	0.47	0.47	0.47
Overconsolidation ratio	*OCR*	-	-	1.82	1.83	1.83	5	5	5	5
Pre-overburden pressure	*POP*	-	33	-	-	-	-	-	-	-

Table B.5 Clay material input parameters for Scenario 4.

Scenario 4						
Parameter	**Symbol**	**Unit**	**Clay 1**	**Clay 2**	**Clay 3**	**Clay 4**
General						
Material model	Model	-	NGI-ADP	NGI-ADP	NGI-ADP	NGI-ADP
Type of behaviour	Type	-	Undrained (C)	Undrained (C)	Undrained (C)	Undrained (C)
Dry weight	γ_{unsat}	[kN/m^3]	16.3	16.3	16.3	16.3
Wet weight	γ_{sat}	[kN/m^3]	16.3	16.3	16.3	16.3
Parameters						
Ratio unloading/reloading shear modulus over active shear strength	$G_{ur}/s^A{}_u$	-	82	85	88	90
Shear strain at failure in triaxial compression	$\gamma_f{}^C$	[%]	2	2	2	2
Shear strain at failure in triaxial extension	$\gamma_f{}^E$	[%]	4	4	4	4
Shear strain at failure in direct simple shear	$\gamma_f{}^{DSS}$	[%]	3	3	3	3
Reference active shear strength	$s^A{}_{u,ref}$	[kPa]	17.8	21.5	28.2	34.7
Ratio triaxial compressive shear strength over active shear strength	$s^{C,TX}{}_u/s^A{}_u$	-	0.99	0.99	0.99	0.99
Reference depth	y_{ref}	[m]	-3	-4.5	-7.5	-10.5
Increase of active shear strength with depth	$s^A{}_{u,inc}$	[kPa/m]	2.44	2.23	2.19	2.19
Ratio of passive shear strength over active shear strength	$s^P{}_u/s^A{}_u$	-	0.63	0.59	0.55	0.50
Initial mobilization	$\tau_0/s^A{}_u$	-	0.24	0.30	0.30	0.30
Ratio of direct simple shear strength over active shear strength	$s^{DSS}{}_u/s^A{}_u$	-	0.73	0.69	0.67	0.63
Undrained Poisson's ratio	ν_u	-	0.495	0.495	0.495	0.495
Groundwater						
Horizontal permeability	k_x	[m/day]	-	-	-	-
Vertical permeability	k_y	[m/day]	-	-	-	-
Initial void ratio	e_{init}	-	1.88	1.84	1.80	1.75
Change of permeability	c_k	-	-	-	-	-
Interfaces						
Interface strength	-	-	Rigid	Rigid	Rigid	Rigid
Interface reduction strength	R_{inter}	-	1	1	1	1
Initial						
K_0 determination	-	-	Manual	Manual	Manual	Manual
Lateral earth pressure coefficient	$K_{0,x}$	-	0.72	0.68	0.68	0.68
Overconsolidation ratio	*OCR*	-	-	-	-	-
Pre-overburden pressure	*POP*	-	.	-	-	-

C. Construction sequences

Table C.1 Construction sequence for Scenario 1.

Scenario 1			
Phase	**Procedure**	**Time**	**Description**
Initial phase	K_0 - procedure	-	Activating the soil and the initial groundwater level
Phase 1	Consolidation	15	Excavation 0.5 m
Phase 2	Consolidation	15	Excavation 1 m
Phase 3	Consolidation	30	Groundwater lowering 2 m
Phase 4	Consolidation	15	Excavation 1.5 m
Phase 5	Consolidation	15	Excavation 2 m
Phase 6	Consolidation	30	Groundwater lowering 3 m
Phase 7	Consolidation	15	Excavation 2.5 m
Phase 8	Consolidation	15	Excavation 3 m
Phase 9	Consolidation	30	Groundwater lowering 4 m
Phase 10	Consolidation	15	Excavation 3.5 m
Phase 11	Consolidation	15	Excavation 4 m
Phase 12	Consolidation	30	Groundwater lowering 5 m
Phase 13	Consolidation	15	Excavation 4.5 m
Phase 14	Consolidation	15	Excavation 5 m
Phase 15	Phi-c reduction	-	Short-term factor of safety
Phase 16	Consolidation	30	Groundwater lowering 6 m
Phase 17	Consolidation	14 600	Consolidation 40 years
Phase 18	Phi-c reduction	-	Long-term factor of safety

Table C.2 Construction sequence for Scenario 2.

Scenario 2			
Phase	**Procedure**	**Time**	**Description**
Initial phase	K_0 - procedure	-	Activating the soil and the initial groundwater level
Phase 1	Consolidation	21	Installation of the composite material
Phase 2	Consolidation	15	Excavation 0.5 m
Phase 3	Consolidation	15	Excavation 1 m
Phase 4	Consolidation	30	Groundwater lowering 2 m
Phase 5	Consolidation	15	Excavation 1.5 m
Phase 6	Consolidation	15	Excavation 2 m
Phase 7	Consolidation	30	Groundwater lowering 3 m
Phase 8	Consolidation	15	Excavation 2.5 m
Phase 9	Consolidation	15	Excavation 3 m
Phase 10	Consolidation	30	Groundwater lowering 4 m
Phase 11	Consolidation	15	Excavation 3.5 m
Phase 12	Consolidation	15	Excavation 4 m
Phase 13	Consolidation	30	Groundwater lowering 5 m
Phase 14	Consolidation	15	Excavation 4.5 m
Phase 15	Consolidation	15	Excavation 5 m
Phase 16	*Phi-c* reduction	-	Short-term factor of safety

Table C.3 Construction sequence for Scenario 3.

Scenario 3			
Phase	**Procedure**	**Time**	**Description**
Initial phase	K_0 - procedure	-	Activating the soil and the initial groundwater level
Phase 1	Consolidation	21	Installation of the composite material
Phase 2	Consolidation	15	Excavation 0.5 m
Phase 3	Consolidation	15	Excavation 1 m
Phase 4	Consolidation	30	Groundwater lowering 2 m
Phase 5	Consolidation	15	Excavation 1.5 m
Phase 6	Consolidation	15	Excavation 2 m
Phase 7	Consolidation	30	Groundwater lowering 3 m
Phase 8	Consolidation	15	Excavation 2.5 m
Phase 9	Consolidation	15	Excavation 3 m
Phase 10	Consolidation	30	Groundwater lowering 4 m
Phase 11	Consolidation	15	Excavation 3.5 m
Phase 12	Consolidation	15	Excavation 4 m
Phase 13	Consolidation	30	Groundwater lowering 5 m
Phase 14	Consolidation	15	Excavation 4.5 m
Phase 15	Consolidation	15	Excavation 5 m
Phase 16	Phi-c reduction	-	Short-term factor of safety
Phase 17	Consolidation	30	Groundwater lowering 6 m
Phase 18	Consolidation	14 600	Consolidation 40 years
Phase 19	Phi-c reduction	-	Long-term factor of safety

Table C.4 Construction sequence for Scenario 4.

Scenario 4		
Phase	**Procedure**	**Description**
Initial phase	K_0 - procedure	Activating the soil and the initial groundwater level
Phase 1	Plastic	Excavation 0.5 m
Phase 2	Plastic	Excavation 1 m
Phase 3	Plastic	Excavation 1.5 m
Phase 4	Plastic	Excavation 2 m
Phase 5	Plastic	Excavation 2.5 m
Phase 6	Plastic	Excavation 3 m
Phase 7	Plastic	Excavation 3.5 m
Phase 8	Plastic	Excavation 4 m
Phase 9	Plastic	Excavation 4.5 m
Phase 10	Plastic	Excavation 5 m
Phase 11	Phi-c reduction	Undrained factor of safety

D. Sensitivity analysis

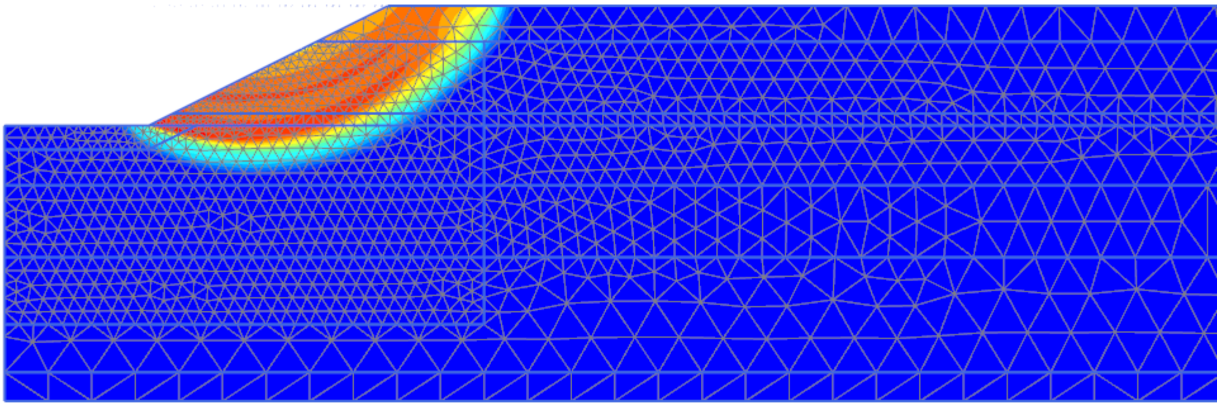

Figure D.1 Incremental displacements for short-term phi-c reduction in Scenario 1 for an induced artesian pressure of 180 kPa.

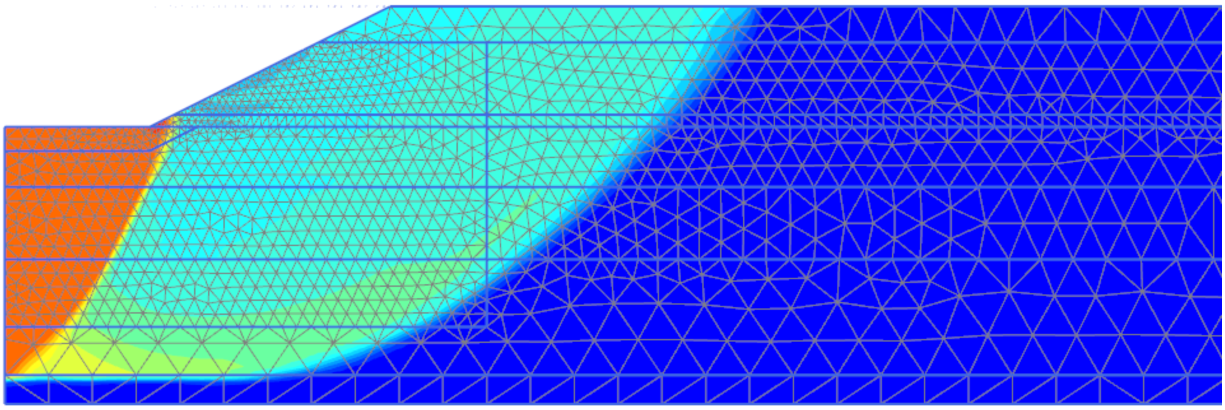

Figure D.2 Incremental displacements for short-term phi-c reduction in Scenario 1 for an induced artesian pressure of 190 kPa.

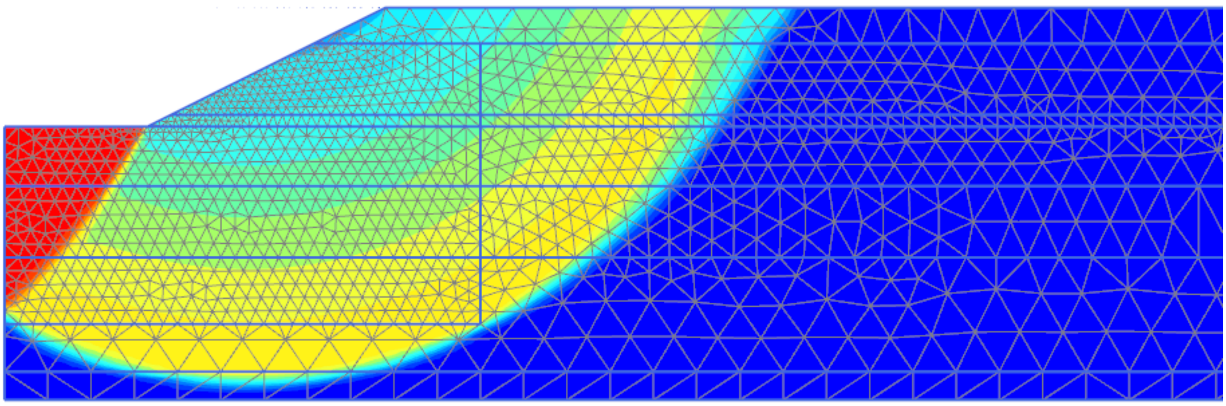

Figure D.3 Incremental displacements for short-term phi-c reduction in Scenario 2 for an induced artesian pressure of 180 kPa.

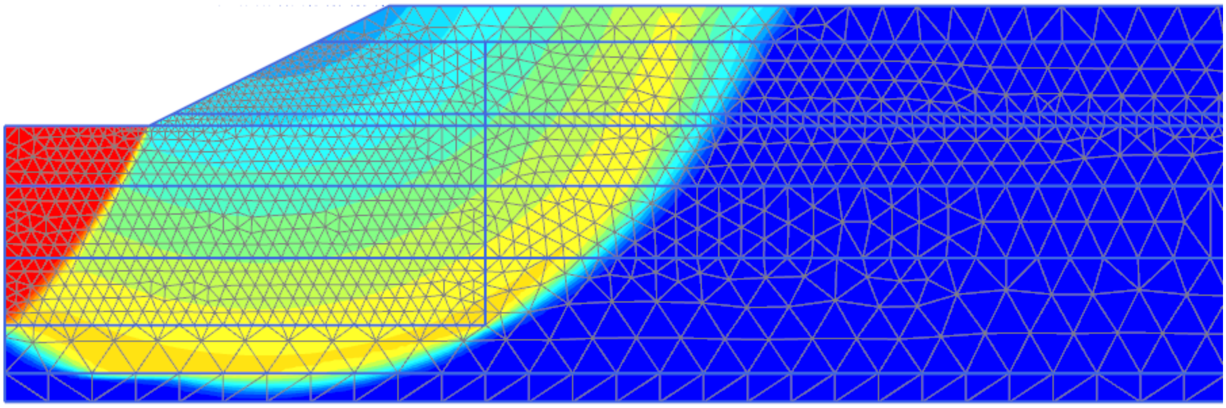

Figure D.4 Incremental displacements for short-term phi-c reduction in Scenario 2 for an induced artesian pressure of 190 kPa.

DEPARTMENT OF ARCHITECTURE AND CIVIL ENGINEERING
DIVISION OF GEOLOGY & GEOTECHNICS
CHALMERS UNIVERSITY OF TECHNOLOGY
Gothenburg, Sweden 2021
www.chalmers.se

CHALMERS
UNIVERSITY OF TECHNOLOGY